Development of an in situ laser-induced fluorescence spectrometer for real-time analysis of bioaerosols

Dissertation

Zur Erlangung des Grades

‘Doktor rerum naturalium (Dr. rer. nat.)‘

im Promotionsfach Chemie

am Fachbereich Chemie, Pharmazie und Geowissenschaften

der Johannes Gutenberg-Universität in Mainz

Paul Crutzen Graduate School

Minghui Zhang

geb. am 05.10.1989 in Shandong, China

Mainz, Germany, April 2019

I hearby declare that I wrote the dissertation submitted without any unauthorised external assistance and used only sources acknowledged in the work. All textual passages which are appropriated verbatim or paraphrased from published and unpublished texts as well as all information obtained from oral sources are duly indicated and listed in accordance with bibliographical rules. In carrying out this research, I complied with the rules of standard scientific practice as formulated in the statutes of the Johannes Gutenberg University, Mainz, to ensure standard scientific practice.

April 2, 2019
Minghui Zhang

Abstract

Characteristic particle size, fluorescence intensity and fluorescence spectra are important features to detect and categorize bioaerosols. In this thesis, I developed a size-resolved single-particle fluorescence spectrometer (S2FS), which enables measurement of fluorescence spectra dispersed in 512 channels between 370 nm and 610 nm with excitation wavelength (λ_{ex}) at 355 nm. Moreover, it can simultaneously measure aerodynamic diameters of aerosol particles from 0.5 μm to 20 μm (52 channels, logarithmic size scale). The S2FS consists of an aerodynamic particle sizer and a fluorescence spectrometer with a 355-nm laser excitation source and an intensified charge-coupled device (ICCD) as detector.

Preliminary ambient measurement in Mainz (Germany, central Europe) shows that an emission peak at ~440 nm was frequently observed for fluorescent fine particles (0.5-1 μm), suggesting the occurrence of dipicolinic acid (DPA), which constitutes a significant fraction of bacterial endospores and exists exclusively in bacterial endospores. Fluorescent fine particles account for 2.8% on average, based on the number fraction in the fine mode. Fluorescence coarse particles (> 1 μm) exhibit emission peaks at ~440 nm, ~450 nm, and ~470 nm, suggesting the existence of agglomerated bacterial endospores, pollen fragments, and fungal spores in the coarse mode. Fluorescent coarse particles account for 8.9% on average based on the number fraction, with strongest occurrence observed during a thunderstorm and in the morning.

I further demonstrate that the volume of single particles can be used as the single parameter to calibrate the intensity of an online/in situ fluorescence spectrometer (OFS). Among the materials tested, nicotinamide adenine dinucleotide (NADH), cellulose, and chitin exhibit fluorescence scaling with the volume of the particle. After the fluorescence intensity is calibrated by volume, the fluorescence spectra are nearly the same for particles with different sizes. This method implies that the fluorescence intensity can be compared and scaled between different online/in situ fluorescence spectrometers.

The last part is to explore the potential interference of biogenic secondary organic aerosols (SOA). I measured the fluorescence property of fresh SOA and aged SOA in the *particle* phase by using the S2FS. Fresh SOA were generated by the reaction of limonene or α-pinene with ozone (O_3) while aged SOA were generated by the reaction of limonene or α-pinene with ozone (O_3) in the presence of ammonia. Preliminary results show that fresh SOA exhibit fluorescence from 400-500 nm with the emission peaking at ~470 nm while aged SOA cover a broader range from 400-610 nm with the emission peaking at ~480 nm with λ_{ex} = 355 nm. The fractions of fluorescent fresh SOA and fluorescent aged SOA are 1-4% and 6-10%, respectively. Relative humidity (RH) influences fluorescence of fresh SOA in the shorter wavelength while RH influences fluorescence aged SOA mainly in the longer wavelength.

Contents

1 Introduction

1.1 Bioaerosols in the atmosphere

Bioaerosols are also termed as primary biological aerosol particles (PBAP) (Despres et al., 2012;Frohlich-Nowoisky et al., 2016), which mean they are directly emitted from the biological community. Biogenic secondary organic aerosols (BSOA) (Hallquist et al., 2009) are oxidation products of biogenic volatile organic compounds (BVOC), but they are not classified as PBAP. In terrestrial ecosystems, PBAP consist of viruses, bacteria and archaea, fungal and fern spores, pollen from vascular plants, algae and lichens from cryptogamic covers, and fragments of animal and plant matter (Despres et al., 2012). In marine ecosystems, PBAP consist of viruses, bacteria and archaea, fungi, protozoa, algae, fragments and exudates of phytoplankton emitted from sea surface microlayer (SML) (Hawkins and Russell, 2010;Frohlich-Nowoisky et al., 2016). In the coarse mode (> 1 μm), PBAP account for 4-10% in urban and rural environments (Gabey et al., 2011;Huffman et al., 2010) and 30% in rainforest environments (Huffman et al., 2012) based on the number concentrations. In the fine mode (< 1 μm), the fraction of PBAP decreases to ~7% (Schneider et al., 2011). However, a large fraction of ~30% has been reported for fine particles (0.4-1 μm) (MatthiasMaser and Jaenicke, 1995) although the number fraction could be much lower by taking into account the particle below 0.4 μm.

PBAP can influence climate by acting as ice nuclei (IN) (Wilson et al., 2015;Poschl et al., 2010). PBAP can account for ~33% of the ice-crystal residues at high altitude (Pratt et al., 2009) although on a global scale PBAP account for < 1% of the IN (Hoose et al., 2010). In precipitation and fresh snow samples (Christner et al., 2008), rainforest aerosol samples (Prenni et al., 2009;Poschl et al., 2010), or exudates from marine phytoplankton cells (Wilson et al., 2015), PBAP were observed to be IN active at high temperatures. Some types of PBAP can act as IN since they have similar chemical bonding and crystallographic structures to those of ice (Knopf et al., 2011). Some types of PBAP such as pollen are likely to participate as giant cloud condensation nuclei (GCCN), which are effective in changing the intensity and amount of precipitation although the concentration of GCCN is low in the atmosphere (Mohler et al., 2007). Moreover, some species of PBAP are pathogens or

allergens for humans, animals, and plants, and they have been identified in northern America (Brodie et al., 2007), central Europe (Frohlich-Nowoisky et al., 2009) or eastern Asia (Cao et al., 2014).

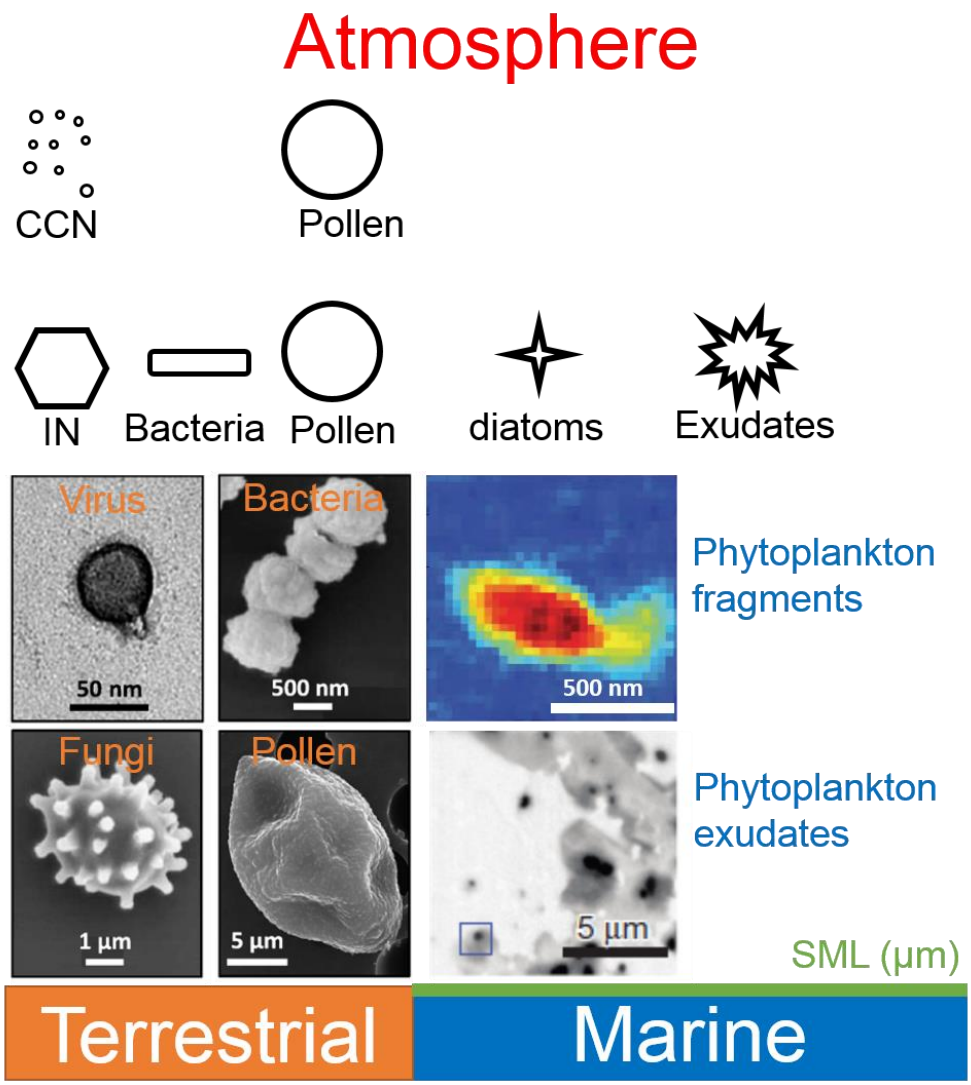

Figure 1. PBAP in the atmosphere are directly emitted from terrestrial ecosystems and marine ecosystems. In terrestrial ecosystems, PBAP consist of viruses, bacteria and archaea, fungal and fern spores, pollen from vascular plants, etc. In marine ecosystems, PBAP consist of viruses, bacteria and archaea, fungi, protozoa, algae, fragments and exudates of phytoplankton emitted from sea surface microlayer (SML). They may affect climate by acting as ice nuclei (IN) or giant cloud condensation nuclei (GCCN). The figure is adapted from (Frohlich-Nowoisky et al., 2016).

1.2 Real-time analysis of bioaerosols

The approaches for analysis of bioaerosols fall into offline techniques and online (also termed as real-time or in situ) techniques. Offline techniques mean first collecting samples on a filter from the air; afterwards, the filter is analyzed by fluorescence and electron microscopy, polymerase chain reaction (PCR), chromatography, mass spectrometry, electrochemical, immunochemical, or immunological methods (Despres et al., 2012). Offline techniques enable comprehensive analysis of PBAP, e.g., by gene sequencing PBAP can be identified at the species level (Cao et al., 2014). The disadvantage is that aerosol sampling and subsequent offline analysis require intensive laboratory work and have low time resolution (hours/days) (Despres et al., 2012). Besides, some viable bioaerosols may reproduce on the filter during the aerosol sampling process, thus influencing the subsequent quantification of bioaerosols.

Online techniques are also termed as real-time techniques or in situ techniques, which can directly analyze airborne bioareosols without the need of the filter. These methods consist of aerosol mass spectrometry (Schneider et al., 2011), Raman spectroscopy (Sowoidnich and Kronfeldt, 2012), laser-induced breakdown spectroscopy (Hybl et al., 2003), and laser/light-induced fluorescence (LIF) spectrometers (Huang et al., 2008). Among them, LIF spectrometers have been frequently used in recent years to quantify bioaerosols in the atmosphere (Gabey et al., 2010;Huffman et al., 2010;Perring et al., 2015). Several commercial LIF spectrometers have been developed and commonly used including the Ultraviolet Aerodynamic Particle Sizer (UV-APS) (Huffman et al., 2012) and the Wideband Integrated Bioaerosol Sensor (WIBS) (Toprak and Schnaiter, 2013). These commercial instruments measure the fluorescence intensity by using photomultiplier tubes (PMT) as sensor. In order to measure the dispersed fluorescence spectra at different emission wavelengths, the number of channels of PMT has been extended from 1 channel to 32 channels (Crouzy et al., 2016). Higher-resolution fluorescence spectra have been achieved in non-commercial applications, e.g., by particle-fluorescence spectrometer (PFS) (Pinnick et al., 1998) or dual-wavelength particle-fluorescence spectrometer (DPFS) (Pan et al., 2014) using an intensified charge-coupled device (ICCD) with 1024 channels.

Apart from the fluorescence property, simultaneous measurement of particle size is also important. Firstly, some types of PBAP exhibit characteristic size distributions. For example, a characteristic peak at ~3 μm has been observed in many studies and probably can be explained by fungal spores (Huffman et al., 2012;Huffman et al., 2010;Healy et al., 2014;Schumacher et al., 2013). Secondly, the size information of a single particle is also a fundamental factor concerning health effects. Fine particles can penetrate deep into lungs, which may eventually lead to tissue damage and cardiovascular problems (Polichetti et al., 2009). Thirdly, the fluorescence intensity scales with the size of particles (Hill et al., 2015). Fluorescence intensities are difficult to compare without accounting for the size of particles.

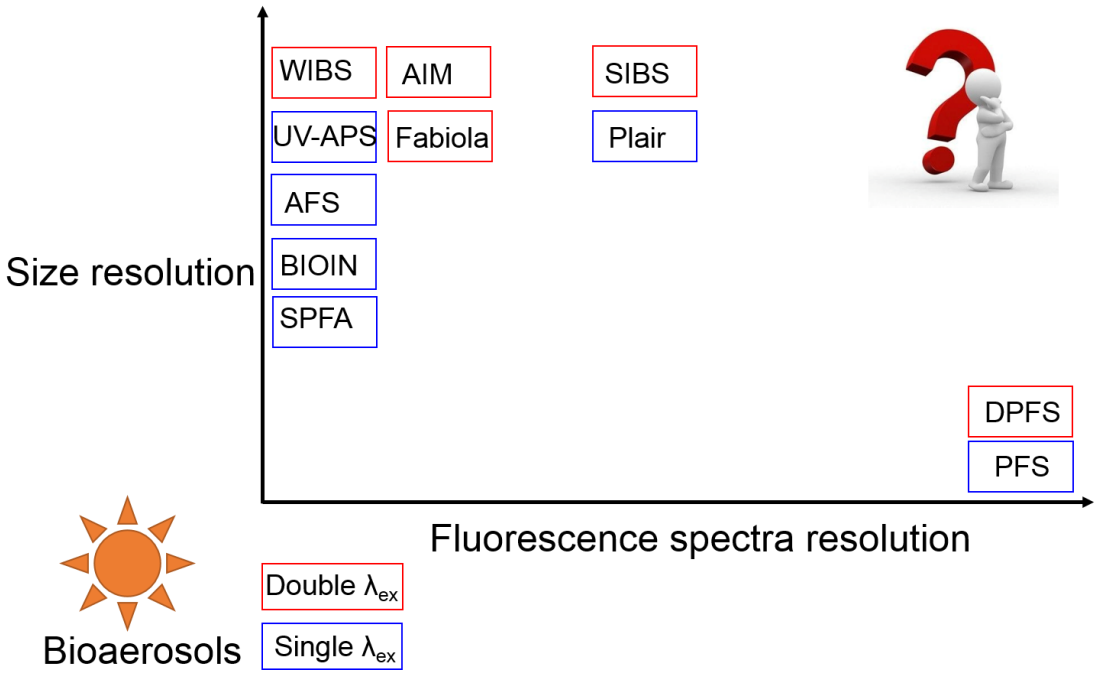

Figure 2. Laser/light-induced fluorescence (LIF) spectrometers for analysis of bioaerosols. Most of the commercial instruments can measure the fluorescence intensity and the size of the particle simultaneously, but the fluorescence spectra resolution is low. Particle-fluorescence spectrometer (PFS) and dual-wavelength particle-fluorescence spectrometer (DPFS) enable measurement of high-resolution fluorescence spectra, but the size information of the particle is of low resolution. This figure is adapted from (Pohlker et al., 2012).

1.3 Research objectives

The major objective of this PhD project is to develop an in situ LIF spectrometer to simultaneously measure high-resolution fluorescence spectra and aerodynamic diameters. Most of the commercial LIF instruments can measure the fluorescence intensity and the size of the particle simultaneously, but the fluorescence spectra resolution is low (Figure 2). Particle-fluorescence spectrometer (PFS) and dual-wavelength particle-fluorescence spectrometer (DPFS) enable measurement of high-resolution fluorescence spectra, but the size information of the particle is of low resolution (Figure 2). The new LIF spectrometer enables the simultaneous measurement of high-resolution fluorescence spectra and high-resolution aerodynamic diameters. After the development and evaluation of the new LIF spectrometer in the lab, the new LIF spectrometer is applied for atmospheric measurement.

The second objective is to develop a method to calibrate fluorescence intensity of online/in situ fluorescence spectrometers. Fluorescence intensity of LIF spectrometer is commonly applied as an arbitrary unit, which limits comparisons between different instruments. In order to facilitate comparisons, a standard fluorescence intensity calibration method is needed by using one single parameter.

The third objective is to measure the potential inference of fresh secondary organic aerosols (SOA) and aged SOA. Fresh biogenic secondary organic aerosols (SOA) and aged SOA are potentially interfering particles since they have been reported to exhibit fluorescence in the liquid phase. But the fluorescence property of fresh SOA and aged SOA in the *particle* phase has not been measured. The third objective of this PhD project is to quantify the potential inference of fresh secondary organic aerosols (SOA) and aged SOA.

2 Results and conclusions

2.1 Individual studies

2.1.1 Size-resolved single-particle fluorescence spectrometer for real-time analysis of bioaerosols: laboratory evaluation and atmospheric measurement

A size-resolved singe-aerosol fluorescence spectrometer (S2FS) to simultaneously measure fluorescence spectra and aerodynamic diameters was developed, tested in the lab, and applied for atmospheric measurement. The peak position and fluorescence index of biofluorophores measured by the S2FS were consistent with those measured by the offline spectrometer. Measurement of cellulose and chitin demonstrates that the S2FS is probably more sensitive than the FL3 channel of the WIBS, thus enabling the measurement of weakly fluorescent particles.

PAH exhibited fluorescence patterns overlapping with those of biofluorophores. PAH are normally coated on the surface of combustion-related particles, rather than exist as pure substances. The comparison between measured fluorescence spectra calculated fluorescence spectra support the mechanism that the fluorescence of PAH is quenched by particle bulk materials in the combustion-related particles. 355 nm is an effective excitation wavelength to distinguish bioaerosols from combustion-related aerosols.

Ambient measurement suggests that the fluorophore content and composition of bioaerosols are different for fine and coarse particles. The emission peak at ~440 nm was frequently observed for fluorescent fine particles (0.5-1.0 μm) and the peak at ~440 nm might be used as a tracer for bacterial endospores. During the thunderstorm, fluorescent coarse particles (> 1.0 μm) exhibited the emission peaking at 450 nm, which can probably be explained by phenolic compounds in the pollen fragments. In the early morning, fluorescent coarse particles (> 1.0 μm) exhibited the emission peaking at ~440 nm or 470 nm, which suggests the existence of agglomerated bacterial endospores and fungal spores, respectively.

2.1.2 Intensity calibration of an online/in situ fluorescence spectrometer (OFS) using the volume of single particles

Online/in situ fluorescence spectrometers (OFS) have been widely used to analyze bio-aerosols in real-time for atmospheric research. Fluorescence intensity of OFS is commonly applied as an arbitrary unit, which limits comparisons between different instruments. In order to facilitate comparisons, a standard fluorescence intensity calibration method is needed by using one parameter. Here the volume of the single particle has been used as the single parameter to calibrate the fluorescence intensity.

In the size range between 1 μm and 3 μm, the fluorescence intensity of NADH, cellulose, and chitin show power law based exponent of ~3, which suggests that the fluorescence intensity is proportional to the particle volume. Quinine in the core of the particle does not contribute the observed fluorescence, which might explain the lower value of quinine of 2.6. Riboflavin reveals a smaller exponent value of 1.2 suggesting that the fluorescence intensity of riboflavin increases with the diameter of the particle. Quenching of fluorescence or the cooperative effect of shielding of absorption and quenching of fluorescence could happen for riboflavin particles

Among the materials tested, nicotinamide adenine dinucleotide (NADH), cellulose, chitin, and quinine exhibit fluorescence scaling with the volume of the particle. After the fluorescence intensity is corrected by volume, the fluorescence spectra are nearly the same for particles with different sizes. This method implies that the fluorescence intensity can be compared and scaled between different OFS.

λ_{ex} and λ_{em} used in the S2FS (λ_{ex} = 355 nm, λ_{em} = 370-610 nm) were similar to those of the FL3 sensor used in the WIBS (λ_{ex} = 370 nm, λ_{em} = 420-650 nm), the Ultraviolet Aerodynamic Particle Sizer (UV-APS, λ_{ex} = 355 nm, λ_{em} = 420-575 nm), or the Plair detector (λ_{ex} = 337 nm, λ_{em} = 390-600 nm, so the above results might be applied to these instruments as well.

2.1.3 Fluorescence of fresh and aged biogenic secondary organic aerosols (SOA)

The fluorescence spectra of fresh SOA and aged SOA have been measured in the *particle* phase for the first time. Fresh SOA were generated by the reaction of limonene or α-pinene with ozone (O_3) while aged SOA were generated by the reaction of limonene or α-pinene with ozone (O_3) in the presence of ammonia. Preliminary results show that fresh SOA exhibit fluorescence from 400-500 nm with the emission peaking at ~467 nm or ~478 nm while aged SOA cover a broader range from 400-610 nm with the emission peaking at ~480 nm with λ_{ex} = 355 nm. The fractions of fluorescent fresh SOA and fluorescent aged SOA are 1-4% and 6-10%, respectively.

Relative humidity (RH) influences fluorescence of fresh SOA in the shorter wavelength while RH influences fluorescence aged SOA mainly in the longer wavelength. One possible mechanism to explain the RH effect is that the hydration state of particles is different under different RH. In order to test this mechanism, a Nafion dryer with a sheath flow of 5 LPM was used in front of the DMA. The fluorescence spectra of SOA particles with the Nafion dryer are nearly the same as those without the Nafion dryer, suggesting that the difference of fluorescence is not caused by the hydration state of particles. The other possible mechanism is that RH influenced the final chemical compounds. Although the molar fraction of chromophores induced by RH was small (2%), these products have a significant influence on the absorption property and the fluorescence property of aerosol particles.

The assignment of the fluorescence spectra to individual chemical compounds in mixtures of fresh SOA and aged SOA is based on the published literatures. The relatively weak fluorescence of fresh SOA could probably be explained by carbonyl while the chemical compounds of aged SOA are more complex. The nitrogen containing heterocycles including a coupled 2,5-dimethylpyrrole unit or a substituted dihydropyridine could possibly explain fluorescence of aged SOA.

2.2 Summary and outlook

In summary, a new in situ fluorescence spectrometer named as size-resolved single-particle fluorescence spectrometer (S2FS) was developed. With this new instrument, some new discoveries were made and can be summarized as follows:

(i) Fluorescence spectra for atmospheric aerosol particles below 1 μm have not been measured before, but these smaller particles have more adverse health effects since they can penetrate deeper into lungs. The fluorescence emission peak at ~440 nm for fluorescent fine particles (0.5-1 μm) was frequently observed, suggesting the occurrence of dipicolinic acid (DPA), which is a chemical compound composing a significant fraction of bacterial endospores and exists exclusively in bacterial endospores. Fluorescent coarse particles exhibited multiple fluorescence emission modes. During the thunderstorm, fluorescent coarse particles (> 1 μm) exhibited the peak emission at ~450 nm, which can probably be explained by phenolic compounds existing in pollen fragments. In the early morning, fluorescent coarse particles (> 1.0 μm) exhibited the emission peaking at ~440 nm or 470 nm, which suggests the existence of agglomerated bacterial endospores and fungal spores, respectively. These results demonstrate that the high-resolution fluorescence spectra are necessary since the peak positions are quite close for atmospheric aerosols.

(ii) NADH, cellulose, and chitin are good candidates for calibrating the fluorescence intensity of online/in situ fluorescence spectrometers (OFS). The volume calibrated fluorescence spectra of particles with different sizes are nearly the same. This means the volume calibrated spectra depend on the species of chemicals and settings of in situ fluorescence spectrometers, rather than on the size of the particle. The calibration factor of NADH, cellulose, and chitin should be the same and can be used for atmospheric measurement results as well.

(iii) Fresh SOA exhibit fluorescence from 400-500 nm with the emission peaking at ~467 nm or ~478 nm while aged SOA cover a broader range from 400-610 nm with the emission peaking at ~480 nm with λ_{ex} = 355 nm. The fluorescence of fresh SOA could possibly be explained by carbonyl while the florescence of aged SOA could be due to nitrogen containing heterocycles. These fluorescence spectra results suggest that fluorescent fine particles during atmospheric measurement in Mainz (Central Europe) are

not biogenic fresh SOA or biogenic aged SOA since the fluorescent fine particles have the emission peaking at ~440 nm or ~450 nm.

The above peak position assignment constrains the previous abundant biofluorophors to a few major biofluorophores. The assignment of peak positions to biofluorophores and PBAP is tentative and a long-term atmospheric measurement including nighttime observation will be conducted in the future to better probe the relationship between fluorescence spectra and the type of bioaerosols. Besides, the instrument can be further updated with better performance. The laser energy of this instrument is in the order of μJ to obtain the molecular fluorescence information (S2FS-version 1). When the laser is replaced with a new laser with the energy in the order of mJ, the elemental information can be obtained (S2FS-version 2). The particle will become fragments when the laser energy is in the order of mJ, and the fragments can be further analyzed by installing mass spectrometry behind the optics chamber (S2FS-version 3).

A References

Brodie, E. L., DeSantis, T. Z., Parker, J. P. M., Zubietta, I. X., Piceno, Y. M., and Andersen, G. L.: Urban aerosols harbor diverse and dynamic bacterial populations, P. Natl. Acad. Sci. USA, 104, 299-304, 10.1073/pnas.0608255104, 2007.

Cao, C., Jiang, W. J., Wang, B. Y., Fang, J. H., Lang, J. D., Tian, G., Jiang, J. K., and Zhu, T. F.: Inhalable Microorganisms in Beijing's PM2.5 and PM10 Pollutants during a Severe Smog Event, Environ. Sci. Technol., 48, 1499-1507, 10.1021/es4048472, 2014.

Christner, B. C., Morris, C. E., Foreman, C. M., Cai, R. M., and Sands, D. C.: Ubiquity of biological ice nucleators in snowfall, Science, 319, 1214-1214, 10.1126/science.1149757, 2008.

Crouzy, B., Stella, M., Konzelmann, T., Calpini, B., and Clot, B.: All-optical automatic pollen identification: Towards an operational system, Atmos. Environ., 140, 202-212, 10.1016/j.atmosenv.2016.05.062, 2016.

Despres, V. R., Huffman, J. A., Burrows, S. M., Hoose, C., Safatov, A. S., Buryak, G., Frohlich-Nowoisky, J., Elbert, W., Andreae, M. O., Poschl, U., and Jaenicke, R.: Primary biological aerosol particles in the atmosphere: a review, Tellus B, 64, ARTN 15598 10.3402/tellusb.v64i0.15598, 2012.

Frohlich-Nowoisky, J., Pickersgill, D. A., Despres, V. R., and Poschl, U.: High diversity of fungi in air particulate matter, P. Natl. Acad. Sci. USA, 106, 12814-12819, 10.1073/pnas.0811003106, 2009.

Frohlich-Nowoisky, J., Kampf, C. J., Weber, B., Huffman, J. A., Pohlker, C., Andreae, M. O., Lang-Yona, N., Burrows, S. M., Gunthe, S. S., Elbert, W., Su, H., Hoor, P., Thines, E., Hoffmann, T., Despres, V. R., and Poschl, U.: Bioaerosols in the Earth system: Climate, health, and ecosystem interactions, Atmos. Res., 182, 346-376, 10.1016/j.atmosres.2016.07.018, 2016.

Gabey, A. M., Gallagher, M. W., Whitehead, J., Dorsey, J. R., Kaye, P. H., and Stanley, W. R.: Measurements and comparison of primary biological aerosol above and below a tropical forest canopy using a dual channel fluorescence spectrometer, Atmos. Chem. Phys., 10, 4453-4466, 10.5194/acp-10-4453-2010, 2010.

Gabey, A. M., Stanley, W. R., Gallagher, M. W., and Kaye, P. H.: The fluorescence properties of aerosol larger than 0.8 mu m in urban and tropical rainforest locations, Atmos. Chem. Phys., 11, 5491-5504, 10.5194/acp-11-5491-2011, 2011.

Hallquist, M., Wenger, J. C., Baltensperger, U., Rudich, Y., Simpson, D., Claeys, M., Dommen, J., Donahue, N. M., George, C., Goldstein, A. H., Hamilton, J. F., Herrmann, H., Hoffmann, T., Iinuma, Y., Jang, M., Jenkin, M. E., Jimenez, J. L., Kiendler-Scharr, A., Maenhaut, W., McFiggans, G., Mentel, T. F., Monod, A., Prevot, A. S. H., Seinfeld, J. H., Surratt, J. D., Szmigielski, R., and Wildt, J.: The formation, properties and impact of secondary organic aerosol: current and emerging issues, Atmos. Chem. Phys., 9, 5155-5236, DOI 10.5194/acp-9-5155-2009, 2009.

Hawkins, L. N., and Russell, L.: Polysaccharides, Proteins, and Phytoplankton Fragments: Four Chemically Distinct Types of Marine Primary Organic Aerosol Classified by Single Particle Spectromicroscopy, Adv. Meteorol., Artn 612132 10.1155/2010/612132, 2010.

Healy, D. A., Huffman, J. A., O'Connor, D. J., Pohlker, C., Poschl, U., and Sodeau, J. R.: Ambient measurements of biological aerosol particles near Killarney, Ireland: a comparison between real-time fluorescence and microscopy techniques, Atmos. Chem. Phys., 14, 8055-8069, 10.5194/acp-14-8055-2014, 2014.

Hill, S. C., Williamson, C. C., Doughty, D. C., Pan, Y. L., Santarpia, J. L., and Hill, H. H.: Size-dependent fluorescence of bioaerosols: Mathematical model using fluorescing and absorbing molecules in bacteria, J. Quant. Spectrosc. Ra., 157, 54-70, 10.1016/j.jqsrt.2015.01.011, 2015.

Hoose, C., Kristjansson, J. E., and Burrows, S. M.: How important is biological ice nucleation in clouds on a global scale?, Environ. Res. Lett., 5, Artn 024009 10.1088/1748-9326/5/2/024009, 2010.

Huang, H. C., Pan, Y. L., Hill, S. C., Pinnick, R. G., and Chang, R. K.: Real-time measurement of dual-wavelength laser-induced fluorescence spectra of individual aerosol particles, Opt. Express, 16, 16523-16528, Doi 10.1364/Oe.16.016523, 2008.

Huffman, J. A., Treutlein, B., and Poschl, U.: Fluorescent biological aerosol particle concentrations and size distributions measured with an Ultraviolet Aerodynamic Particle Sizer (UV-APS) in Central Europe, Atmos. Chem. Phys., 10, 3215-3233, 2010.

Huffman, J. A., Sinha, B., Garland, R. M., Snee-Pollmann, A., Gunthe, S. S., Artaxo, P., Martin, S. T., Andreae, M. O., and Poschl, U.: Size distributions and temporal variations of biological aerosol particles in the Amazon rainforest characterized by microscopy and real-time UV-APS fluorescence techniques during AMAZE-08, Atmos. Chem. Phys., 12, 11997-12019, 10.5194/acp-12-11997-2012, 2012.

Hybl, J. D., Lithgow, G. A., and Buckley, S. G.: Laser-induced breakdown spectroscopy detection and classification of biological aerosols, Appl. Spectrosc., 57, 1207-1215, Doi 10.1366/000370203769699054, 2003.

Knopf, D. A., Alpert, P. A., Wang, B., and Aller, J. Y.: Stimulation of ice nucleation by marine diatoms, Nat. Geosci., 4, 88-90, 10.1038/Ngeo1037, 2011.

MatthiasMaser, S., and Jaenicke, R.: The size distribution of primary biological aerosol particles with radii >0.2 mu m in an urban rural influenced region, Atmos. Res., 39, 279-286, Doi 10.1016/0169-8095(95)00017-8, 1995.

Mohler, O., DeMott, P. J., Vali, G., and Levin, Z.: Microbiology and atmospheric processes: the role of biological particles in cloud physics, Biogeosciences, 4, 1059-1071, 2007.

Pan, Y. L., Hill, S. C., Santarpia, J. L., Brinkley, K., Sickler, T., Coleman, M., Williamson, C., Gurton, K., Felton, M., Pinnick, R. G., Baker, N., Eshbaugh, J., Hahn, J., Smith, E., Alvarez, B., Prugh, A., and Gardner, W.: Spectrally-resolved fluorescence cross sections of aerosolized biological live agents and simulants using five excitation wavelengths in a BSL-3 laboratory, Opt. Express, 22, 8165-8189, 10.1364/Oe.22.008165, 2014.

Perring, A. E., Schwarz, J. P., Baumgardner, D., Hernandez, M. T., Spracklen, D. V., Heald, C. L., Gao, R. S., Kok, G., McMeeking, G. R., McQuaid, J. B., and Fahey, D. W.: Airborne observations of regional variation in fluorescent aerosol across the United States, J. Geophys. Res-Atmos., 120, 1153-1170, 10.1002/2014jd022495, 2015.

Pinnick, R. G., Hill, S. C., Nachman, P., Videen, G., Chen, G., and Chang, R. K.: Aerosol fluorescence spectrum analyzer for rapid measurement of single micrometer-sized airborne biological particles, Aerosol Sci. Tech., 28, 95-104, Doi 10.1080/02786829808965514, 1998.

Pohlker, C., Huffman, J. A., and Poschl, U.: Autofluorescence of atmospheric bioaerosols - fluorescent biomolecules and potential interferences, Atmos. Meas. Tech., 5, 37-71, 10.5194/amt-5-37-2012, 2012.

Polichetti, G., Cocco, S., Spinali, A., Trimarco, V., and Nunziata, A.: Effects of particulate matter (PM10, PM2.5 and PM1) on the cardiovascular system, Toxicology, 261, 1-8, 10.1016/j.tox.2009.04.035, 2009.

Poschl, U., Martin, S. T., Sinha, B., Chen, Q., Gunthe, S. S., Huffman, J. A., Borrmann, S., Farmer, D. K., Garland, R. M., Helas, G., Jimenez, J. L., King, S. M., Manzi, A., Mikhailov, E., Pauliquevis, T., Petters, M. D., Prenni, A. J., Roldin, P., Rose, D., Schneider, J., Su, H., Zorn, S. R., Artaxo, P., and Andreae, M. O.: Rainforest Aerosols as Biogenic Nuclei of Clouds and Precipitation in the Amazon, Science, 329, 1513-1516, 10.1126/science.1191056, 2010.

Pratt, K. A., DeMott, P. J., French, J. R., Wang, Z., Westphal, D. L., Heymsfield, A. J., Twohy, C. H., Prenni, A. J., and Prather, K. A.: In situ detection of biological particles in cloud ice-crystals, Nat. Geosci., 2, 397-400, 10.1038/Ngeo521, 2009.

Prenni, A. J., Petters, M. D., Kreidenweis, S. M., Heald, C. L., Martin, S. T., Artaxo, P., Garland, R. M., Wollny, A. G., and Poschl, U.: Relative roles of biogenic emissions and Saharan dust as ice nuclei in the Amazon basin, Nat. Geosci., 2, 401-404, 10.1038/Ngeo517, 2009.

Schneider, J., Freutel, F., Zorn, S. R., Chen, Q., Farmer, D. K., Jimenez, J. L., Martin, S. T., Artaxo, P., Wiedensohler, A., and Borrmann, S.: Mass- spectrometric identification of primary biological particle markers and application to pristine submicron aerosol measurements in Amazonia, Atmos. Chem. Phys., 11, 11415-11429, 10.5194/acp-11-11415-2011, 2011.

Schumacher, C. J., Pohlker, C., Aalto, P., Hiltunen, V., Petaja, T., Kulmala, M., Poschl, U., and Huffman, J. A.: Seasonal cycles of fluorescent biological aerosol particles in boreal and semi-arid forests of Finland and Colorado, Atmos. Chem. Phys., 13, 11987-12001, 10.5194/acp-13-11987-2013, 2013.

Sowoidnich, K., and Kronfeldt, H. D.: Multispectral diode laser based shifted excitation Raman difference spectroscopy for biological sample identification, Advanced

Environmental, Chemical, and Biological Sensing Technologies Ix, 8366, Artn 836603 10.1117/12.918253, 2012.

Toprak, E., and Schnaiter, M.: Fluorescent biological aerosol particles measured with the Waveband Integrated Bioaerosol Sensor WIBS-4: laboratory tests combined with a one year field study, Atmos. Chem. Phys., 13, 225-243, 10.5194/acp-13-225-2013, 2013.

Wilson, T. W., Ladino, L. A., Alpert, P. A., Breckels, M. N., Brooks, I. M., Browse, J., Burrows, S. M., Carslaw, K. S., Huffman, J. A., Judd, C., Kilthau, W. P., Mason, R. H., McFiggans, G., Miller, L. A., Najera, J. J., Polishchuk, E., Rae, S., Schiller, C. L., Si, M., Temprado, J. V., Whale, T. F., Wong, J. P. S., Wurl, O., Yakobi-Hancock, J. D., Abbatt, J. P. D., Aller, J. Y., Bertram, A. K., Knopf, D. A., and Murray, B. J.: A marine biogenic source of atmospheric ice-nucleating particles, Nature, 525, 234-238, 10.1038/nature14986, 2015.

B Abbreviations

Short name	Description
a.u.	Arbitrary units
APS	Aerodynamic particle sizer
BSOA	Biogenic secondary organic aerosols
BVOC	Biogenic volatile organic compounds
CCN	Cloud condensation nuclei
D_a	Aerodynamic diameter
DMA	Differential Mobility Analyzer
DPA	Dipicolinic acid
DPFS	Dual-wavelength particle-fluorescence spectrometer
DSO	Digital storage oscilloscope
FAP	Fluorescent aerosol particles
FPSL	Fluorescent polystyrene latex
FWHM	Full width at half maximum
GCCN	Giant cloud condensation nuclei
ICCD	Intensified-charge-coupled device

IN	Ice nuclei
LIF	Laser/light-induced fluorescence
NAD^+	Oxidation form of nicotinamide adenine dinucleotide
NADH	Nicotinamide adenine dinucleotide
NADPH	Nicotinamide adenine dinucleotide phosphate
$N_{F,c}$	The number concentration of coarse fluorescent particles
$N_{F,f}$	The number concentration of fine fluorescent particles
$N_{T,c}$	The number concentration of total coarse particles
$N_{T,f}$	The number concentration of total fine particles
OFS	Online/in situ fluorescence spectrometers
OPS	Optical particle sizer
PAH	Polycyclic aromatic hydrocarbons
PBAP	Primary biological aerosol particles

PCR	Polymerase chain reaction
PFS	Particle-fluorescence spectrometer
PMT	Photo-multiplier tubes
RH	Relative humidity
S2FS	Size-resolved single-particle fluorescence spectrometer
SML	Surface microlayer
SOA	Secondary organic aerosols
TAP	Total aerosol particles
UV-APS	Ultraviolet Aerodynamic Particle Sizer
WIBS	Wideband Integrated Bioaerosol Sensor
λ_{ex}	Excitation wavelength
λ_{em}	Emission wavelength

C Personal list of publications

Journal articles

1. **M. Zhang**, T. Klimach, N. Ma, T. Könemann, C. Pöhlker, Z. Wang, N. Scheck, U. Kuhn, U. Pöschl, H. Su, Y. Cheng, Size-resolved Single-particle Fluorescence Spectrometer (S2FS) for real-time analysis of bioaerosols: Laboratory evaluation and atmospheric measurement, submitted, 2019.

2. **M. Zhang**, U. Pöschl, H. Su, Y. Cheng, Intensity calibration of an online/in situ fluorescence spectrometer (OFS) using the volume of single particles, to be submitted, 2019.

3. **M. Zhang**, U. Pöschl, H. Su, Y. Cheng, Fluorescence of fresh and aged biogenic secondary organic aerosols (SOA), in preparation, 2019.

4. X. Yu, Z. Wang, **M. Zhang**, U. Kuhn, Z. Xie, Y. Cheng, U. Pöschl, H. Su, Ambient measurement of fluorescent aerosol particles with a WIBS in the Yangtze River Delta of China: potential impacts of combustion-related aerosol particles, *Atmospheric Chemistry and Physics* 16 (17), 11337-11348, 2016

5. **M. Zhang**, X. Hou, J. Wang, Y. Tian, X. Fan, J. Zhai, L. Jiang, Light and pH cooperative nanofluidic diode using a spiropyran-functionalized single nanochannel, *Advanced Materials* 24 (18), 2424-2428, 2012

6. **M. Zhang**, Z. Meng, J Zhai, L. Jiang, Photo-induced current amplification in L-histidine modified nanochannels based on a highly charged photoacid in solution, *Chemical Communications* 49 (23), 2284-2286, 2013

7. J. Wang, **M. Zhang**, J. Zhai, L. Jiang, Theoretical simulation of the ion current rectification (ICR) in nano-pores based on the Poisson–Nernst–Planck (PNP) model, *Physical Chemistry Chemical Physics* 16 (1), 23-32, 2014

8. Y. Xu, **M. Zhang**, T. Tian, Y. Shang, Z. Meng, J. Jiang, J. Zhai, Y. Wang, Mimicking how plants control CO2 influx: CO2 activation of ion current rectification in nanochannels, *NPG Asia Materials* 7 (9), 215, 2015

9. Y. Kong, X. Fan, **M. Zhang**, X. Hou, Z. Liu, J. Zhai, L. Jiang, Nanofluidic diode based on branched alumina nanochannels with tunable ionic rectification, *ACS applied materials & interfaces* 5 (16), 7931-7936, 2013

10. Z. Meng, H. Bao, J. Wang, C Jiang, **M. Zhang**, J. Zhai, L. Jiang, Artificial Ion Channels Regulating Light-Induced Ionic Currents in Photoelectrical Conversion Systems, *Advanced Materials* 26 (15), 2329-2334, 2014

Poster presentations

1. **M. Zhang**, T. Klimach, N. Ma, Z. Wang, T. Könemann, C. Pöhlker, N. Scheck, U. Kuhn, U. Pöschl, H. Su, Y. Cheng, Size-resolved Single-particle Fluorescence Spectrometer (S2FS) for Real-time Measurements of Biological Aerosols and Non-biological Fluorescent Aerosols, *EGU General Assembly Conference Abstracts* 20, 14774, 2018

2. **M. Zhang**, T. Klimach, N. Ma, Z. Wang, T. Könemann, C. Pöhlker, N. Scheck, U. Kuhn, U. Pöschl, H. Su, Y. Cheng, Size-resolved Single-particle Fluorescence Spectrometer (S2FS) for measurement of biological aerosols, *AGU Fall Meeting*, 2018

D Individual studies

D.1 Zhang et al., submitted, 2019

Size-resolved single-particle fluorescence spectrometer (S2FS) for real-time analysis of bioaerosols: Laboratory evaluation and atmospheric measurement

Minghui Zhang,[†] Thomas Klimach,[†] Nan Ma,[§] Tobias Könemann,[†] Christopher Pöhlker,[†] Zhibin Wang,[¶,†] Uwe Kuhn,[†] Nelli Scheck,[‡] Ulrich Pöschl,[†] Hang Su,[*,§,†] and Yafang Cheng[*,†]

[†]Multiphase Chemistry Department, Max Planck Institute for Chemistry, 55128 Mainz, Germany

[‡]Particle Chemistry Department, Max Planck Institute for Chemistry, 55128 Mainz, Germany

[§]Center for Air pollution and Climate Change Research, Institute for Environmental and Climate Research (ECI), Jinan University, 511443 Guangzhou, China

[¶]Research Center for Air Pollution and Health, College of Environmental and Resource Sciences, Zhejiang University, 310058 Hangzhou, China

Size-resolved Single-particle Fluorescence Spectrometer (S2FS) for Real-time Analysis of Bioaerosols: Laboratory Evaluation and Atmospheric Measurement

Journal:	*Environmental Science & Technology*
Manuscript ID	Draft
Manuscript Type:	Article
Date Submitted by the Author:	n/a
Complete List of Authors:	Zhang, Minghui; Max Planck Institute for Chemistry, Multiphase Chemistry Department Klimach, Thomas; Max-Planck-Institut fur Chemie, Multiphase Chemistry Department Ma, Nan; Jinan University, Institute for Environmental and Climate Research (ECI) Könemann, Tobias; Max Planck Institute for Chemistry, Multiphase Chemistry Department Poehlker, Christopher; Max Planck Institute for Chemistry Wang, Zhibin; Zhejiang University, College of Environmental and Resource Sciences; Max Planck Institute for Chemistry Kuhn, Uwe; Max Planck Institute for Chemistry Scheck, Nelli; Max Planck Institute for Chemistry, Particle Chemistry Department Pöschl, Ulrich; Max Planck Institute for Chemistry, Multiphase Chemistry Department Su, Hang; Jinan University, Institute for Environmental and Climate Research (ECI); Max Planck Institute for Chemistry, Multiphase Chemistry Department Cheng, Yafang; Max Planck Institute for Chemistry, Multiphase Chemistry Department

Size-resolved Single-particle Fluorescence Spectrometer (S2FS) for Real-time Analysis of Bioaerosols: Laboratory Evaluation and Atmospheric Measurement

Minghui Zhang,[†] Thomas Klimach,[†] Nan Ma,[§] Tobias Könemann,[†] Christopher Pöhlker,[†] Zhibin Wang,[¶,†] Uwe Kuhn,[†] Nelli Scheck,[‡] Ulrich Pöschl,[†] Hang Su,[*,§,†] and Yafang Cheng[*,†]

[†]Multiphase Chemistry Department, Max Planck Institute for Chemistry, 55128 Mainz, Germany

[‡]Particle Chemistry Department, Max Planck Institute for Chemistry, 55128 Mainz, Germany

[§]Center for Air pollution and Climate Change Research, Institute for Environmental and Climate Research (ECI), Jinan University, 511443 Guangzhou, China

[¶]Research Center for Air Pollution and Health, College of Environmental and Resource Sciences, Zhejiang University, 310058 Hangzhou, China

ABSTRACT

Characteristic particle size, fluorescence intensity and fluorescence spectra are important features to detect and categorize bioaerosols. A prototype Size-resolved Single-particle Fluorescence Spectrometer (S2FS) was developed to simultaneously measure aerodynamic diameters and fluorescence spectra. The S2FS consists of an aerodynamic particle sizer and a fluorescence spectrometer with a 355-nm laser excitation source and an intensified charge-coupled device (ICCD) as detector. Emission spectra are dispersed in 512 channels from 370 to 610 nm, where a major portion of biological fluorescence emission occurs. Preliminary ambient measurement in Mainz (Germany, central Europe) show that an emission peak at ~440 nm was frequently observed for fluorescent fine particles (0.5-1 μm), suggesting the occurrence of dipicolinic acid (DPA), which constitutes a significant fraction of bacterial endospores and exists exclusively in bacterial endospores. Fluorescent fine particles accounted for 2.8% on average, based on the number fraction in the fine mode. Fluorescence coarse particles (> 1 μm) exhibited emission peaks at ~440 nm, ~450 nm, and ~470 nm, suggesting the existence of agglomerated bacterial endospores, pollen fragments, and fungal spores in the coarse mode. Fluorescent coarse particles accounted for 8.9% on average based on the number fraction, with strongest occurrence observed during a thunderstorm and in the morning.

1 INTRODUCTION

Primary biological aerosol particles (PBAP), also termed as bioaerosols, have important impact on human health[1] and may influence cloud formation and precipitation by acting as ice nuclei (IN)[2] or giant cloud condensation nuclei (GCCN)[3]. The approaches for analysis of PBAP fall into offline techniques[4, 5] and online (also termed as real-time or in situ) techniques[6, 7]. Offline techniques enable comprehensive analysis of PBAP, e.g., by gene sequencing PBAP can be

identified at the species level[8]. The disadvantage is that aerosol sampling and subsequent offline analysis require intensive laboratory work and have low time resolution (hours/days)[9]. High time resolution is required to understand its formation and transformation mechanisms. To analyze PBAP in real-time with high time resolution, laser/light-induced fluorescence (LIF) spectrometers[10-12] are commonly used based on the fluorescence of biofluorophores being excited at certain wavelengths[13, 14].

Several commercial LIF spectrometers have been developed and commonly used such as the Ultraviolet Aerodynamic Particle Sizer (UV-APS)[15-18] and the Wideband Integrated Bioaerosol Sensor (WIBS)[19-23]. These commercial instruments measure the fluorescence intensity by using photomultiplier tubes (PMT) as the sensor. In order to measure dispersed fluorescence spectra at different emission wavelengths, the number of channels of PMT has been extended from 1-channel to 8-channel[24], 16-channel[25, 26], or 32-channel[27-30]. Higher-resolution fluorescence spectra have been achieved in non-commercial applications, e.g., by Pinnick et al.[31], Saari et al.[32] and Pan et al.[33] using an intensified charge-coupled device (ICCD) with 1024 channels.

Apart from fluorescence properties, simultaneous measurement of particle size is also important. Firstly, some types of PBAP exhibit characteristic size distributions. For example, a characteristic peak at ~3 μm has been observed in many studies and probably can be explained by fungal spores[16, 34-36]. Secondly, the size information of a single particle is also a fundamental factor concerning health effects. Fine particles can penetrate deep into lungs, which may eventually lead to tissue damage and cardiovascular problems[37]. Thirdly, the fluorescence intensity scales with the size of particles[38, 39]. Fluorescence intensities are difficult to compare without accounting for the size of particles.

Either optical particle sizer (OPS) or aerodynamic particle sizer (APS) is commonly used for LIF spectrometers. The advantage of OPS is that it can measure particles up to 100 μm[30] while the APS measures particles limited below 20 μm[15-18]. The disadvantage of OPS is that the elastic scattering intensity is subject to non-unique and non-monotonic response function due to oscillations in the Lorenz-Mie response curves when the diameter of particles is in the same order as the incident light[40, 41]. In our case, APS[42] was used for measuring the size of the single particle with the advantage that the time-of-flight has a monotonic response to the diameter of particles (Figure S1).

Here we develop a size-resolved single-particle fluorescence spectrometer (S2FS), which enables measurement of the fluorescence spectra dispersed in 512 channels between 370 nm and 610 nm with excitation wavelength (λ_{ex}) at 355 nm. Moreover, it can simultaneously measure the aerodynamic diameters of aerosol particles from 0.5 μm to 20 μm (52 channels, logarithmic size scale).

2 MATERIALS AND METHODS

2.1 Technical Description of the S2FS.

The S2FS utilizes the optical chamber of a UV-APS[15-18] in which a red laser (λ = 655 nm) passes through a calcite beam splitter to produce two red laser beams (Figure 1a). On the one hand, the two red laser beams are used to measure aerodynamic diameters based on time-of-flight of single particles[42, 43]. The detectable size range of aerodynamic diameters is between 0.5 and 20 μm (Figure S1). On the other hand, the red lasers are used to trigger the 355-nm excitation laser, which is positioned slightly downstream of the second red laser beam. This UV laser is pulsed by a Nd:YAG crystal with a pulse energy between 17 and 20 μJ, which utilizes an actively Q-switched, high-repetition laser system (Explorer One XP, Spectra Physics, USA). The pulse

width (FWHM, full width at half maximum) of the UV laser is ~10 ns. After excitation, elliptical mirrors focus the fluorescence signal on a slit of a spectrograph. The slit width is 1 mm corresponding to a spectral resolution of ~15 nm[29]. A filter is placed in front of the slit to get rid of the residual UV light.

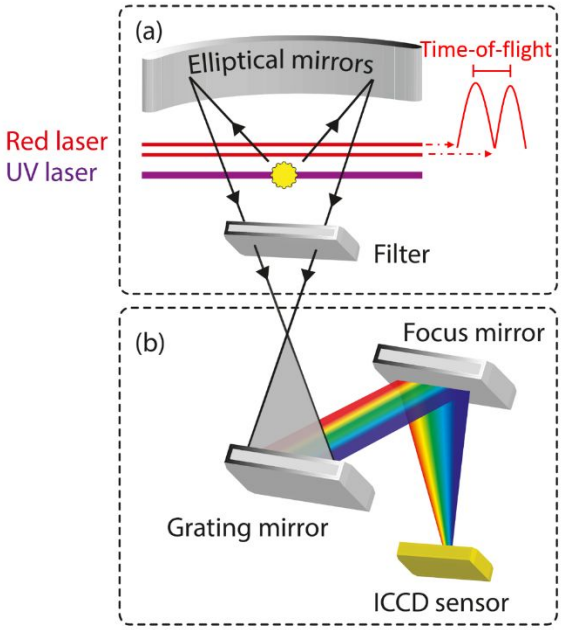

Figure 1. Construction of the size-resolved single-particle fluorescence spectrometer (S2FS), which consists of (**a**) an aerodynamic particle sizer and (**b**) a fluorescence spectrometer including a 355-nm excitation laser and an intensified charge-coupled device (ICCD) detector.

The fluorescence spectrometer consists of an optical fiber, a high performance imaging spectrograph, and an ICCD sensor (Figure 1b). The optical fiber has a numeric aperture of 0.5 with a diameter of 1 mm (Thorlabs GmbH, Germany). The spectrograph is an IsoPlane SCT-320 imaging spectrograph (Princeton Instruments, USA).

The detector is an efficient back-illuminated ICCD camera system (PI-MAX4: 512EMB-HBF, Princeton Instruments, USA). The ICCD gain was set to the maximum of 100 without suffering from saturation of the detector during laboratory and atmospheric measurement.

The ICCD, the UV laser and the digital storage oscilloscope (DSO) are synchronized to ensure that the fluorescence spectrum and the aerodynamic diameter for the same particle are measured (Figure S2).

2.2 Generation of Fluorescent Materials

Detailed information of tested materials in the lab can be found in Table S1. Ambient measurement was performed on the roof of the Max Planck Institute for Chemistry in the daytime from 31 May 2017 to 8 June 2017. The location is surrounded by a city in the north and east and a rural region in the south and west[34].

3 RESULTS AND DISCUSSION

3.1 Performance of the S2FS

In order to evaluate the performance of the S2FS, we used selected pure biofluorophores and pollen as sample aerosols. Figure 2 (solid lines) shows that the peaks of averaged spectra of nicotinamide adenine dinucleotide (NADH) and riboflavin by the S2FS were located at ~450 nm and ~562 nm, respectively. These results are consistent with those detected by the offline spectrometer (at ~452 nm and ~564 nm; dashed lines). Apart from the peak position, the fluorescence index (defined as the ratio of emission intensities at 450 nm and 500 nm following 355-nm excitation)[44] of NADH measured by the S2FS is 1.76, which is consistent with that of 1.77 measured by the offline spectrometer (Figure 2).

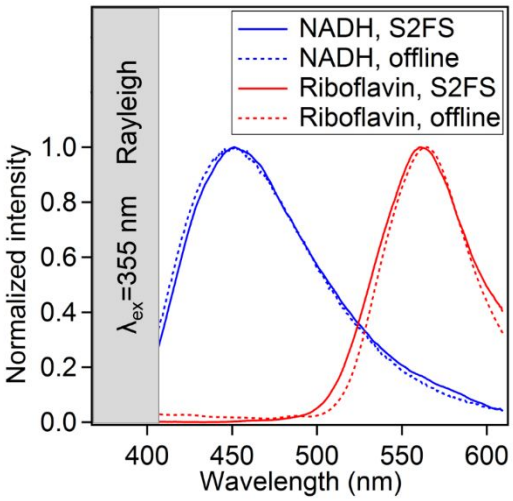

Figure 2. Normalized spectra of NADH and riboflavin by the S2FS compared to those by the offline spectrometer. The solid lines indicate the spectra by the S2FS, which were smoothed every 32 pixels and normalized to the maximum. The shaded area indicates the first order Rayleigh scattering of excitation light of the offline spectrometer.

Pollen revealed two fluorescence modes with λ_{ex} = 355 nm. *Ambrosia artemisiifolia*, *Sambucus nigra*, and *Urtica dioica* exhibited an emission peak at ~450 nm and *Artemisia vulgaris* exhibited an emission peak at ~460 nm (Figure S3a). *Betula pendula* exhibited an emission peak at ~480 nm and *Olea europaea* exhibited an emission peak at ~510 nm (Figure S3b). The pronounced peak at ~450 nm or ~460 nm is assigned to phenolic compounds in the cell wall while the peak at ~480 nm or ~510 nm probably can be explained by carotenoid pigments[45].

The sensitivity of different LIF spectrometers may vary between each other, thus influencing the quantification of concentration of PBAP in the atmospheric measurement[35]. The excitation (λ_{ex}) and emission (λ_{em}) wavelengths used in the S2FS (λ_{ex} = 355 nm, λ_{em} = 370-610 nm) are similar to those used in the FL3 channel of the WIBS (λ_{ex} = 370 nm, λ_{em} = 420-650 nm). In order to compare the sensitivity of the S2FS, we used relatively weak fluorescent materials such as

cellulose and chitin. By using the S2FS, the fluorescence counting efficiencies of cellulose and chitin particles with an aerodynamic diameter of 3 μm were 67% and 51%, respectively (Figure S4a). Savage et al.[20] reported that cellulose and chitin with an optical diameter of 3 μm emitted very weak fluorescence in the FL3 channel of the WIBS. According to our measurement with the WIBS, only 2% of cellulose and chitin particles with an optical diameter of 3 μm were above the background threshold in the FL3 channel of the WIBS (Figure S4b). These results demonstrate that the S2FS is probably more sensitive than the FL3 channel of the WIBS, thus enabling measurement of particles with very weak fluorescence signals. The possible reason is that the gain of the sensor was set to the maximum for the S2FS while the gain of the sensor was set with low values for the WIBS[35] or the UV-APS[16] in order to avoid saturation of the sensor or to reduce the possible interference of non-biological artifacts. During our measurement in the lab and in the ambient environment, saturation of the sensor was not observed; therefore, the gain of the sensor was set to the maximum for all of measurement.

Our measurement shows that fluorescence signals from a single particle are not strong enough to produce a complete spectrum dispersed in 512 channels (Figure S5). Here, we define N as the minimum number of particles needed to obtain the complete fluorescence spectrum (Figure S6a). N was determined to be between 100 and 3000 for test particles, which was proportional to the square root of the number of electrons detected by the ICCD sensor for a single particle (Figure S6b).

Although atmospheric aerosol particles are of heterogeneous compositions, ambient measurement[16, 34-36] suggests that one type of aerosols could probably dominate PBAP during a certain period. For example, fungal spores constitute the major part of PBAP in the morning[16, 34-

[36]. This lays the foundation for the fluorescence spectra process by averaging over multiple particles during a certain period in ambient measurement.

Highly fluorescent particles such as *Ambrosia artemisiifolia* pollen and *Olea europaea* pollen can be distinguished on a single particle level without averaging over multiple particles when the fluorescence spectrum is binned from 512 channels to 8 channels (Figure S7).

3.2 Potential Interfering Particles

PBAP often exhibit fluorescence[13], and that is why LIF spectrometers can be used to detect them. However, non-PBAP may also be fluorescent[46]. Polycyclic aromatic hydrocarbons (PAH) exhibited fluorescence in the overlapping region with that of biofluorophores (Figure 3a). PAH can often be found on the surface of combustion-related particles[47], rather than exist as pure substances.

Here we tested combustion-related particles including diesel soot and biomass burning particles. Diesel soot and biomass burning particles exhibited very weak fluorescence signals with λ_{ex} = 355 nm (Figure 3b) compared to pure PAH. Lamberg et al.[48] reported that total PAH accounted for ~2% of PM_1 (median value) while pyrene and fluoranthene accounted for ~40% (median value) of total PAH in typical small-scale combustion appliances. Robinson et al.[39] reported that the fluorescence intensity of particles scaled with the volume of the particle. Assuming that no quenching effect happened, the fluorescence intensity of biomass burning particles with an aerodynamic diameter of 3 μm was calculated as follows:

$$I_{\text{biomass of 3 μm}} = I_{\text{pyrene of 1 μm}} * (3/1)^3 * 2\% * 40\%$$

The calculated fluorescence intensity of biomass burning particles (Figure 3c) was higher than that measured by the S2FS (Figure 3b). Therefore, our calculation supports the mechanism previously proposed by Panne et al.[47] that the fluorescence of PAH is efficiently quenched by particle bulk materials.

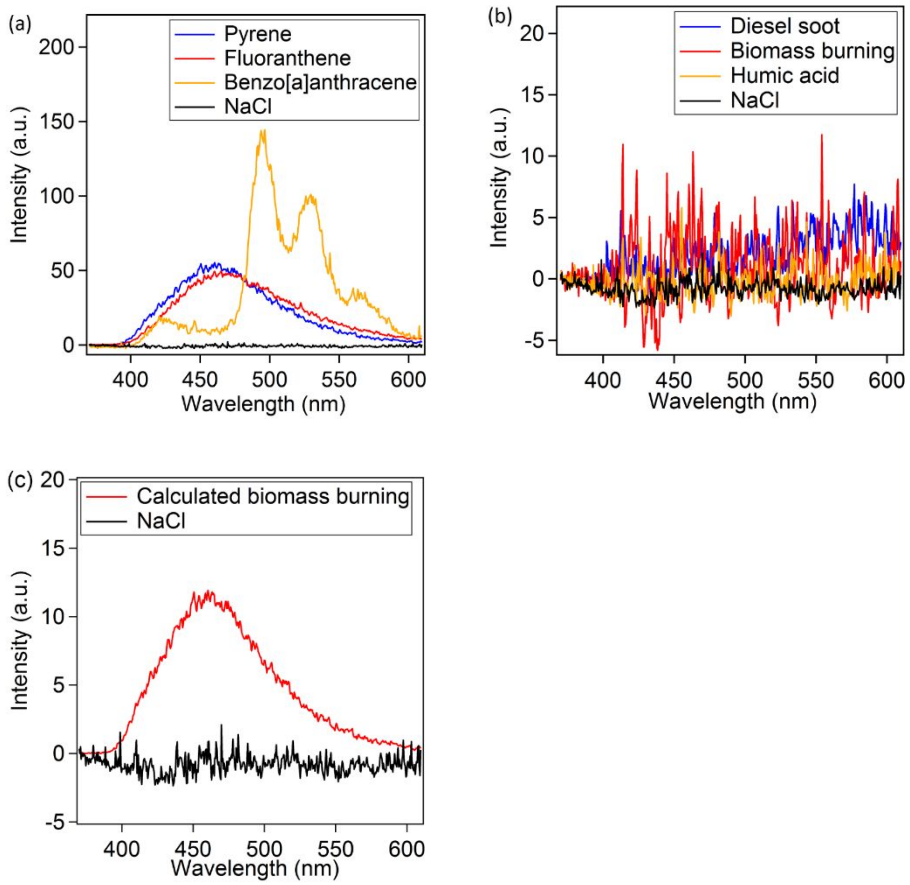

Figure 3. Fluorescence spectra for PAH and combustion-related particles. (**a**) Averaged S2FS spectra of PAH particles with an aerodynamic diameter of 1 μm. (**b**) Averaged S2FS spectra of combustion-related particles and humic acid particles with an aerodynamic diameter of 3 μm. (**c**) Calculated fluorescence spectra of biomass burning particles with an aerodynamic diameter of 3 μm assuming that no quenching effect happened.

When λ_{ex} was changed from 355 nm to 263 nm, Pan et al.[49] reported that combustion-related particles exhibited strong fluorescence in the same range as that of pollen[28] by normalizing the fluorescence intensity to the elastic scattering intensity of the particle. The strong fluorescence with λ_{ex} =263 nm was ascribed to the combinations of tyrosine-like, tryptophan-like, and humic-like substances[49].

The above results can better explain previous ambient measurement in the Yangtze River Delta of China by our group with the WIBS[46]. Type ABC particles (defined as particles that are simultaneously detected in channels FL1 λ_{ex} = 280 nm, λ_{em} = 310-400 nm, FL2 λ_{ex} = 280 nm, λ_{em} = 420-650 nm and FL3 λ_{ex} = 370 nm, λ_{em} = 420-650 nm) showed a good correlation with fractions of combustion-related particles[46]. The measurement by the S2FS shows that pure combustion-related particles exhibited very weak fluorescence with λ_{ex} = 355 nm (close to 370 nm used in FL3 of the WIBS). The above two observations suggest that type ABC particles measured by the WIBS are probably internally mixed particles of PBAP and combustion-related particles.

Apart from combustion-related particles, humic acid particles with an aerodynamic diameter of 3 μm also exhibited very weak fluorescence in the solid phase (Figure 3b) although the fluorescence intensity of humic acid was reported to be high in the liquid phase[18].

3.3 Ambient Atmospheric Application

Dispersed fluorescence spectra have been measured for atmospheric aerosol particles above 10 μm[30], 3 μm[50], or above 1 μm[29]. Meanwhile, fluorescence spectra for atmospheric aerosol particles below 1 μm have not been measured before, but these smaller particles have more adverse health effects since they can penetrate deeper into lungs[37]. A fluorescence emission peak

at ~440 nm for fluorescent fine particles (0.5-1 μm) was frequently observed on 31 May, 3 June, 4 June, and 5 June (Figure 4b, bottom panel). The emission peak at ~440 nm suggests the occurrence of dipicolinic acid (DPA), which is a chemical compound composing a significant fraction of bacterial endospores and existing exclusively in bacterial endospores[13, 51, 52]. This is supported by the offline measurement of DPA with an emission peak at ~440 nm (Figure S8). A fluorescence emission peak at ~450 nm for fluorescent fine particles was observed on 1 June and 2 June, which might be due to NAD(P)H or pteridine[13] in the bacteria. Fluorescent fine particles accounted for ~2.8% in the fine mode with an averaged concentration of ~0.035 cm^{-3} (Figure 4a, Table 1).

Fluorescent coarse particles exhibited multiple fluorescence emission modes. During a thunderstorm on 3 June, fluorescent coarse particles (> 1 μm) exhibited an emission peak at ~450 nm (Figure 4b, top panel), which can probably be explained by phenolic compounds[45] existing in pollen fragments. This is supported by frequently reported thunderstorm asthma events caused by pollen fragments[53]. In the morning of 5 June, fluorescent coarse particles exhibited an emission peak at ~440 nm, suggesting that these fluorescent coarse particles are probably agglomerated bacterial endospores[13, 51]. In the morning of 7 June, fluorescent coarse particles exhibited an emission peak at ~470 nm, which might be explained by ergosterol existing in fungal spores[13]. Fluorescent coarse particles accounted for ~8.9% in the coarse mode with an averaged concentration of ~0.031 cm^{-3} (Figure 4a, Table 1), which is in the same range as that measured by the UV-APS in Mainz[34].

The assignment of peak positions to biofluorophores and PBAP is tentative and a long-term atmospheric observation including nighttime observation will be performed in the future to better probe the relationship of fluorescence spectra and the type of PBAP.

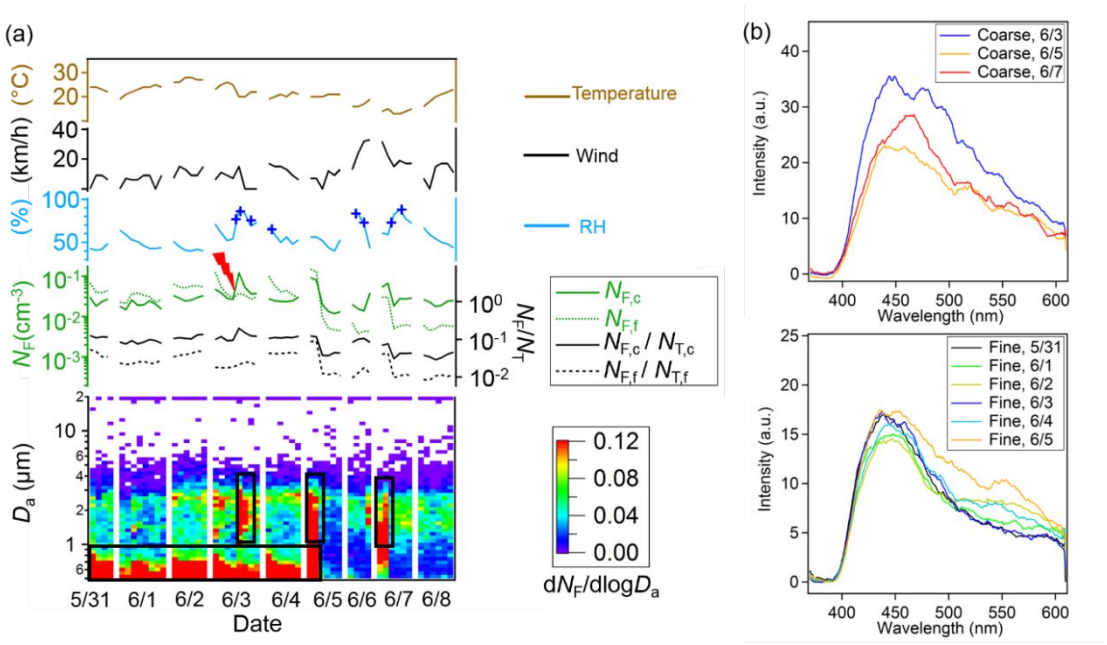

Figure 4. Fluorescence measurement data for atmospheric aerosol particles. (**a**) Time series of fluorescent aerosol particles (FAP) concentrations and corresponding meteorological conditions such as temperature, wind speed and relative humidity (RH). Middle panel left y-axis is integrated total FAP number (N_F) and middle panel right y-axis is number ratio of integrated FAP to total aerosol particles (TAP, N_T). The solid line indicates coarse particles and the dashed line indicates fine particles. Bottom panel is FAP number size distribution (dN_F/dlogD_a) for each 1-hour sampling time. The blue crosses represent rain events and the red scar represents the thunderstorm. The black rectangles represent the period of averaged particles. (**b**) Averaged fluorescence spectra of atmospheric fluorescent aerosol particles over a certain period in the coarse mode (top panel) and in the fine mode (bottom panel), which were smoothed over 32 pixels.

Table 1. Integrated number concentrations of coarse TAP, coarse FAP, fine TAP, and fine FAP measured by the S2FS from 31 May 2017 to 8 June 2017.

Number		**Values**
$N_{T,c}$ (cm^{-3})	Mean	0.38
	Median	0.28
$N_{F,c}$ (cm^{-3})	Mean	0.031
	Median	0.025
$N_{F,c}/N_{T,c}$ (%)	Mean	8.88
	Median	9.62
$N_{T,f}$ (cm^{-3})	Mean	1.16
	Median	0.98
$N_{F,f}$ (cm^{-3})	Mean	0.035
	Median	0.031
$N_{F,f}/N_{T,f}$ (%)	Mean	2.76
	Median	2.29

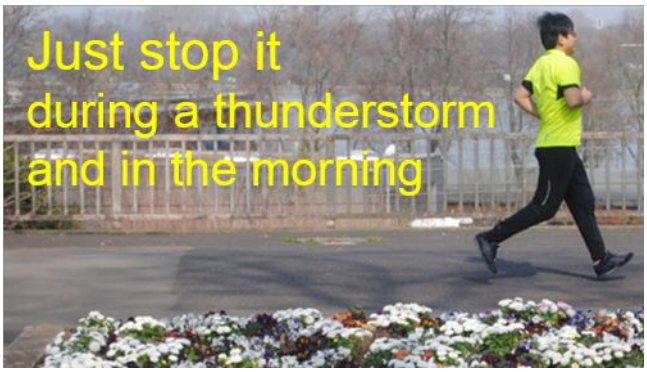

Table of content (**TOC**).

ASSOCIATED CONTENT

Supporting Information

The supporting information is available free of charge on the website. Additional information about technical details and particular topics (PDF).

AUTHOR INFORMATION

Corresponding Author

*H. Su, Phone: +49 (0) 61313057300; e-mail: h.su@mpic.de

*Y. Cheng, Phone: +49 (0) 61313057200; e-mail: yafang.cheng@mpic.de

Notes

The authors declare no competing financial interest.

ACKNOWLEDGMENTS

We acknowledge the National Natural Science Foundation of China (91644218), EU-BACCHUS project (No. 603445), and Guangdong Innovative and Entrepreneurial Research Team Program (2016ZT06N263). J. Schneider is acknowledged for his kind help with UV-APS. M. Zhang would like to thank China Scholarship Council (CSC). This work is supported by the Max Planck Society (MPG).

ABBREVIATIONS

a.u.	Arbitrary units
APS	Aerodynamic particle sizer
D_a	Aerodynamic diameter
DPA	Dipicolinic acid
DSO	Digital storage oscilloscope
FAP	Fluorescent aerosol particles
GCCN	Giant cloud condensation nuclei
FWHM	Full width at half maximum
ICCD	Intensified-charge-coupled device
IN	Ice nuclei
LIF	Laser/light-induced fluorescence

NADH	Nicotinamide adenine dinucleotide
NADPH	Nicotinamide adenine dinucleotide phosphate
$N_{F,c}$	The number concentration of coarse fluorescent particles
$N_{F,f}$	The number concentration of fine fluorescent particles
$N_{T,c}$	The number concentration of total coarse particles
$N_{T,f}$	The number concentration of total fine particles
OPS	Optical particle sizer
PAH	Polycyclic aromatic hydrocarbons
PBAP	Primary biological aerosol particles
PMT	Photo-multiplier tubes
RH	Relative humidity
S2FS	Size-resolved single-particle fluorescence spectrometer

TAP	Total aerosol particles
UV-APS	Ultraviolet Aerodynamic Particle Sizer
WIBS	Wideband Integrated Bioaerosol Sensor
λ_{ex}	Excitation wavelength
λ_{em}	Emission wavelength

REFERENCES

1. Lacey, J.; Dutkiewicz, J., Bioaerosols and Occupational Lung-Disease. *J. Aerosol Sci.* **1994,** *25*, (8), 1371-1404.
2. Poschl, U.; Martin, S. T.; Sinha, B.; Chen, Q.; Gunthe, S. S.; Huffman, J. A.; Borrmann, S.; Farmer, D. K.; Garland, R. M.; Helas, G.; Jimenez, J. L.; King, S. M.; Manzi, A.; Mikhailov, E.; Pauliquevis, T.; Petters, M. D.; Prenni, A. J.; Roldin, P.; Rose, D.; Schneider, J.; Su, H.; Zorn, S. R.; Artaxo, P.; Andreae, M. O., Rainforest Aerosols as Biogenic Nuclei of Clouds and Precipitation in the Amazon. *Science* **2010,** *329*, (5998), 1513-1516.
3. Mohler, O.; DeMott, P. J.; Vali, G.; Levin, Z., Microbiology and atmospheric processes: the role of biological particles in cloud physics. *Biogeosciences* **2007,** *4*, (6), 1059-1071.
4. Jaenicke, R., Abundance of cellular material and proteins in the atmosphere. *Science* **2005,** *308*, (5718), 73-73.
5. Du, P. R.; Du, R.; Ren, W. S.; Lu, Z. D.; Fu, P. Q., Seasonal variation characteristic of inhalable microbial communities in PM2.5 in Beijing city, China. *Sci. Total Environ.* **2018,** *610*, 308-315.
6. Konemann, T.; Savage, N. J.; Huffman, J. A.; Pohlker, C., Characterization of steady-state fluorescence properties of polystyrene latex spheres using off- and online spectroscopic methods. *Atmos. Meas. Tech.* **2018,** *11*, (7), 3987-4003.
7. Xu, Z. Q.; Wu, Y.; Shen, F. X.; Chen, Q.; Tan, M. M.; Yao, M. S., Bioaerosol Science, Technology, and Engineering: Past, Present, and Future. *Aerosol Sci. Tech.* **2011,** *45*, (11), 1337-1349.
8. Cao, C.; Jiang, W. J.; Wang, B. Y.; Fang, J. H.; Lang, J. D.; Tian, G.; Jiang, J. K.; Zhu, T. F., Inhalable Microorganisms in Beijing's PM2.5 and PM10 Pollutants during a Severe Smog Event. *Environ. Sci. Technol.* **2014,** *48*, (3), 1499-1507.
9. Frohlich-Nowoisky, J.; Pickersgill, D. A.; Despres, V. R.; Poschl, U., High diversity of fungi in air particulate matter. *P. Natl. Acad. Sci. USA* **2009,** *106*, (31), 12814-12819.

10. Hill, S. C.; Pinnick, R. G.; Niles, S.; Pan, Y. L.; Holler, S.; Chang, R. K.; Bottiger, J.; Chen, B. T.; Orr, C. S.; Feather, G., Real-time measurement of fluorescence spectra from single airborne biological particles. *Field Anal. Chem. Tech.* **1999,** *3*, (4-5), 221-239.
11. Sivaprakasam, V.; Huston, A. L.; Scotto, C.; Eversole, J. D., Multiple UV wavelength excitation and fluorescence of bioaerosols. *Opt. Express* **2004,** *12*, (19), 4457-4466.
12. Taketani, F.; Kanaya, Y.; Nakamura, T.; Koizumi, K.; Moteki, N.; Takegawa, N., Measurement of fluorescence spectra from atmospheric single submicron particle using laser-induced fluorescence technique. *J. Aerosol. Sci.* **2013,** *58*, 1-8.
13. Pohlker, C.; Huffman, J. A.; Poschl, U., Autofluorescence of atmospheric bioaerosols - fluorescent biomolecules and potential interferences. *Atmos. Meas. Tech.* **2012,** *5*, (1), 37-71.
14. Ma, Z. M.; Liu, C.; Niu, N.; Chen, Z. J.; Li, S. J.; Liu, S. X.; Li, J., Seeking Brightness from Nature: J-Aggregation-Induced Emission in Cellulolytic Enzyme Lignin Nanoparticles. *Acs Sustain. Chem. Eng.* **2018,** *6*, (3), 3169-3175.
15. Hairston, P. P.; Ho, J.; Quant, F. R., Design of an instrument for real-time detection of bioaerosols using simultaneous measurement of particle aerodynamic size and intrinsic fluorescence. *J. Aerosol Sci.* **1997,** *28*, (3), 471-82.
16. Huffman, J. A.; Sinha, B.; Garland, R. M.; Snee-Pollmann, A.; Gunthe, S. S.; Artaxo, P.; Martin, S. T.; Andreae, M. O.; Poschl, U., Size distributions and temporal variations of biological aerosol particles in the Amazon rainforest characterized by microscopy and real-time UV-APS fluorescence techniques during AMAZE-08. *Atmos. Chem. Phys.* **2012,** *12*, (24), 11997-12019.
17. Agranovski, V.; Ristovski, Z.; Hargreaves, M.; Blackall, P. J.; Morawska, L., Real-time measurement of bacterial aerosols with the UVAPS: performance evaluation. *J. Aerosol Sci.* **2003,** *34*, (3), 301-317.
18. Brosseau, L. M.; Vesley, D.; Rice, N.; Goodell, K.; Nellis, M.; Hairston, P., Differences in detected fluorescence among several bacterial species measured with a direct-reading particle sizer and fluorescence detector. *Aerosol Sci. Tech.* **2000,** *32*, (6), 545-558.
19. Kaye, P. H.; Stanley, W. R.; Hirst, E.; Foot, E. V.; Baxter, K. L.; Barrington, S. J., Single particle multichannel bio-aerosol fluorescence sensor. *Opt. Express* **2005,** *13*, (10), 3583-3593.
20. Savage, N. J.; Krentz, C. E.; Konemann, T.; Han, T. T.; Mainelis, G.; Pohlker, C.; Huffman, J. A., Systematic characterization and fluorescence threshold strategies for the wideband integrated bioaerosol sensor (WIBS) using size-resolved biological and interfering particles. *Atmos. Meas. Tech.* **2017,** *10*, (11), 4279-4302.
21. Toprak, E.; Schnaiter, M., Fluorescent biological aerosol particles measured with the Waveband Integrated Bioaerosol Sensor WIBS-4: laboratory tests combined with a one year field study. *Atmos. Chem. Phys.* **2013,** *13*, (1), 225-243.
22. Crawford, I.; Gallagher, M. W.; Bower, K. N.; Choularton, T. W.; Flynn, M. J.; Ruske, S.; Listowski, C.; Brough, N.; Lachlan-Cope, T.; Fleming, Z. L.; Foot, V. E.; Stanley, W. R., Real-time detection of airborne fluorescent bioparticles in Antarctica. *Atmos. Chem. Phys.* **2017,** *17*, (23), 14291-14307.
23. O'Connor, D. J.; Healy, D. A.; Hellebust, S.; Buters, J. T. M.; Sodeau, J. R., Using the WIBS-4 (Waveband Integrated Bioaerosol Sensor) Technique for the On-Line Detection of Pollen Grains. *Aerosol Sci. Tech.* **2014,** *48*, (4), 341-349.
24. Ruske, S.; Topping, D. O.; Foot, V. E.; Kaye, P. H.; Stanley, W. R.; Crawford, I.; Morse, A. P.; Gallagher, M. W., Evaluation of machine learning algorithms for classification of primary biological aerosol using a new UV-LIF spectrometer. *Atmos. Meas. Tech.* **2017,** *10*, (2), 695-708.

25. Wilson, G. A.; DeFreez, R. K., Multispectral diode laser induced fluorescence biological particle sensor. *Optically Based Biological and Chemical Sensing for Defence* **2004,** *5617*, 46-52.
26. Konemann, T.; Savage, N.; Klimach, T.; Walter, D.; Frohlich-Nowoisky, J.; Su, H.; Poschl, U.; Huffman, J. A.; Pohlker, C., Spectral Intensity Bioaerosol Sensor (SIBS): an instrument for spectrally resolved fluorescence detection of single particles in real time. *Atmos. Meas. Tech.* **2019,** *12*, (2), 1337-1363.
27. Pan, Y. L.; Cobler, P.; Rhodes, S.; Potter, A.; Chou, T.; Holler, S.; Chang, R. K.; Pinnick, R. G.; Wolf, J. P., High-speed, high-sensitivity aerosol fluorescence spectrum detection using a 32-anode photomultiplier tube detector. *Rev. Sci. Instrum.* **2001,** *72*, (3), 1831-1836.
28. Pan, Y. L.; Hill, S. C.; Pinnick, R. G.; House, J. M.; Flagan, R. C.; Chang, R. K., Dual-excitation-wavelength fluorescence spectra and elastic scattering for differentiation of single airborne pollen and fungal particles. *Atmos. Environ.* **2011,** *45*, (8), 1555-1563.
29. Pan, Y. L.; Pinnick, R. G.; Hill, S. C.; Chang, R. K., Particle-Fluorescence Spectrometer for Real-Time Single-Particle Measurements of Atmospheric Organic Carbon and Biological Aerosol. *Environ. Sci. Technol.* **2009,** *43*, (2), 429-434.
30. Crouzy, B.; Stella, M.; Konzelmann, T.; Calpini, B.; Clot, B., All-optical automatic pollen identification: Towards an operational system. *Atmos. Environ.* **2016,** *140*, 202-212.
31. Pinnick, R. G.; Hill, S. C.; Nachman, P.; Videen, G.; Chen, G.; Chang, R. K., Aerosol fluorescence spectrum analyzer for rapid measurement of single micrometer-sized airborne biological particles. *Aerosol Sci. Tech.* **1998,** *28*, (2), 95-104.
32. Saari, S. E.; Putkiranta, M. J.; Keskinen, J., Fluorescence spectroscopy of atmospherically relevant bacterial and fungal spores and potential interferences. *Atmos. Environ.* **2013,** *71*, 202-209.
33. Pan, Y. L.; Hill, S. C.; Santarpia, J. L.; Brinkley, K.; Sickler, T.; Coleman, M.; Williamson, C.; Gurton, K.; Felton, M.; Pinnick, R. G.; Baker, N.; Eshbaugh, J.; Hahn, J.; Smith, E.; Alvarez, B.; Prugh, A.; Gardner, W., Spectrally-resolved fluorescence cross sections of aerosolized biological live agents and simulants using five excitation wavelengths in a BSL-3 laboratory. *Opt. Express* **2014,** *22*, (7), 8165-8189.
34. Huffman, J. A.; Treutlein, B.; Poschl, U., Fluorescent biological aerosol particle concentrations and size distributions measured with an Ultraviolet Aerodynamic Particle Sizer (UV-APS) in Central Europe. *Atmos. Chem. Phys.* **2010,** *10*, (7), 3215-3233.
35. Healy, D. A.; Huffman, J. A.; O'Connor, D. J.; Pohlker, C.; Poschl, U.; Sodeau, J. R., Ambient measurements of biological aerosol particles near Killarney, Ireland: a comparison between real-time fluorescence and microscopy techniques. *Atmos. Chem. Phys.* **2014,** *14*, (15), 8055-8069.
36. Schumacher, C. J.; Pohlker, C.; Aalto, P.; Hiltunen, V.; Petaja, T.; Kulmala, M.; Poschl, U.; Huffman, J. A., Seasonal cycles of fluorescent biological aerosol particles in boreal and semi-arid forests of Finland and Colorado. *Atmos. Chem. Phys.* **2013,** *13*, (23), 11987-12001.
37. Polichetti, G.; Cocco, S.; Spinali, A.; Trimarco, V.; Nunziata, A., Effects of particulate matter (PM10, PM2.5 and PM1) on the cardiovascular system. *Toxicology* **2009,** *261*, 1-8.
38. Hill, S. C.; Williamson, C. C.; Doughty, D. C.; Pan, Y. L.; Santarpia, J. L.; Hill, H. H., Size-dependent fluorescence of bioaerosols: Mathematical model using fluorescing and absorbing molecules in bacteria. *J. Quant. Spectrosc. Ra.* **2015,** *157*, 54-70.

39. Robinson, E. S.; Gao, R. S.; Schwarz, J. P.; Fahey, D. W.; Perring, A. E., Fluorescence calibration method for single-particle aerosol fluorescence instruments. *Atmos. Meas. Tech.* **2017,** *10*, (5), 1755-1768.
40. Picard, R. H., Absorption and Scattering of Light by Small Particles - Bohren,C, Huffman,D. *Opt. Eng.* **1984,** *23*, (2), 48-48.
41. Salt, K.; Noble, C. A.; Prather, K. A., Aerodynamic particle sizing versus light scattering intensity measurement as methods for real time particle sizing coupled with time-of-flight mass spectrometry. *Anal. Chem.* **1996,** *68*, (1), 230-234.
42. Wilson, J. C.; Liu, B. Y. H., Aerodynamic Particle-Size Measurement by Laser-Doppler Velocimetry. *J. Aerosol Sci.* **1980,** *11*, (2), 139-150.
43. Volckens, J.; Peters, T. M., Counting and particle transmission efficiency of the aerodynamic particle sizer. *J. Aerosol Sci.* **2005,** *36*, (12), 1400-1408.
44. Lee, H. J.; Laskin, A.; Laskin, J.; Nizkorodov, S. A., Excitation-Emission Spectra and Fluorescence Quantum Yields for Fresh and Aged Biogenic Secondary Organic Aerosols. *Environ. Sci. Technol.* **2013,** *47*, (11), 5763-5770.
45. Pohlker, C.; Huffman, J. A.; Forster, J. D.; Poschl, U., Autofluorescence of atmospheric bioaerosols: spectral fingerprints and taxonomic trends of pollen. *Atmos. Meas. Tech.* **2013,** *6*, (12), 3369-3392.
46. Yu, X. W.; Wang, Z. B.; Zhang, M. H.; Kuhn, U.; Xie, Z. Q.; Cheng, Y. F.; Poschl, U.; Su, H., Ambient measurement of fluorescent aerosol particles with a WIBS in the Yangtze River Delta of China: potential impacts of combustion-related aerosol particles. *Atmos. Chem. Phys.* **2016,** *16*, (17), 11337-11348.
47. Panne, U.; Knoller, A.; Kotzick, R.; Niessner, R., On-line and in-situ detection of polycyclic aromatic hydrocarbons (PAH) on aerosols via thermodesorption and laser-induced fluorescence spectroscopy. *Fresen J. Anal. Chem.* **2000,** *366*, (4), 408-414.
48. Lamberg, H.; Nuutinen, K.; Tissari, J.; Ruusunen, J.; Yli-Pirila, P.; Sippula, O.; Tapanainen, M.; Jalava, P.; Makkonen, U.; Teinila, K.; Saarnio, K.; Hillamo, R.; Hirvonen, M. R.; Jokiniemi, J., Physicochemical characterization of fine particles from small-scale wood combustion. *Atmos. Environ.* **2011,** *45*, (40), 7635-7643.
49. Pan, Y. L.; Houck, J. D. T.; Clark, P. A.; Pinnick, R. G., Single particle size and fluorescence spectra from emissions of burning materials in a tube furnace to simulate burn pits. *Appl. Phys. B-Lasers O* **2013,** *112*, (1), 89-98.
50. Pinnick, R. G.; Hill, S. C.; Pan, Y. L.; Chang, R. K., Fluorescence spectra of atmospheric aerosol at Adelphi, Maryland, USA: measurement and classification of single particles containing organic carbon. *Atmos. Environ.* **2004,** *38*, (11), 1657-1672.
51. Alimova, A.; Katz, A.; Savage, H. E.; Shah, M.; Minko, G.; Will, D. V.; Rosen, R. B.; McCormick, S. A.; Alfano, R. R., Native fluorescence and excitation spectroscopic changes in Bacillus subtilis and Staphylococcus aureus bacteria subjected to conditions of starvation. *Appl. Optics* **2003,** *42*, (19), 4080-4087.
52. Slieman, T. A.; Nicholson, W. L., Role of dipicolinic acid in survival of Bacillus subtilis spores exposed to artificial and solar UV radiation. *Appl. Environ. Microb.* **2001,** *67*, (3), 1274-1279.
53. Kornei, K., METEOROLOGY Australian state forecasts deadly thunderstorm asthma. *Science* **2018,** *359*, (6374), 380-380.

Supporting Information for

Size-resolved Single-particle Fluorescence Spectrometer (S2FS) for Real-time Analysis of Bioaerosols: Laboratory Evaluation and Atmospheric Measurement

Minghui Zhang,[†] Thomas Klimach,[†] Nan Ma,[§] Tobias Könemann,[†] Christopher Pöhlker,[†] Zhibin Wang,[¶,†] Uwe Kuhn,[†] Nelli Scheck,[‡] Ulrich Pöschl,[†] Hang Su,[*,§,†] and Yafang Cheng[*,†]

[†]Multiphase Chemistry Department, Max Planck Institute for Chemistry, 55128 Mainz, Germany

[‡]Particle Chemistry Department, Max Planck Institute for Chemistry, 55128 Mainz, Germany

[§]Center for Air pollution and Climate Change Research, Institute for Environmental and Climate Research (ECI), Jinan University, 511443 Guangzhou, China

[¶]Research Center for Air Pollution and Health, College of Environmental and Resource Sciences, Zhejiang University, 310058 Hangzhou, China

Corresponding Author

[*]H. Su, Phone: +49 (0) 61313057300; e-mail: h.su@mpic.de

[*]Y. Cheng, Phone: +49 (0) 61313057200; e-mail: yafang.cheng@mpic.de

Supporting Information includes 29 pages, 19 figures, and 2 tables.

Relationship between the aerodynamic diameter and the time-of-flight

The detectable size range of aerodynamic diameters is between 0.5 and 20 µm and the corresponding time-of-flight of the particle is between 0.7 µs and 3.7 µs.

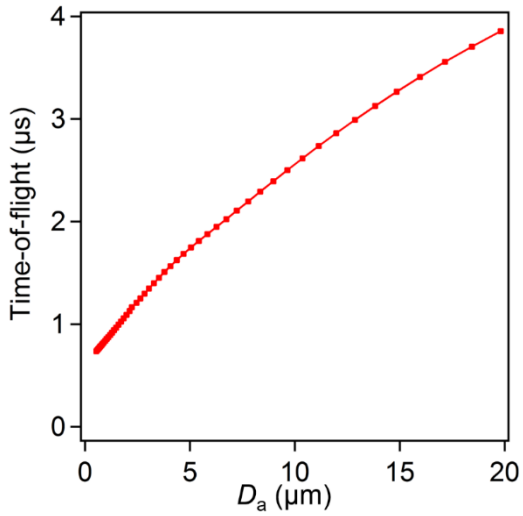

Figure S1. Dependence of the time-of-flight on the aerodynamic diameter. Note that each APS device has an individual relationship[1].

Technical description of the spectrograph

The size of the sensor was chosen to be 8 mm, and then the optics of the spectrometer was designed around the detector[2]: The focal length is 320 mm, and the groove density of the grating is150 gr mm^{-1}, which means the groove spacing of the grating is 6.6 * 10^3 nm. The grating is a ruled diffraction grating with 500 nm blaze wavelength.

The diffraction grating equation is the following[2]:

$$\sin \alpha + \sin \beta_m = -m\lambda/d$$

where α, angle of incidence; β_m, angle of diffraction; m, order of diffraction; λ, wavelength; d is the groove spacing of the grating. Therefore, different λ have different β_m, which correspond to different locations of the detector.

The spectral range is 240 nm in our case, which is dependent on groove density (groove spacing) of the grating[2]. For our application, the range was set between 370 nm and 610 nm, which represents a spectral hot spot where a major portion of biological fluorescence emission occurs[3].

The wavelength of the spectrometer was calibrated by the IntellCal spectral calibration system with a Hg/Ne atomic emission light source.

Technical description of ICCD sensor

The ICCD has a data-transfer rate of a few milliseconds, resulting in a data-transfer rate of ~300 Hz. If two aerosol particles pass by the UV laser at the time interval shorter than 0.33 milliseconds, the second aerosol particle can not be recorded by the ICCD. The particle will be detected by the red laser but the fluorescence measurement will not be recorded. This problem does not influence the calculation of the fraction of fluorescent aerosol particles (FAP), but influences the concentration of FAP. In order to overcome this problem, the concentration of FAP was corrected by multiplying with the ratio of total to measured particles (also termed as the correction factor) in each size bin, as already used by the WIBS[4-6].

The analog-to-digital unit (the conversion factor from electrons into digital counts) of the microchannel plate (MCP) gain per electron was 909 when the ICCD gain was set to be 100. Therefore, the number of electrons was calculated as dividing the sum fluorescence intensity by 909. The number of photons emitted by the particles is 4 to 16 times higher than the number of electrons detected by the detector by taking the efficiency of the elliptical mirrors, optical fiber, spectrograph, and the ICCD sensor into account.

Background noise consists of the ICCD noise (read noise, Poisson noise, and fixed-pattern noise)[7] and the inherent signal from the optical chamber[6]. Here the ICCD noise was determined by measuring the signal five times with 100 ns for each time while keeping the shutter closed. The ICCD noise was subtracted from the measured signals of individual particles. To determine the inherent signal from the optical chamber, a forced signal was used to trigger the UV laser and the fluorescence spectra were measured and regarded as the background noise, similarly to the WIBS technique[4-6].

Background measurement was performed every 2 hours. The nozzle surface was cleaned when the background was observed to increase, which happened roughly every two days for ambient measurement. In the lab, the nozzle needs to be cleaned from every 10 minutes to a few hours, depending on the type of particles.

Synchronization methods

Once the UV laser was fired, an electrical pulse would be generated to trigger the ICCD detector, opening its shutter for 100 ns. Afterwards, the ICCD transmitted an auxiliary port output (AUX OUT) signal to trigger a channel (channel B in Figure S2) of the digital storage oscilloscope (DSO). A second channel (channel A in Figure S2) of the DSO was connected with the detector of two red laser beams to measure the time-of-flight signal of the particle. The advantage of the DSO is that it could record the data before triggering; therefore, the time-of-flight signal of the red laser beams was recorded even though the triggering happened afterwards. The amount of fluorescence spectra and time-of-flight signals is the same. In this synchronization way, the fluorescence spectrum and the aerodynamic diameter for the same particle are measured.

When using parallel triggering (Figure S2a), the number of signals measured by the DSO is larger than that of the ICCD since the maximum working frequency of the DSO is higher than that of the ICCD. With the serial triggering (Figure S2b), the size information and the fluorescent signal can be retrieved for the same individual particle. In our case, the serial triggering is preferred over parallel triggering.

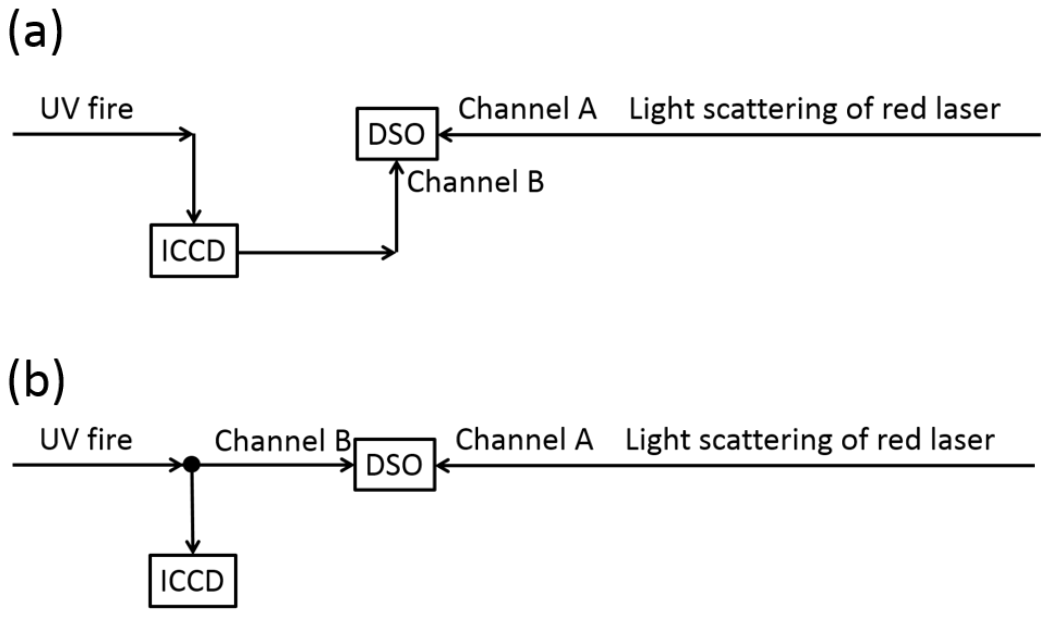

Figure S2. Two possible synchronization methods: (**a**) serial triggering of ICCD and DSO by the UV laser, or (**b**) parallel triggering of ICCD and DSO by the UV laser.

Offline Measurement

Offline measurement was performed to validate the accuracy of the S2FS. The offline spectrometer was a Horiba dual-FL spectrometer (Horiba, Japan). Several milligrams of powdered materials were placed on to the black surface holder and the slit width of the spectrometer was set to be 10 nm with λ_{ex} = 355 nm. Dipicolinic acid (DPA) was dissolved in ethanol with a concentration of $4*10^{-3}$ M.

WIBS Measurement

WIBS measurement of cellulose and chitin particles was performed to intercompare the sensitivity of the S2FS. The WIBS-4A was purchased from Droplet Measurement Technologies (DMT, USA).

Chemicals and aerosolization methods

Either liquid aerosolization or powder aerosolization was used for aerosol generation. PAH were dissolved with isopropanol with the concentration of 0.5 mM. The solution was subsequently nebulized by a Portable Atomizer Aerosol Generator (Model 3079A, TSI Inc., St. Paul, MN, USA). A silica gel drier was used to dry particles after nebulization. NaCl was dissolved in water with the concentration of 0.5 mM. Afterwards, NaCl particles were generated by liquid aerosolization method. The relative humidity (RH) was measured by a RH sensor, which was connected to the outlet of the optics chamber. The RH varied between 19-24% during measurement for water-soluble chemicals.

Biofluorophores, combustion-related particles and pollen were aerosolized by using powder aerosolization[5, 8]. In brief, compressed air was flushed through a glass vial filled with solid chemicals while a magnetic bar stirred the powdered chemicals.

Table S1. The Details of Chemicals and Corresponding Aerosolization Methods.

Chemicals	**Company**	**CAS number**	**Aerosolization method**	**Aerodynamic diamter used for analysis**
Beta-nicotinamide adenine dinucleotide reduced, disodium salt hydrate (NADH)	Sigma-Aldrich Chemie GmbH (Germany)	606-68-8	Powder	1.5 μm, 2 μm, 2.5 μm
Riboflavin	Sigma-Aldrich Chemie GmbH (Germany)	83-88-5	Powder	1.5 μm, 2 μm, 2.5 μm
Cellulose	Sigma-Aldrich Chemie GmbH (Germany)	9004-34-6	powder	3 μm
Chitin	TCI Deutschland GmbH (Germany)	1398-61-4	powder	3 μm
Ambrosia artemisiifolia (comon ragweed)	Bonapol A.S., Czech Republic	-	Powder	10-16 μm
Artemisia vulgaris (common mugwort)	Bonapol A.S., Czech Republic		Powder	10-14 μm
Betula pendula (White birch)	Bonapol A.S., Czech Republic		Powder	7-15 μm

Olea europaea (European olive)	Bonapol A.S., Czech Republic	-	Powder	9-13 μm
Sambucus nigra (Elder)	Bonapol A.S., Czech Republic		Powder	7-18 μm
Urtica dioica (Nettle)	Bonapol A.S., Czech Republic		Powder	7-11 μm
Pyrene	Sigma-Aldrich Chemie GmbH (Germany)	129-00-0	Liquid	1 μm
Fluoranthene	Sigma-Aldrich Chemie GmbH (Germany)	206-44-0	Liquid	1 μm
Benzo[a]anthracene	Sigma-Aldrich Chemie GmbH (Germany)	56-55-3	Liquid	1 μm
Humic acid	Carl Roth GmbH (Germany)	1415-93-6	Powder	3 μm
Diesel soot	National Institute of Standards and Technology (NIST; Gaithersburg, MD, USA)	SRM 2975	Powder	3 μm
Biomass burning particles[a]	Self-made	Self-made	Powder	3 μm
Polystyrene latex (PSL)	Thermo Scientific	-	Liquid	0.6 μm,0.8 μm, 1 μm, 1.8 μm

Fluorescent polystyrene latex (FPSL)	Thermo Scientific	-	Liquid	0.6 μm,0.8 μm, 1 μm, 2.1 μm
NaCl	Sigma-Aldrich Chemie GmbH (Germany)	7647-14-5	Liquid	1 μm
Dipicolinic acid (DPA)	Sigma-Aldrich Chemie GmbH (Germany)	499-83-2	Offline measurement	-

[a]Biomass burning particles were obtained by burning wheat. A glass slide was placed on top of the fire to collect biomass burning particles.

Performance of the S2FS

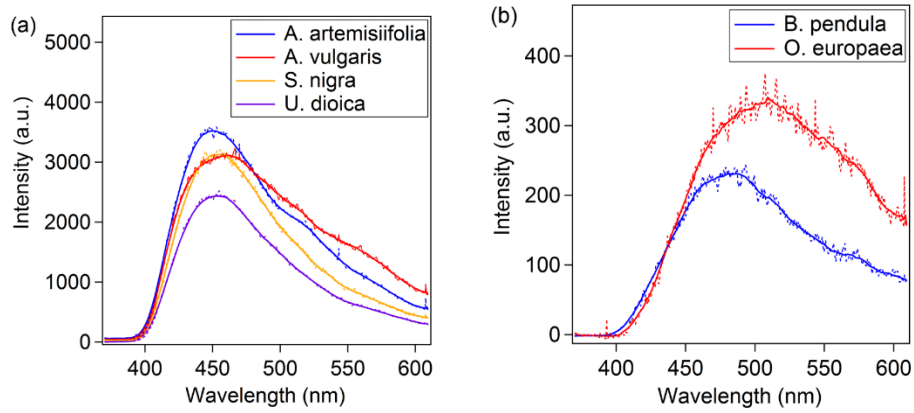

Figure S3. Averaged fluorescence spectra of 300 individual pollen grains by the S2FS. Solid lines indicate that the spectra were smoothed every 32 pixels and dashed lines indicate the raw spectra without smoothing.

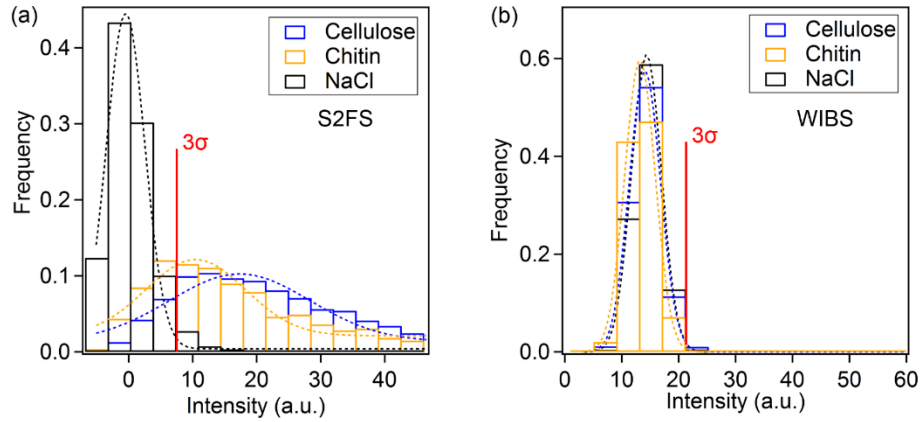

Figure S4. Fluorescence intensity distribution of cellulose and chitin (**a**) with an aerodynamic diameter of 3 μm observed by the S2FS or (**b**) with an optical diameter of 3 μm observed by the WIBS. The fluorescence intensity is binned into 16 channels and frequency means the ratio of particles in each channel to the number of total particles. Dashed lines represent Gaussian fits. The threshold was calculated as the average plus 3 times the standard deviation of the background intensity.

Individual spectrum of the single pollen

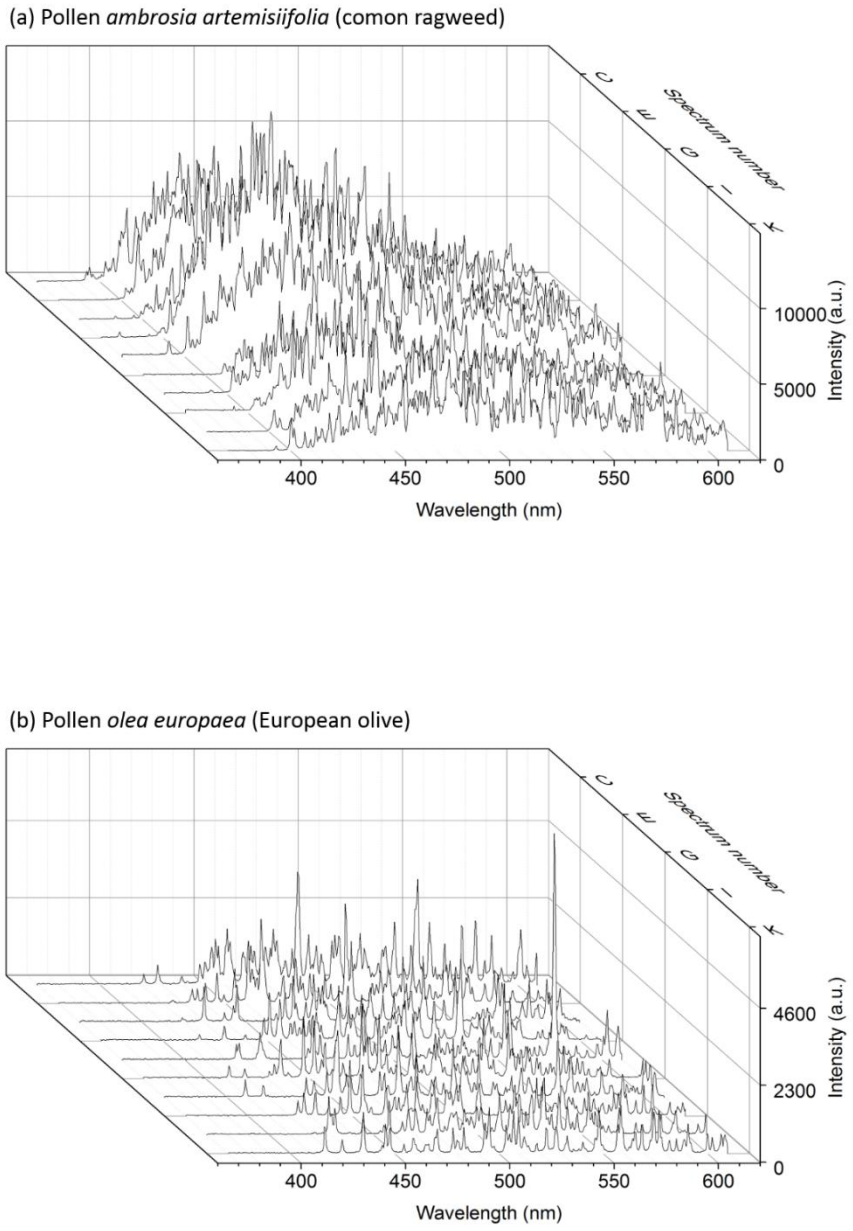

Figure S5. Individual spectrum of the single particle of (**a**) *Ambrosia artemisiifolia* pollen and (**b**) *Olea europaea* pollen.

The minimum number of particles needed to obtain the complete fluorescence spectrum

In practice, *N* was determined when the deviation between the averaged fluorescence spectrum over a certain number of particles (*N*) and the averaged fluorescence spectrum over *N+100* particles was below a certain threshold, which was manually set as $2*10^{-6}$ in our case (Figure S6a).

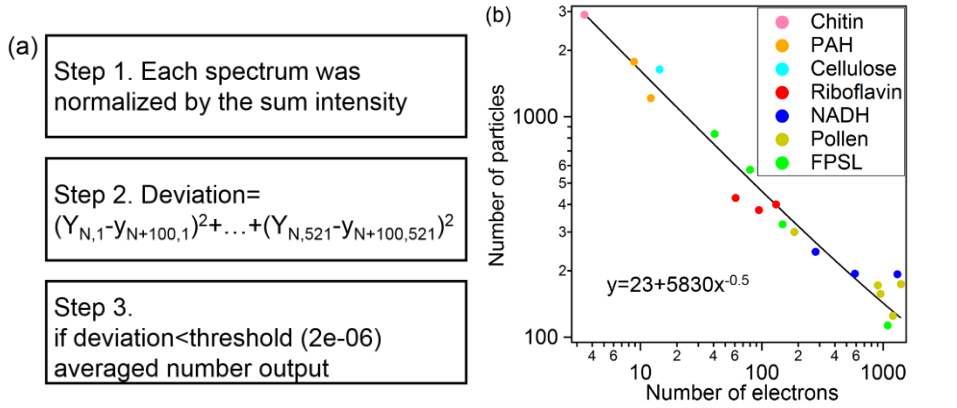

Figure S6. (**a**) Procedure to calculate the number of particles to obtain the complete fluorescence spectrum as a function of number of electrons detected by the ICCD sensor. (**b**) The number of particles needed to obtain the complete fluorescence spectrum is between 100 and 3000. The black solid line indicates a power fit with an exponential value of -0.5. The detailed information of particles can be found in Table S1.

Cluster analysis of single pollen particles

Pinnick et al.[9] have used a hierarchical cluster analysis to cluster atmospheric aerosol particles into 12 main categories on a single particle level. A hierarchical cluster analysis means combining spectra that have the largest overlap until the largest dot product exceed a manually set threshold[9]. The fluorescence spectrum was binned from 512 channels to 8 channels. Afterwards, the fluorescence spectra were combined that have the largest overlap until the largest dot product exceeded a manually set threshold[9]. *Ambrosia artemisiifolia* pollen and *Olea europaea* pollen can be distinguished on a single particle level by using this hierarchical cluster analysis method (Figure S7). Meanwhile, for atmospheric aerosol particles during our measurement, fluorescence only appeared on a few pixels (Figure S9). Therefore, the fluorescence spectra of fluorescent particles were averaged over a certain period.

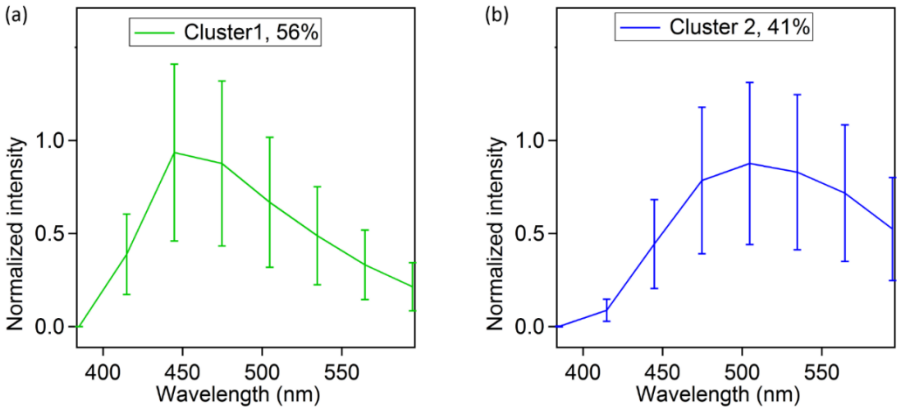

Figure S7. Cluster analysis of single pollen particles by the S2FS. Each species of pollen contained 300 individual single particles. The fluorescence spectrum was binned from 512 channels to 8 channels. The threshold was set as 0.9. This hierarchical cluster analysis method was applied to analyze the above two species of pollen, which can separate them based on the fluorescence spectrum. Cluster 1 represents *Ambrosia artemisiifolia* pollen and cluster 2 represents *Olea europaea* pollen.

Comparison of atmospheric fluorescent aerosol particles in the fine mode to the spectrum of DPA

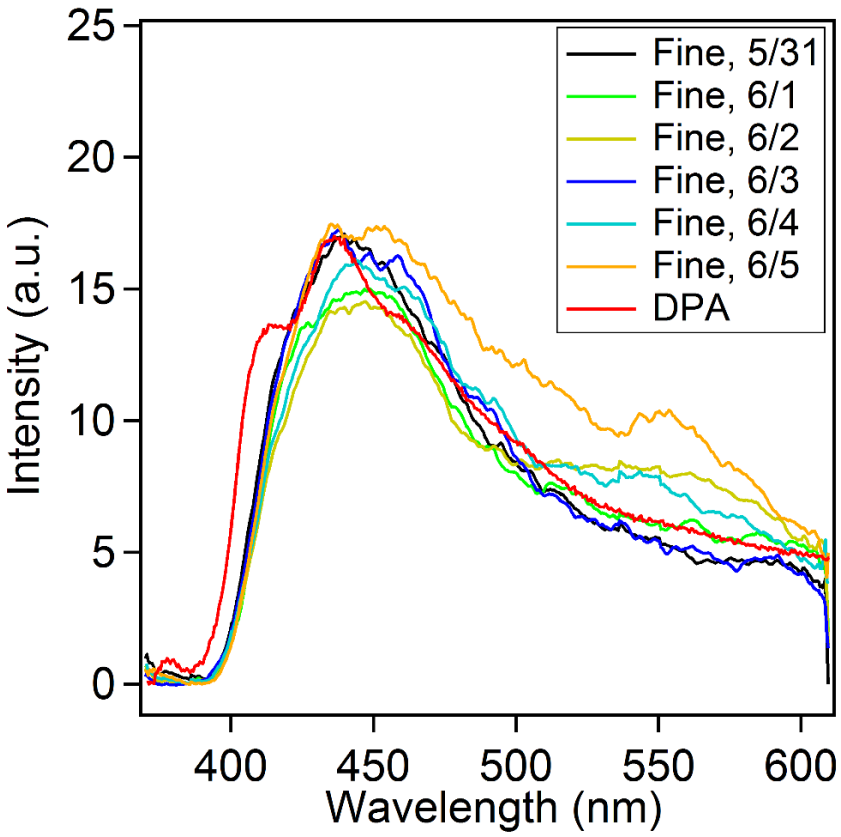

Figure S8. Comparison of averaged fluorescence spectra of atmospheric fluorescent aerosol particles in the fine mode to the spectrum of DPA measured by the offline spectrometer. The peak intensity of DPA was normalized to the same range as that of atmospheric fluorescent aerosol particles in the fine mode. The spectra observed on 31 May, 3 June, 4 June, and 5 June fit well to the spectrum of DPA measured by the offline spectrometer.

Individual spectrum of the single aerosol particle in ambient air

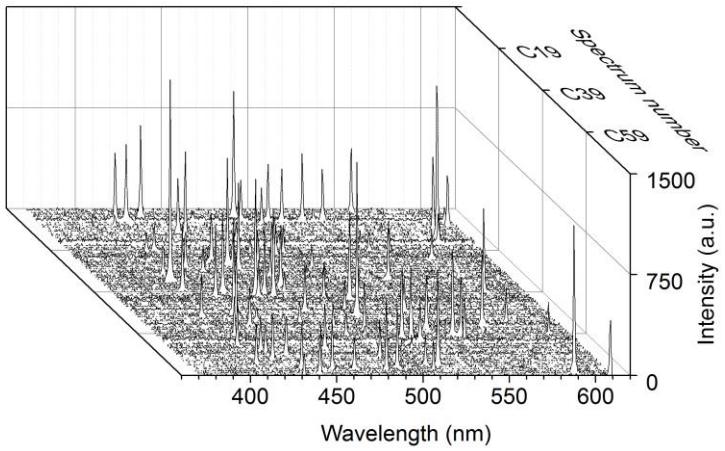

Figure S9. Individual spectrum of the single atmospheric aerosol particle. The signal appeared only on a few pixels.

Fluorescence spectra of background noise

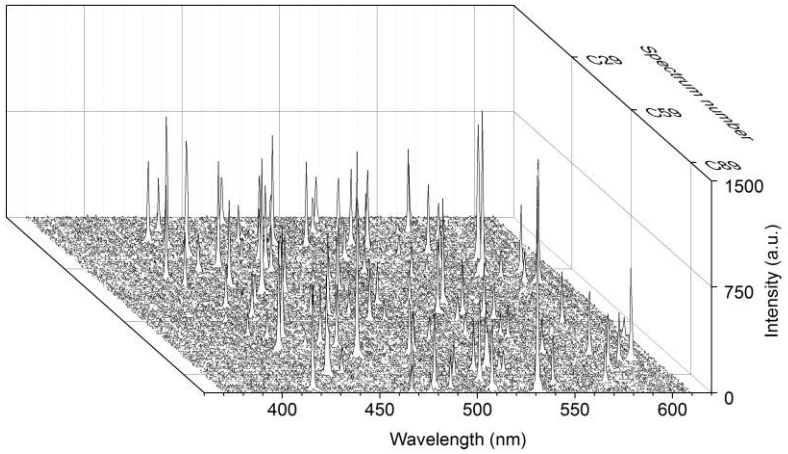

Figure S10. Individual spectrum of background noise. The signal also appeared only on a few pixels.

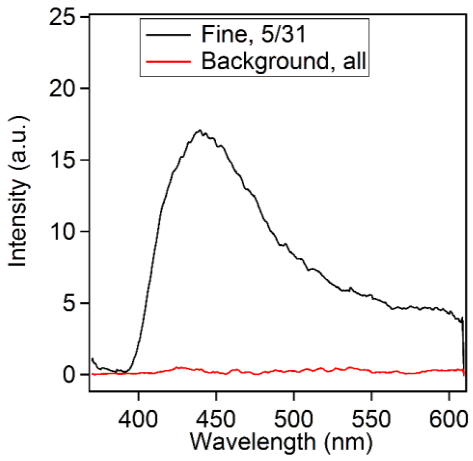

Figure S11. Comparison of fluorescent fine particles to background noise. The background noise was averaged signal of 50,000 forced trigger signals.

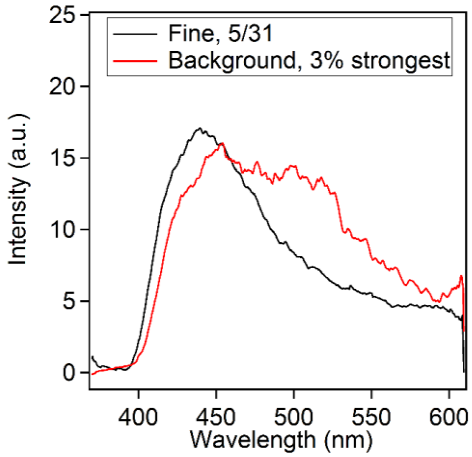

Figure S12. Comparison of fluorescent particles to strongest 3% background noise. The background noise was averaged spectrum of top 3% strongest signals of 50,000 forced trigger signals. The fluorescence intensity of the strongest background noise was in the same range as that fluorescent particles, but the peak position was different.

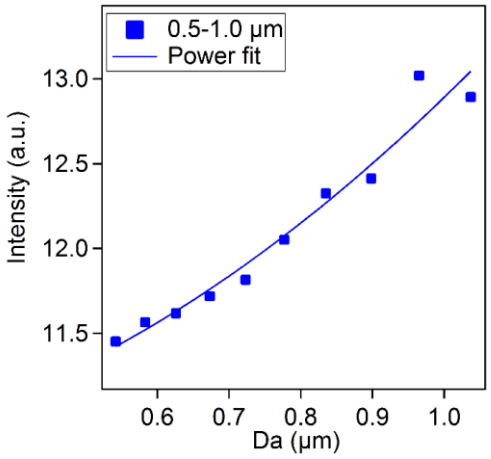

Figure S13. The fluorescence intensity of fluorescent fine particles scaled with the surface of particles, which further suggests that the measured signal is not background signal.

Averaged fluorescence spectra of atmospheric particles

Figure S14 shows the averaged fluorescence spectra of all of the fluorescent particles during the 9-daytime measurement period. Since the fluorescence intensity is a function of particle size[10, 11], the fluorescence intensity was normalized by the sum intensity or the maximum intensity in each size bin (Figure 14a, 14b). Both of them indicate that the peak position shifted to a longer wavelength when the size increased. The peak position was located at ~440 nm for $PM_{0.5\text{-}1}$ and the peak position was at ~465 nm for $PM_{1.1\text{-}2.5}$ (Figure 14c). Meanwhile, $PM_{2.6\text{-}20}$ had multiple peaks.

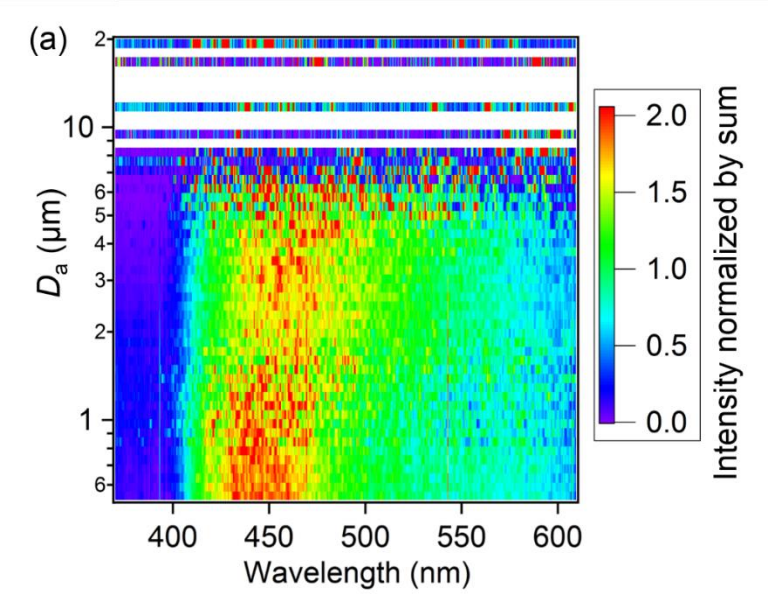

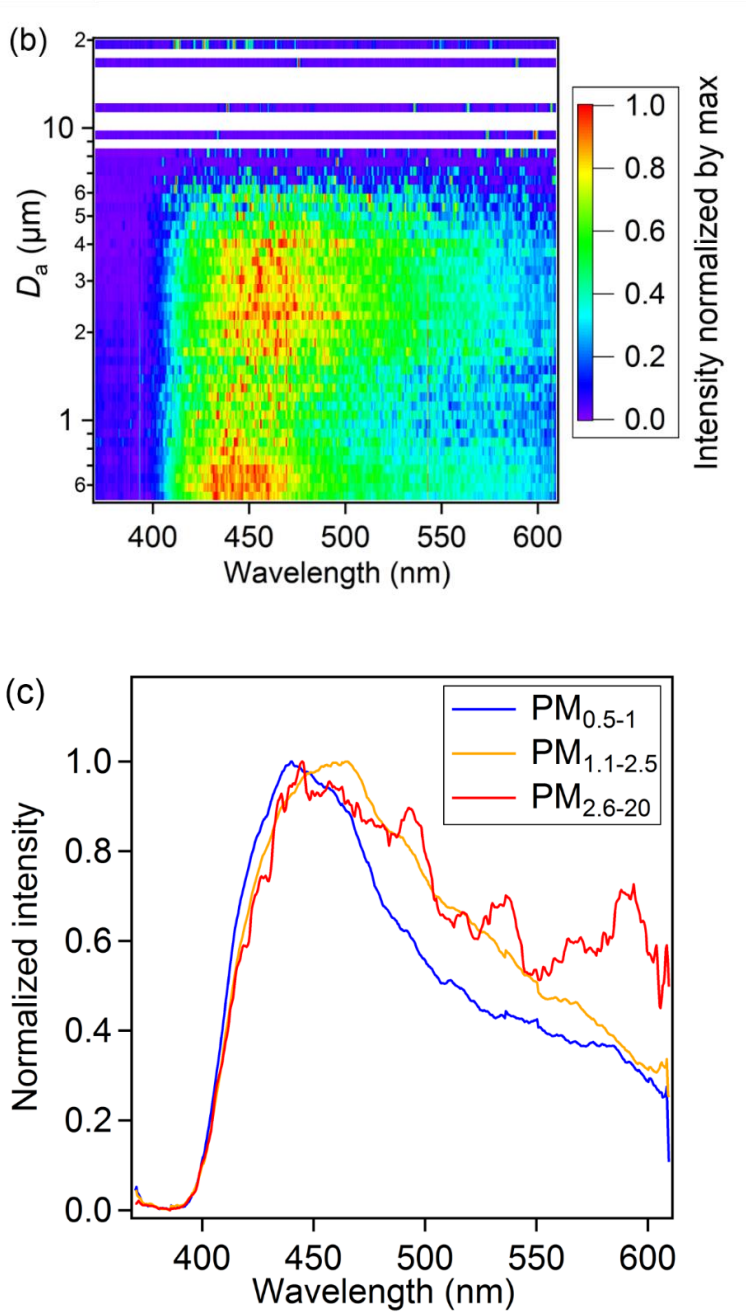

Figure S14. Size-resolved fluorescence spectra for atmospheric fluorescent particles. (**a**) The fluorescence spectra were normalized by the sum intensity while the size was binned to 52 channels. (**b**) The fluorescence spectra were normalized by the maximum intensity while the size was binned to 52 channels. (**c**) The fluorescence spectra were smoothed every 32 pixels and normalized by the maximum intensity while the size was binned to 3 channels.

Gaussian fit to fluorescence spectra of atmospheric aerosol particles

The fluorescence spectra of atmospheric aerosol particles can be fitted well with two Gaussian functions. The fluorescence spectra of $PM_{0.5\text{-}1}$ (0.5-1 μm) can be fitted with two Gaussian peaks at 444 and 534 nm while the fluorescence spectra of $PM_{1.1\text{-}2.5}$ (1.1-2.5 μm) can be fitted with two Gaussian peaks at 449 and 531 nm (Figure S15a, 15b). Meanwhile, the fluorescence spectra of $PM_{2.6\text{-}20}$ (2.6-20 μm) can be fitted with two Gaussian peaks at longer wavelengths of 454 and 570 nm, respectively (Figure S15c). The r^2 value of PM_{20} was relatively low. Apart from the peak position of the fluorescence spectra, the ratio of peak intensities at 450 nm to that at 500 nm was frequently used to distinguish sources of fulvic acids in water[12]. It was observed that a ratio of ~1.9 indicated microbially derived fulvic acids and a ratio of ~1.4 indicated terrestrially derived fulvic acids[12]. For atmospheric aerosols, a difference of the ratio was observed as well. $PM_{0.5\text{-}1}$ (0.5-1 μm) had a higher ratio of 1.61 while $PM_{1.1\text{-}2.5}$ (1.1-2.5 μm) and $PM_{2.6\text{-}20}$ (2.6-20 μm) had a lower ratio of 1.20 and 1.25, respectively (Table S2). These results also suggested that PM_1 may come from different sources compared to $PM_{2.5}$ and PM_{20}.

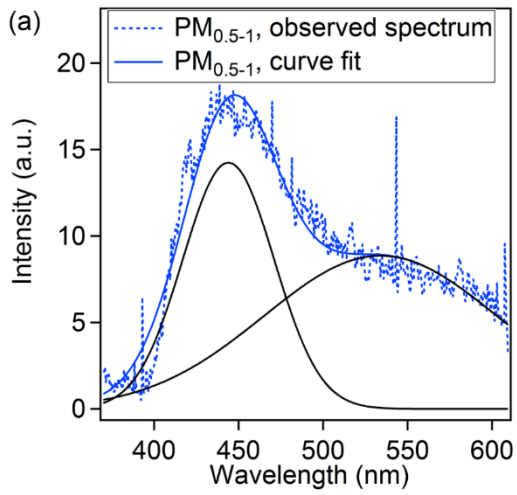

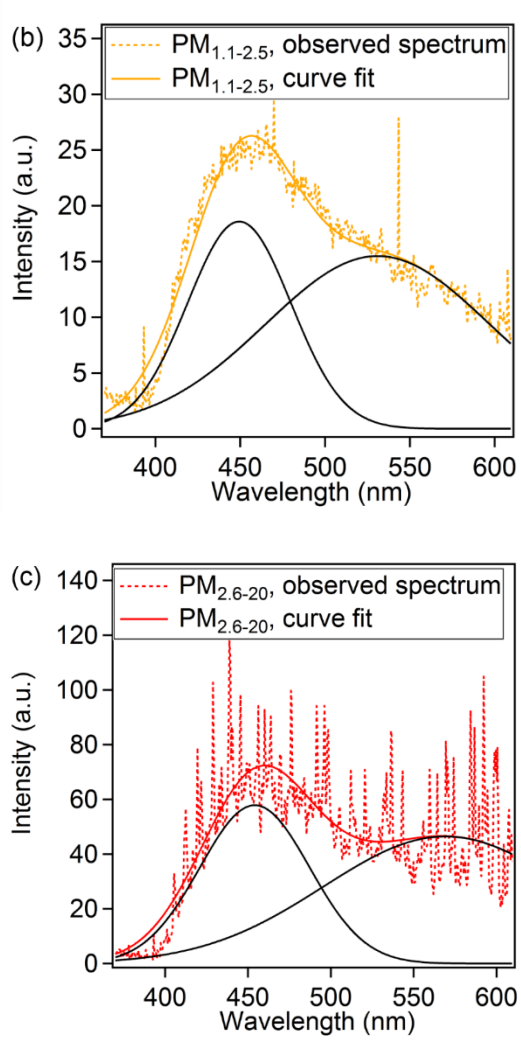

Figure S15. Observed fluorescence spectra of atmospheric aerosol particles and the corresponding Gaussian curve fits.

Table S2. Two Gaussian functions fit to the fluorescence spectra of atmospheric aerosol particles for PM_1, $PM_{1.1\text{-}2.5}$, and $PM_{2.6\text{-}20}$.

	Peak position of Gaussian 1 (nm)	**FWHM of Gaussian 1 (nm)**	**Peak position of Gaussian 2 (nm)**	**FWHM of Gaussian 2 (nm)**	**Ratio of peak intensities**	**r^2 value**
$PM_{0.5\text{-}1}$	444	63	534	162	1.61	0.936
$PM_{1.1\text{-}2.5}$	449	72	531	155	1.20	0.951
$PM_{2.6\text{-}20}$	454	78	570	173	1.25	0.674

Size distributions of pollen

The geometric diameter of the measured pollen was 15-20 μm. The density of corn pollen[13] was ~0.82 * 10^3 kg/m^3, so the calculated aerodynamic diameter was 13-18 μm. Figure S16 shows that pollen had the peak size at ~11 μm or 8 μm, which was close to the calculated aerodynamic diameter. Some pollen also had fragments according to the size distribution. In the manuscript, only the intact pollen was analyzed.

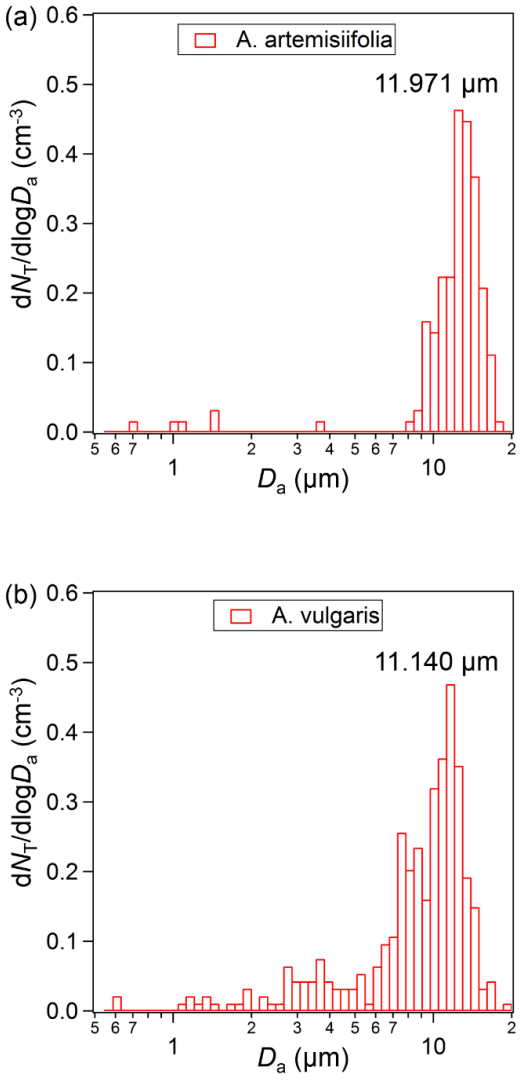

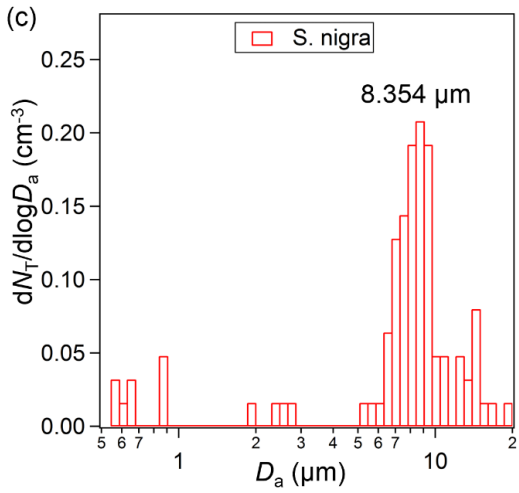
(c)
S. nigra
8.354 µm
0.25
0.20
0.15
0.10
0.05
0.00
dN_T/dlogD_a (cm^-3)
5 6 7
1
2 3 4 5 6 7
10
2
D_a (µm)

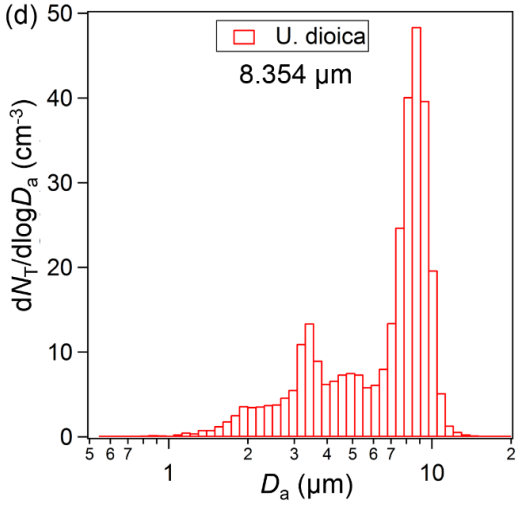
(d)
U. dioica
8.354 µm
50
40
30
20
10
0
dN_T/dlogD_a (cm^-3)
5 6 7
1
2 3 4 5 6 7
10
2
D_a (µm)

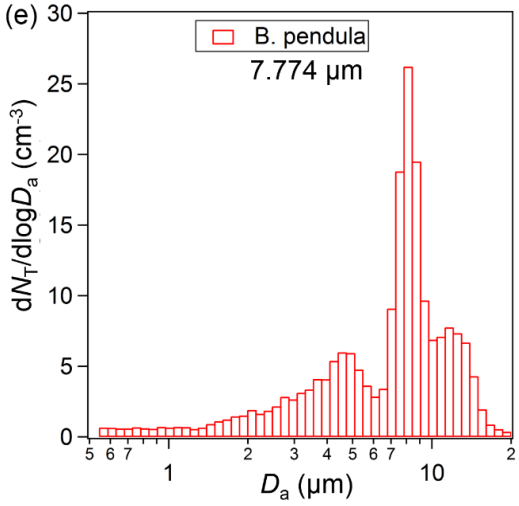
(e)
B. pendula
7.774 µm
30
25
20
15
10
5
0
dN_T/dlogD_a (cm^-3)
5 6 7
1
2 3 4 5 6 7
10
2
D_a (µm)

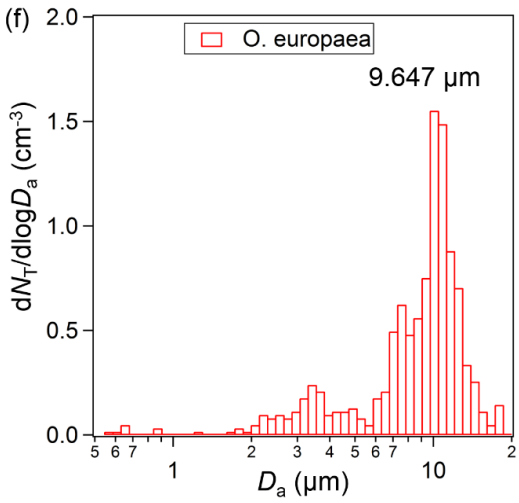

Figure S16. The size distribution of pollen.

Size distributions of standard PSL particles

Standard PSL particles were also measured. The aerodynamic diameter was slightly larger than the geometric diameter since the density of PSL was larger than $1 * 10^3$ kg/m^3.

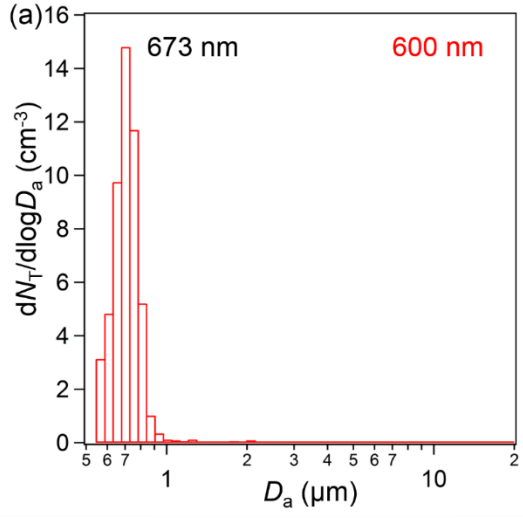

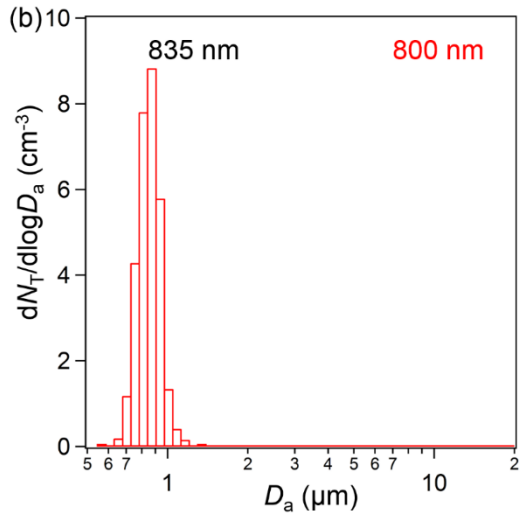

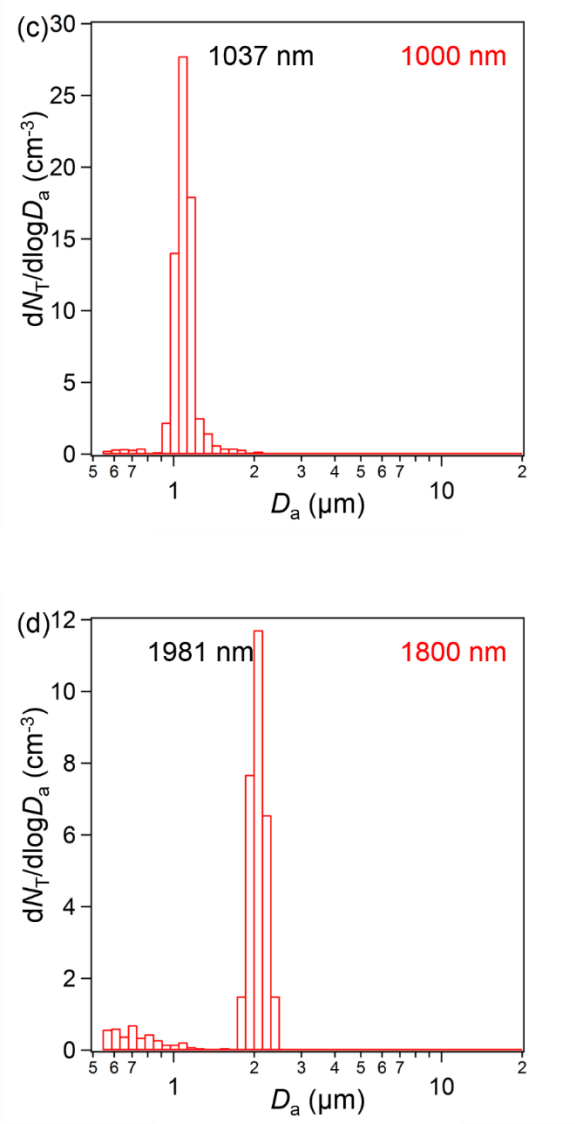

Figure S17. The size distribution of PSLs with (**a**) 600 nm, (**b**) 800 nm, (**c**) 1000 nm, and (**d**) 1800 nm.

Intensity calibration

The quantum efficiency of ICCD sensor and spectrograph was dependent on the emission wavelength. In order to calibrate this effect, a deuterium lamp of DH-mini light source was used. No obvious change of the fluorescence spectra was observed before and after the intensity calibration (IC). Therefore, the results in the manuscript were not corrected for intensity.

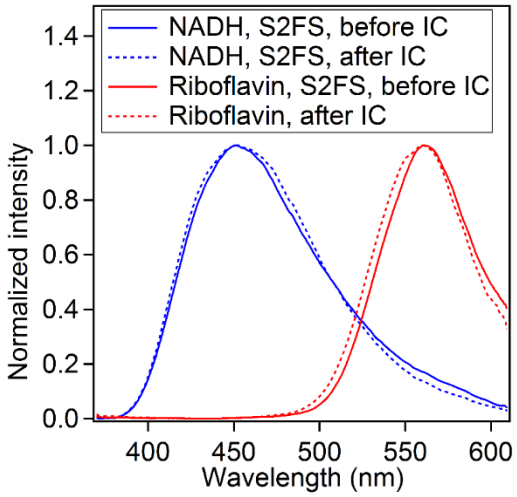

Figure S18. Fluorescence spectra of NADH and riboflavin before and after intensity calibration. No obvious change was observed.

Cleaning the nozzle surface

Struggling against background fluorescence signals is a foremost concern since the number of photons is few[7]. Toprak and Schnaiter[6] reported that background fluorescence is a combination of the detect noise, the variability of the UV intensities, and the fluorescence induced from aerosol particles escaped from the aerosol flow and deposited on the inner walls of the detection chamber. Pan et al.[14] reported that the nozzle surface was also a major source of background signals. The particles accumulate on the nozzle surface during measurement. After cleaning the nozzle surface, the spectra of different materials can be well distinguished (Figure S19). For ambient measurement, the nozzle needs to be cleaned every 2 days; in the laboratory, the nozzle needs to be cleaned from every 10 minutes to a few hours, depending on the species of particles.

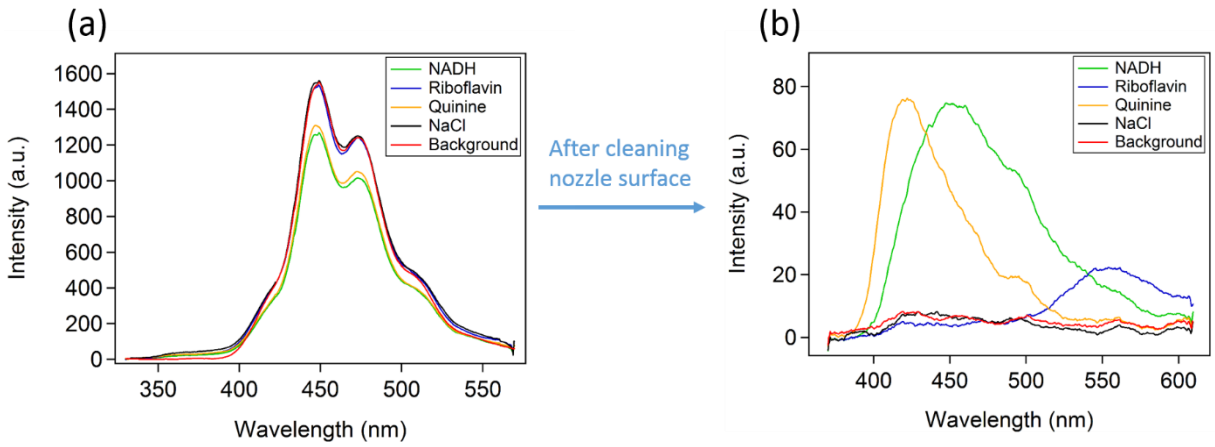

Figure S19. Fluorescence spectra of biomolecule particles. (**a**) After a long time of operation, the nozzle surface was contaminated by fluorescent particles. High background values masked any fluorescence spectra from the sample particles. (**b**) After cleaning the nozzle surface, fluorescence spectra can be clearly distinguished.

References

1. Wilson, J. C.; Liu, B. Y. H., Aerodynamic Particle-Size Measurement by Laser-Doppler Velocimetry. *J. Aerosol Sci.* **1980,** *11*, (2), 139-150.
2. Lerner, J. M., Imaging spectrometer fundamentals for researchers in the biosciences - A tutorial. *Cytom. Part A* **2006,** *69*, (8), 712-734.
3. Pohlker, C.; Huffman, J. A.; Poschl, U., Autofluorescence of atmospheric bioaerosols - fluorescent biomolecules and potential interferences. *Atmos. Meas. Tech.* **2012,** *5*, (1), 37-71.
4. Kaye, P. H.; Stanley, W. R.; Hirst, E.; Foot, E. V.; Baxter, K. L.; Barrington, S. J., Single particle multichannel bio-aerosol fluorescence sensor. *Opt. Express* **2005,** *13*, (10), 3583-3593.
5. Savage, N. J.; Krentz, C. E.; Konemann, T.; Han, T. T.; Mainelis, G.; Pohlker, C.; Huffman, J. A., Systematic characterization and fluorescence threshold strategies for the wideband integrated bioaerosol sensor (WIBS) using size-resolved biological and interfering particles. *Atmos. Meas. Tech.* **2017,** *10*, (11), 4279-4302.
6. Toprak, E.; Schnaiter, M., Fluorescent biological aerosol particles measured with the Waveband Integrated Bioaerosol Sensor WIBS-4: laboratory tests combined with a one year field study. *Atmos. Chem. Phys.* **2013,** *13*, (1), 225-243.
7. Moerner, W. E.; Orrit, M., Illuminating single molecules in condensed matter. *Science* **1999,** *283*, (5408), 1670-1676.
8. Pan, Y. L.; Hill, S. C.; Pinnick, R. G.; House, J. M.; Flagan, R. C.; Chang, R. K., Dual-excitation-wavelength fluorescence spectra and elastic scattering for differentiation of single airborne pollen and fungal particles. *Atmos. Environ.* **2011,** *45*, (8), 1555-1563.
9. Pinnick, R. G.; Hill, S. C.; Pan, Y. L.; Chang, R. K., Fluorescence spectra of atmospheric aerosol at Adelphi, Maryland, USA: measurement and classification of single particles containing organic carbon. *Atmos. Environ.* **2004,** *38*, (11), 1657-1672.
10. Hill, S. C.; Williamson, C. C.; Doughty, D. C.; Pan, Y. L.; Santarpia, J. L.; Hill, H. H., Size-dependent fluorescence of bioaerosols: Mathematical model using fluorescing and absorbing molecules in bacteria. *J. Quant. Spectrosc. Ra.* **2015,** *157*, 54-70.
11. Robinson, E. S.; Gao, R. S.; Schwarz, J. P.; Fahey, D. W.; Perring, A. E., Fluorescence calibration method for single-particle aerosol fluorescence instruments. *Atmos. Meas. Tech.* **2017,** *10*, (5), 1755-1768.
12. McKnight, D. M.; Boyer, E. W.; Westerhoff, P. K.; Doran, P. T.; Kulbe, T.; Andersen, D. T., Spectrofluorometric characterization of dissolved organic matter for indication of precursor organic material and aromaticity. *Limnol. Oceanogr.* **2001,** *46*, (1), 38-48.
13. van Hout, R.; Katz, J., A method for measuring the density of irregularly shaped biological aerosols such as pollen. *J. Aerosol Sci.* **2004,** *35*, (11), 1369-1384.
14. Pan, Y. L.; Pinnick, R. G.; Hill, S. C.; Chang, R. K., Particle-Fluorescence Spectrometer for Real-Time Single-Particle Measurements of Atmospheric Organic Carbon and Biological Aerosol. *Environ. Sci. Technol.* **2009,** *43*, (2), 429-434.

D.2 Zhang et al., to be submitted, 2019

Intensity calibration of an online/in situ fluorescence spectrometer (OFS) using the volume of single particles

Author list to be modified or extended

Minghui Zhang[1], Ulrich Pöschl[1], Hang Su[2,1], and Yafang Cheng[1]

[1]Multiphase Chemistry Department, Max Planck Institute for Chemistry, 55128 Mainz, Germany

[2]Center for Air pollution and Climate Change Research, Institute for Environmental and Climate Research (ECI), Jinan University, 511443 Guangzhou, China

Correspondence to: H. Su (h.su@mpic.de) and Y. Cheng (yafang.cheng@mpic.de)

Keywords: Intensity Calibration, Fluorescence Spectrometer, Bioaerosols, Single Particle, Standard Materials, laser/light-induced fluorescence

Intensity calibration of an online/in situ fluorescence spectrometer (OFS) using the volume of single particles

Author list to be modified or extended

Minghui Zhang[1], Ulrich Pöschl[1], Hang Su[2,1], and Yafang Cheng[1]

[1]Multiphase Chemistry Department, Max Planck Institute for Chemistry, 55128 Mainz, Germany

[2]Center for Air pollution and Climate Change Research, Institute for Environmental and Climate Research (ECI), Jinan University, 511443 Guangzhou, China

Correspondence to: H. Su (h.su@mpic.de) and Y. Cheng (yafang.cheng@mpic.de)

Abstract

Online/in situ fluorescence spectrometers (OFS) have been widely used to analyze bioaerosols in real-time for atmospheric research. Fluorescence intensity of OFS is commonly applied as an arbitrary unit, which limits comparisons between different instruments. In order to facilitate comparisons, a standard fluorescence intensity calibration method is needed by using one parameter. Here the volume of the single particle was used as the single parameter to calibrate the fluorescence intensity of OFS. Among the materials tested, nicotinamide adenine dinucleotide (NADH), cellulose, and chitin exhibit fluorescence scaling with the volume of the particle. After the fluorescence intensity is calibrated by volume, the fluorescence spectra are nearly the same for particles with different sizes. This method implies that the fluorescence intensity can be compared and scaled between different OFS.

1. Introduction

Primary biological aerosol particles (PBAP) (Despres et al., 2012) can impact the health of plants (Brown and Hovmoller, 2002) and human beings (Lacey and Dutkiewicz, 1994), as well as influence the earth system (Frohlich-Nowoisky et al., 2016). The biofluorophores of PBAP exhibit fluorescence (Pohlker et al., 2012) when excited by the UV light without labeling with external dyes, which makes online/in situ fluorescence spectrometers (OFS) (Crawford et al., 2017; Huffman et al., 2010) one of the commonly used instruments to analyze PBAP in real-time. OFS consist of a red laser to obtain the size information and a ultraviolet (UV) light to obtain the fluorescence information. The fluorescence information is either integrated fluorescence intensity (Hairston et al., 1997; Huffman et al., 2012; Huffman et al., 2010; Kaye et al., 2005; Savage et al., 2017; Toprak and Schnaiter, 2013; Yu et al., 2016) or dispersed fluorescence spectrum (Crouzy et al., 2016; Pan et al., 2014; Pan et al., 2009; Pinnick et al., 1998).

Fluorescence intensity is one important factor to distinguish PBAP from other kinds of aerosol particles (Gabey et al., 2010; Savage et al., 2017) or differentiate various types of PBAP (Crawford et al., 2015; Robinson et al., 2013; Sivaprakasam et al., 2011). On the one hand, a particle can be defined as PBAP when the fluorescence intensity of a single particle is above a certain noise threshold (Gabey et al., 2010; Savage et al., 2017). On the other hand, fluorescence intensity distribution patterns are different among several types of PBAP (Crawford et al., 2015; Robinson et al., 2013; Sivaprakasam et al., 2011). However, fluorescence intensity is an arbitrary unit, which may vary between different OFS and may vary when the setting of the same instrument changes.

Recently, Robison et al. (Robinson et al., 2017) recommended using particle mass (d^3) to calibrate OFS. Mixed tryptophan-ammonium sulfate particles were used to calibrate FL1 sensor (λ_{ex} = 280 nm, λ_{em} = 310-400 nm) of the Wideband Integrated Bioaerosol Sensor (WIBS) and quinine particles were used to calibrate the FL2 sensor (λ_{ex} = 280 nm, λ_{em} = 420-650 nm) of the WIBS (Robinson et al., 2017). Two questions remain in terms of this method: (i) Which materials can be used calibrate FL3 sensor (λ_{ex} = 370 nm, λ_{em} = 420-650 nm)? (ii) Are the fluorescence spectra the same after normalizing by the particle mass (d^3)?

In order to probe these two questions, we measured fluorescence of certain materials by using the recently developed size-resolved single-particle fluorescence spectrometer

(S2FS). The excitation wavelength (λ_{ex}) and emission wavelength (λ_{em}) used in the S2FS (λ_{ex} = 355 nm, λ_{em} = 370-610 nm) were similar to those of the FL3 sensor used in the WIBS (λ_{ex} = 370 nm, λ_{em} = 420-650 nm) (Kaye et al., 2005). Besides, the S2FS can measure the dispersed fluorescence spectra, rather than simply measure the integrated fluorescence intensity.

2. Methods

2.1 Aerosol particles generation

Chemicals were purchased from Sigma Aldrich without further purification. All of the aerosol particles were generated by using the compressed air (Pan et al., 2011). Briefly, a glass vial was filled with solid chemicals; afterwards, compressed air was flushed through the glass vial when a magnetic bar stirred the solid chemicals. Neither water nor other solvent was used during aerosolization, which makes chemicals stable during measurement.

Differential mobility analyzer (DMA) was not used; instead, the polydisperse particles were measured. The size and fluorescence spectrum were measured simultaneously for the same particle, so the fluorescence spectrum of the same size can be analyzed afterwards. During our measurement, particles from 1 to 3 μm were analyzed.

2.2 Size-resolved single particle fluorescence spectrometer (S2FS) setup

The S2FS consists of an aerodynamic particle sizer to obtain the size information and a fluorescence spectrometer with a 355-nm excitation laser and an intensified charge-coupled device (ICCD) detector to obtain the fluorescence information. The ICCD gain was set to the maximum at 100. Even at this maximum setting, no saturation effect was observed during measurement.

The measured fluorescence emission is dispersed in 512 channels from 370 to 610 nm, where a major portion of biological fluorescence can be measured in this range.

3. Results and Discussion

Offline fluorescence spectrometers used Raman scatter of water (Lawaetz and Stedmon, 2009) to calibrate the fluorescence intensity. Meanwhile, online/in situ fluorescence spectrometers (OFS) measured particles in the solid state, which makes the using of Raman scatter of water impossible. One advantage of OFS is that the size of the particle can be measured simultaneously. Recently, Robison et al. (Robinson et al., 2017)

have developed particle mass (d^3) to calibrate OFS. But the FL3 sensor (λ_{ex} = 370 nm, λ_{em} = 420-650 nm) was not tested and the dispersed fluorescence spectra were not measured. Here we have measured fluorescence of certain materials by using the recently developed size-resolved single-particle fluorescence spectrometer (S2FS). λ_{ex} and λ_{em} used in the S2FS (λ_{ex} = 355 nm, λ_{em} = 370-610 nm) were similar to those of the FL3 sensor used in the WIBS (λ_{ex} = 370 nm, λ_{em} = 420-650 nm). The other advantage of the S2FS is that it can measure the dispersed fluorescence spectra as well.

3.1 Size-dependent fluorescence intensity

Most of OFS analyzed particles by using the fluorescence intensity. The fluorescence intensity not only depends the type of the particle, but also is a function of the size of the particle. A mathematical model used by Hill et al. (Hill et al., 2015) suggests that fluorescence cross sections scales with volume when the particle size and concentration of fluorophores are small while the fluorescence cross sections are proportional to surface area for larger particles. Lab results (Sivaprakasam et al., 2011) show that a power function fit well between fluorescence intensity and particle size with the exponent value between 1.6 and 3.2.

We have measured certain particles composed of biofluorophores in the solid state. In the size range between 1 μm and 3 μm, the fluorescence intensity of NADH, cellulose, and chitin show power law based exponent of ~3, which suggests that the fluorescence intensity is proportional to the particle volume (Figure 1). According to Robinson et al. (Robinson et al., 2017), quinine in the core of the particle did not contribute the observed fluorescence, which might explain the lower value of quinine of 2.6. Riboflavin reveals a smaller exponent value of 1.2 suggesting that the fluorescence intensity of riboflavin increases with the diameter of the particle. Quenching of fluorescence (Limpouchova and Prochazka, 2016) or the cooperative effect of shielding of absorption and quenching of fluorescence could happen for riboflavin particles (Figure 2).

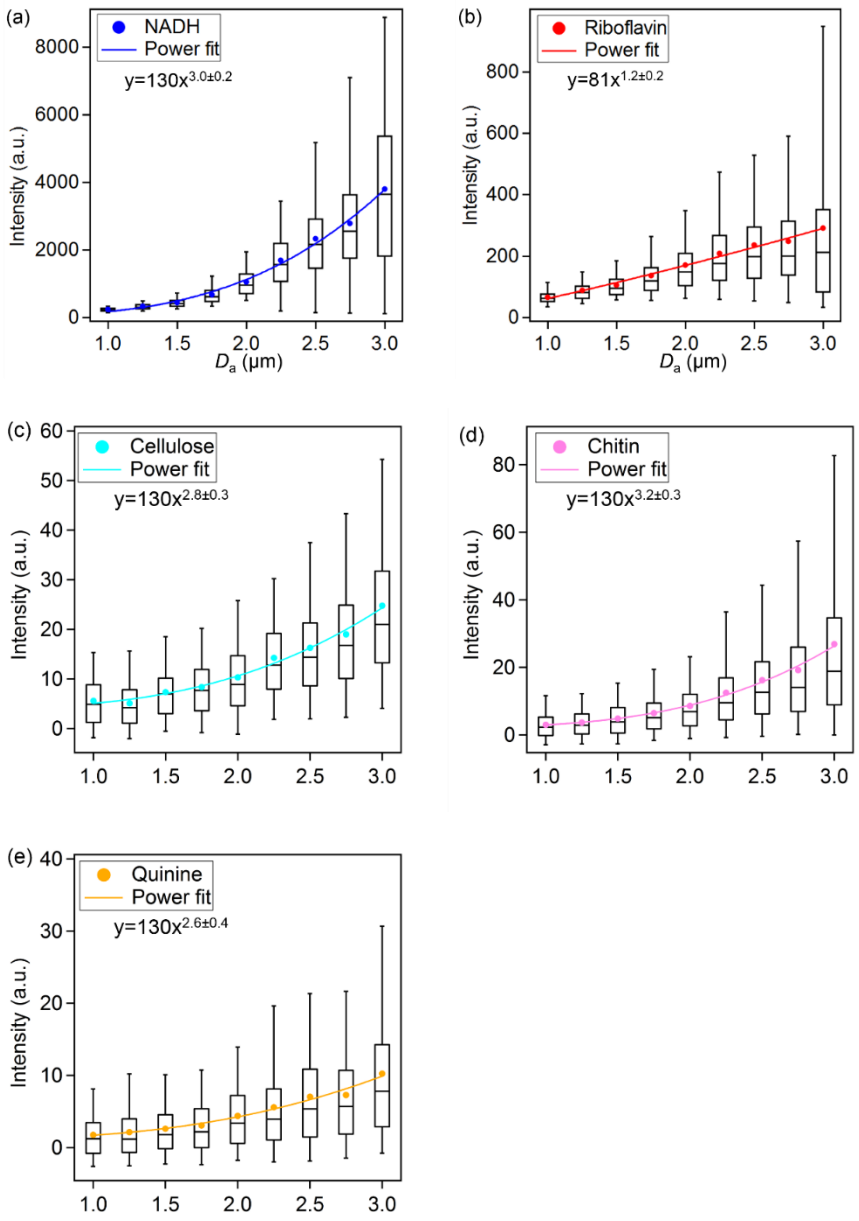

Figure 1. Size dependent fluorescence intensity of (**a**) NADH, (**b**) riboflavin, (**c**) cellulose, (**d**) chitin, and (**e**) quinine of ~300 single particles in each size bin. In the box-whisker plots, dot is arithmetic mean; lower and upper limits of the box represent 25th and 75th percentiles; horizontal bars represent 5th and 95th percentiles. The solid line indicates the power fit to the mean intensity. NADH, cellulose, and chitin exhibit fluorescence scaling with the volume of the particle while riboflavin exhibits fluorescence scaling with the diameter of the particle.

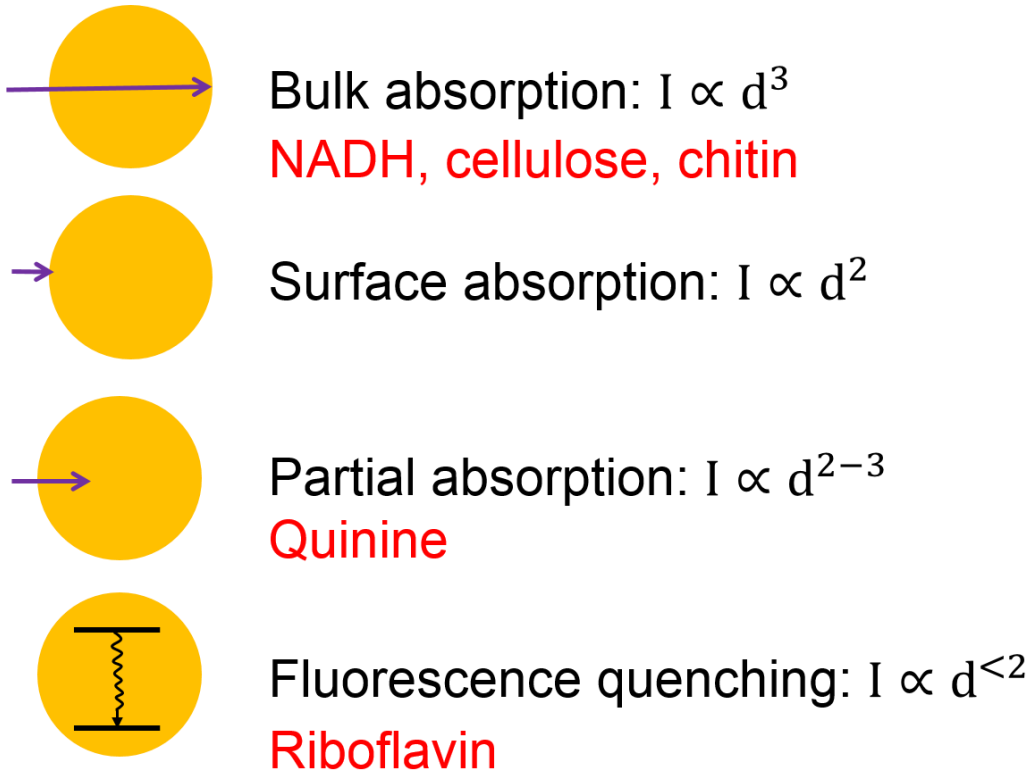

Figure 2. Possible mechanisms explaining the size-dependent fluorescence intensity. Particles composed of NADH, cellulose, and chitin reveal the bulk absorption, resulting in the exponent value of 3. Particles composed of quinine reveal the partial absorption, resulting in the exponent value between 2 and 3. Particles composed of riboflavin have the fluorescence quenching effect, resulting in the exponent value below 2.

3.2 Volume calibrated fluorescence spectra and implications

The raw fluorescence spectra of NADH, cellulose, and chitin depend on the size of the particle. After calibration with the particle volume (d^3), the fluorescence spectra of particles with different aerodynamic diameters are nearly the same (Figure 3). This means that the volume calibrated spectra depend on the species of chemicals and settings of OFS, rather than on the size of the particle.

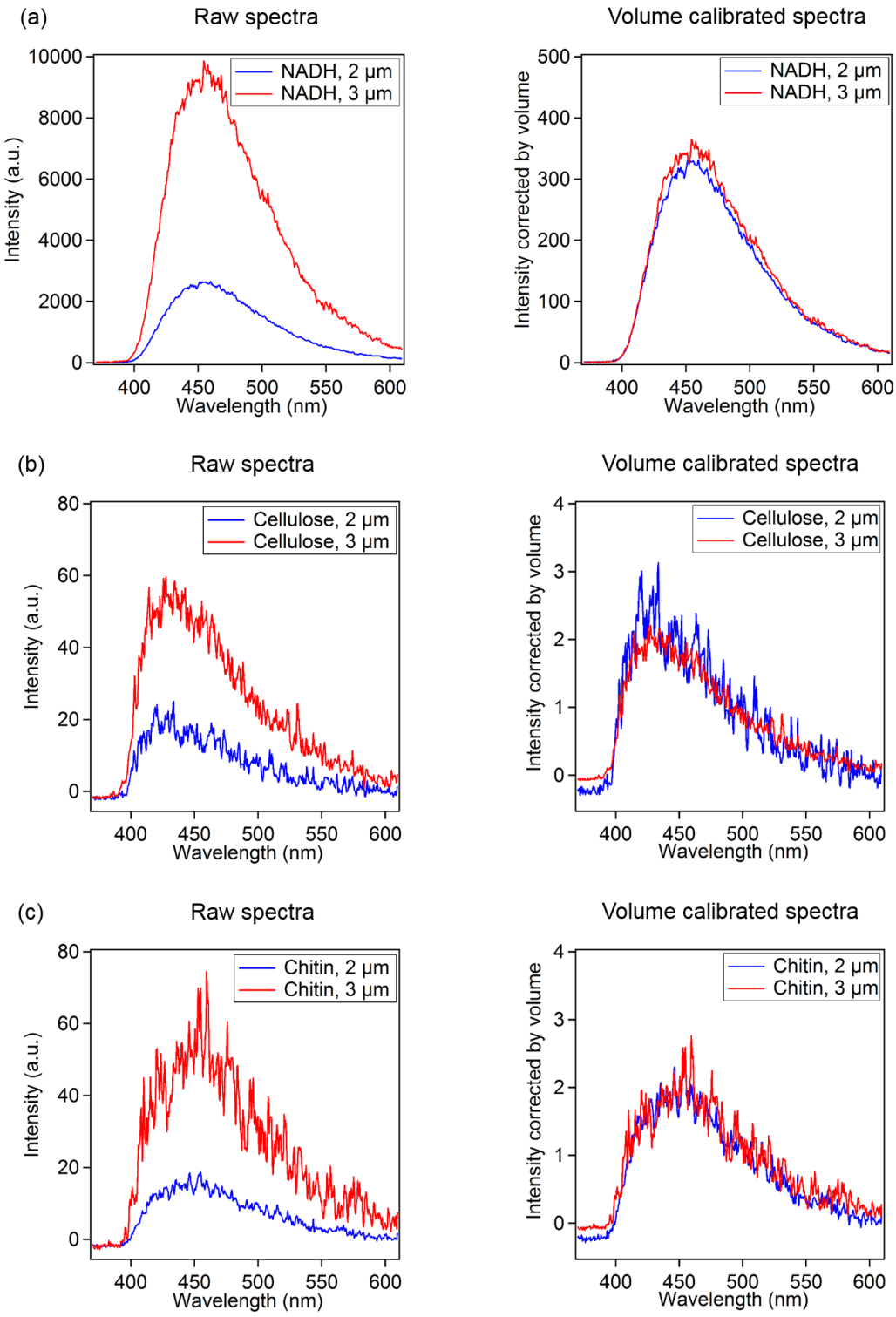

Figure 3. Raw fluorescence spectra of (**a**) NADH, (**b**) cellulose, and (**c**) chitin and the corresponding fluorescence spectra with the fluorescence intensity calibrated by volume. After calibration by volume, the spectra are nearly the same for particles of different sizes.

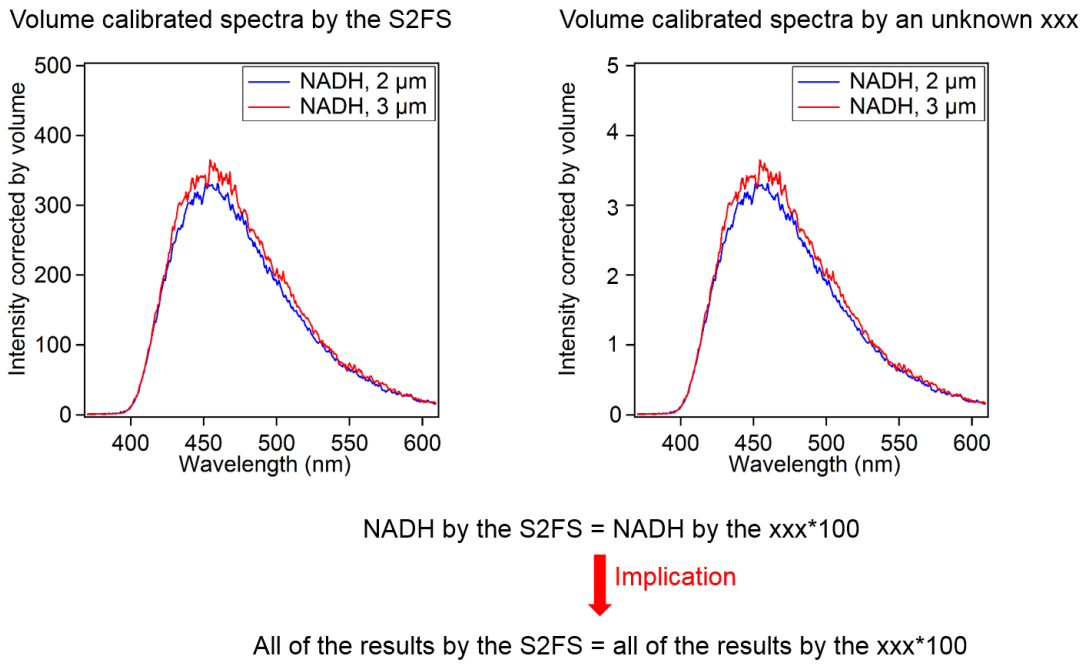

Figure 4. The implication of the volume calibrated fluorescence spectra. In principle, the calibration factor of NADH can be extended to all of the results including other chemicals and ambient measurement.

The volume calibrated fluorescence spectra measured by the S2FS can be compared to other instruments and the calibration factor can be calculated. Take NADH as an example, the peak intensity of volume calibrated spectra of NADH measured by the S2FS is ~350. Imagine the peak intensity of volume calibrated spectra of NADH measured by an unknown OFS (xxx) is ~3.5. The calibration factor is 100, which implies that all of the results measured by S2FS including other chemicals and ambient measurement equal to those measured by the unknown spectrometer times 100 (Figure 4).

4. Conclusion

In conclusion, NADH, cellulose, and chitin are good candidates for calibrating the fluorescence intensity of OFS. Robison et al. (Robinson et al., 2017) reported that NADH was unstable in solution due to the oxidation form (NAD^+). However, NADH was in the solid state during aerosolization and measurement in our method, which makes it a promising candidate for calibration.

The volume calibrated fluorescence spectra of particles with different sizes are nearly the same. This means the volume calibrated spectra depend on the species of chemicals and settings of OFS, rather than on the size of the particle. The calibration factor of NADH, cellulose, and chitin should be the same and can be used for atmospheric measurement results as well.

λ_{ex} and λ_{em} of the S2FS (λ_{ex} = 355 nm, λ_{em} = 370-610 nm) are similar to those of commonly used OFS including the Ultraviolet Aerodynamic Particle Sizer (UV-APS, λ_{ex} = 355 nm, λ_{em} = 420-575 nm) (Hairston et al., 1997; Huffman et al., 2012; Huffman et al., 2010; Schumacher et al., 2013), the Plair detector (Crouzy et al., 2016) (λ_{ex} = 337 nm, λ_{em} = 390-600 nm), and channel FL3 (λ_{ex} = 370 nm, λ_{em} = 420-650 nm) (Kaye et al., 2005; O'Connor et al., 2014; Robinson et al., 2013; Savage et al., 2017; Toprak and Schnaiter, 2013; Yu et al., 2016) of the WIBS. Therefore, the above results can be extended to these instruments as well.

Acknowledgements

We acknowledge the National Natural Science Foundation of China (91644218), EU-BACCHUS project (No. 603445), and Guangdong Innovative and Entrepreneurial Research Team Program (2016ZT06N263). J. Schneider is acknowledged for his kind help with UV-APS. M. Zhang would like to thank China Scholarship Council (CSC). This work is supported by the Max Planck Society (MPG).

Appendix A: List of acronyms and symbols

Acronym/Symbol	Description
a.u.	Arbitrary units
DMA	Differential mobility analyzer
NAD^+	Oxidation form of nicotinamide adenine dinucleotide
NADH	Nicotinamide adenine dinucleotide
OFS	Online/in situ Fluorescence Spectrometers
PBAP	Primary biological aerosol particles
S2FS	Size-resolved single-particle fluorescence spectrometer
UV-APS	Ultraviolet Aerodynamic Particle Sizer
WIBS	Wideband Integrated Bioaerosol Sensor
λ_{ex}	Excitation wavelength
λ_{em}	Emission wavelength

References

Brown, J. K. M. and Hovmoller, M. S.: Epidemiology - Aerial dispersal of pathogens on the global and continental scales and its impact on plant disease, Science, 297, 537-541, 2002.

Crawford, I., Gallagher, M. W., Bower, K. N., Choularton, T. W., Flynn, M. J., Ruske, S., Listowski, C., Brough, N., Lachlan-Cope, T., Fleming, Z. L., Foot, V. E., and Stanley, W. R.: Real-time detection of airborne fluorescent bioparticles in Antarctica, Atmos Chem Phys, 17, 14291-14307, 2017.

Crawford, I., Ruske, S., Topping, D. O., and Gallagher, M. W.: Evaluation of hierarchical agglomerative cluster analysis methods for discrimination of primary biological aerosol, Atmos Meas Tech, 8, 4979-4991, 2015.

Crouzy, B., Stella, M., Konzelmann, T., Calpini, B., and Clot, B.: All-optical automatic pollen identification: Towards an operational system, Atmos Environ, 140, 202-212, 2016.

Despres, V. R., Huffman, J. A., Burrows, S. M., Hoose, C., Safatov, A. S., Buryak, G., Frohlich-Nowoisky, J., Elbert, W., Andreae, M. O., Poschl, U., and Jaenicke, R.: Primary biological aerosol particles in the atmosphere: a review, Tellus B, 64, 2012.

Frohlich-Nowoisky, J., Kampf, C. J., Weber, B., Huffman, J. A., Pohlker, C., Andreae, M. O., Lang-Yona, N., Burrows, S. M., Gunthe, S. S., Elbert, W., Su, H., Hoor, P., Thines, E., Hoffmann, T., Despres, V. R., and Poschl, U.: Bioaerosols in the Earth system: Climate, health, and ecosystem interactions, Atmos Res, 182, 346-376, 2016.

Gabey, A. M., Gallagher, M. W., Whitehead, J., Dorsey, J. R., Kaye, P. H., and Stanley, W. R.: Measurements and comparison of primary biological aerosol above and below a tropical forest canopy using a dual channel fluorescence spectrometer, Atmos Chem Phys, 10, 4453-4466, 2010.

Hairston, P. P., Ho, J., and Quant, F. R.: Design of an instrument for real-time detection of bioaerosols using simultaneous measurement of particle aerodynamic size and intrinsic fluorescence, J Aerosol Sci, 28, 471-482, 1997.

Hill, S. C., Williamson, C. C., Doughty, D. C., Pan, Y. L., Santarpia, J. L., and Hill, H. H.: Size-dependent fluorescence of bioaerosols: Mathematical model using fluorescing and absorbing molecules in bacteria, J Quant Spectrosc Ra, 157, 54-70, 2015.

Huffman, J. A., Sinha, B., Garland, R. M., Snee-Pollmann, A., Gunthe, S. S., Artaxo, P., Martin, S. T., Andreae, M. O., and Poschl, U.: Size distributions and temporal variations of biological aerosol particles in the Amazon rainforest characterized by microscopy and real-time UV-APS fluorescence techniques during AMAZE-08, Atmos Chem Phys, 12, 11997-12019, 2012.

Huffman, J. A., Treutlein, B., and Poschl, U.: Fluorescent biological aerosol particle concentrations and size distributions measured with an Ultraviolet Aerodynamic Particle Sizer (UV-APS) in Central Europe, Atmos Chem Phys, 10, 3215-3233, 2010.

Kaye, P. H., Stanley, W. R., Hirst, E., Foot, E. V., Baxter, K. L., and Barrington, S. J.: Single particle multichannel bio-aerosol fluorescence sensor, Opt Express, 13, 3583-3593, 2005.

Lacey, J. and Dutkiewicz, J.: Bioaerosols and Occupational Lung-Disease, J Aerosol Sci, 25, 1371-1404, 1994.

Lawaetz, A. J. and Stedmon, C. A.: Fluorescence Intensity Calibration Using the Raman Scatter Peak of Water, Appl Spectrosc, 63, 936-940, 2009.

Limpouchova, Z. and Prochazka, K.: Theoretical Principles of Fluorescence Spectroscopy, Springer Ser Fluores, 16, 91-149, 2016.
O'Connor, D. J., Healy, D. A., Hellebust, S., Buters, J. T. M., and Sodeau, J. R.: Using the WIBS-4 (Waveband Integrated Bioaerosol Sensor) Technique for the On-Line Detection of Pollen Grains, Aerosol Sci Tech, 48, 341-349, 2014.
Pan, Y. L., Hill, S. C., Pinnick, R. G., House, J. M., Flagan, R. C., and Chang, R. K.: Dual-excitation-wavelength fluorescence spectra and elastic scattering for differentiation of single airborne pollen and fungal particles, Atmos Environ, 45, 1555-1563, 2011.
Pan, Y. L., Hill, S. C., Santarpia, J. L., Brinkley, K., Sickler, T., Coleman, M., Williamson, C., Gurton, K., Felton, M., Pinnick, R. G., Baker, N., Eshbaugh, J., Hahn, J., Smith, E., Alvarez, B., Prugh, A., and Gardner, W.: Spectrally-resolved fluorescence cross sections of aerosolized biological live agents and simulants using five excitation wavelengths in a BSL-3 laboratory, Opt Express, 22, 8165-8189, 2014.
Pan, Y. L., Pinnick, R. G., Hill, S. C., and Chang, R. K.: Particle-Fluorescence Spectrometer for Real-Time Single-Particle Measurements of Atmospheric Organic Carbon and Biological Aerosol, Environ Sci Technol, 43, 429-434, 2009.
Pinnick, R. G., Hill, S. C., Nachman, P., Videen, G., Chen, G., and Chang, R. K.: Aerosol fluorescence spectrum analyzer for rapid measurement of single micrometer-sized airborne biological particles, Aerosol Sci Tech, 28, 95-104, 1998.
Pohlker, C., Huffman, J. A., and Poschl, U.: Autofluorescence of atmospheric bioaerosols - fluorescent biomolecules and potential interferences, Atmos Meas Tech, 5, 37-71, 2012.
Robinson, E. S., Gao, R. S., Schwarz, J. P., Fahey, D. W., and Perring, A. E.: Fluorescence calibration method for single-particle aerosol fluorescence instruments, Atmos Meas Tech, 10, 1755-1768, 2017.
Robinson, N. H., Allan, J. D., Huffman, J. A., Kaye, P. H., Foot, V. E., and Gallagher, M.: Cluster analysis of WIBS single-particle bioaerosol data, Atmos Meas Tech, 6, 337-347, 2013.
Savage, N. J., Krentz, C. E., Konemann, T., Han, T. T., Mainelis, G., Pohlker, C., and Huffman, J. A.: Systematic characterization and fluorescence threshold strategies for the wideband integrated bioaerosol sensor (WIBS) using size-resolved biological and interfering particles, Atmos Meas Tech, 10, 4279-4302, 2017.
Schumacher, C. J., Pohlker, C., Aalto, P., Hiltunen, V., Petaja, T., Kulmala, M., Poschl, U., and Huffman, J. A.: Seasonal cycles of fluorescent biological aerosol particles in boreal and semi-arid forests of Finland and Colorado, Atmos Chem Phys, 13, 11987-12001, 2013.
Sivaprakasam, V., Lin, H. B., Huston, A. L., and Eversole, J. D.: Spectral characterization of biological aerosol particles using two-wavelength excited laser-induced fluorescence and elastic scattering measurements, Opt Express, 19, 6191-6208, 2011.
Toprak, E. and Schnaiter, M.: Fluorescent biological aerosol particles measured with the Waveband Integrated Bioaerosol Sensor WIBS-4: laboratory tests combined with a one year field study, Atmos Chem Phys, 13, 225-243, 2013.
Yu, X. W., Wang, Z. B., Zhang, M. H., Kuhn, U., Xie, Z. Q., Cheng, Y. F., Poschl, U., and Su, H.: Ambient measurement of fluorescent aerosol particles with a WIBS in the Yangtze River Delta of China: potential impacts of combustion-related aerosol particles, Atmos Chem Phys, 16, 11337-11348, 2016.

D.3 Zhang et al., in preparation, 2019

Fluorescence of fresh and aged biogenic secondary organic aerosols (SOA)

Author list to be modified or extended

Minghui Zhang,[†] Thorsten Hoffmann,[‡] Guo Li,[†] Uwe Kuhn,[†] Ulrich Pöschl,[†]

Hang Su,[*,§,†] and Yafang Cheng[*,†]

[†]Multiphase Chemistry Department, Max Planck Institute for Chemistry, 55128 Mainz, Germany

[‡]Institute for Inorganic and Analytical Chemistry, Johannes Gutenberg University of Mainz, Duesbergweg 10-14, Mainz 55128, Germany

[§] Center for Air pollution and Climate Change Research, Institute for Environmental and Climate Research (ECI), Jinan University, 511443 Guangzhou, China

Corresponding Author

[*]H. Su, Phone: +49 (0) 61313057300; e-mail: h.su@mpic.de

[*]Y. Cheng, Phone: +49 (0) 61313057200; e-mail: yafang.cheng@mpic.de

Fluorescence of fresh and aged biogenic secondary organic aerosols (SOA)

Author list to be modified or extended

Minghui Zhang,[†] Thorsten Hoffmann,[‡] Guo Li,[†] Uwe Kuhn,[†] Ulrich Pöschl,[†]

Hang Su,[*,§,†] and Yafang Cheng[*,†]

[†]Multiphase Chemistry Department, Max Planck Institute for Chemistry, 55128 Mainz, Germany

[‡]Institute for Inorganic and Analytical Chemistry, Johannes Gutenberg University of Mainz, Duesbergweg 10-14, Mainz 55128, Germany

[§] Center for Air pollution and Climate Change Research, Institute for Environmental and Climate Research (ECI), Jinan University, 511443 Guangzhou, China

Corresponding Author

[*]H. Su, h.su@mpic.de; [*]Y. Cheng, yafang.cheng@mpic.de

Abstract

Laser/light-induced fluorescence (LIF) is one of the commonly used techniques to analyze bioaerosols based on the fact that bioaerosols exhibit fluorescence under ultraviolet (UV) excitation. Fresh biogenic secondary organic aerosols (SOA) and aged SOA are potentially interfering particles since they have been reported to exhibit fluorescence in the liquid phase. Here we measured the fluorescence property of fresh SOA and aged SOA in the *particle* phase by using the recently developed size-resolved single-particle fluorescence spectrometer (S2FS). Fresh SOA were generated by the reaction of limonene or α-pinene with ozone (O_3) while aged SOA were generated by the reaction of limonene or α-pinene with ozone (O_3) in the presence of ammonia. Preliminary results show that fresh SOA exhibit fluorescence from 400-500 nm with the emission peaking at ~467 nm or ~478 nm while aged SOA cover a broader range from 400-610 nm with the emission peaking at ~480 nm with λ_{ex} = 355 nm. The fractions of fluorescent fresh SOA and fluorescent aged SOA are 1-4% and 6-10%, respectively. Relative humidity (RH) influences fluorescence of fresh SOA in the shorter wavelength while RH influences fluorescence aged SOA mainly in the longer wavelength.

1. Introduction

Primary biological aerosol particles (PBAP) are of great interest to atmospheric chemists[1, 2] and epidemiologists[3]. Part of the motivation is due to that PBAP are ubiquitous all over the world, no matter in the pristine Amazon rainforest[4] or in the industrialized megacity[5]. PBAP consist of viruses, bacteria and archaea, fungal and fern spores, pollen from vascular plants, algae and lichens from cryptogamic covers, and fragments of animal and plant matter[6].

The quantification of PBAP in the atmosphere is attracting more attention in recent years. Offline techniques enable measurement of the averaged information of PBAP over a certain period, which include staining particles with a protein dye[7], offline aerosol mass spectrometric technique (AMS)[8], and quantitative polymerase chain reaction analysis (qPCR)[9]. Online techniques can analyze the PBAP in real-time with high time-resolution, which include aerosol mass spectrometry[10, 11], laser-induced breakdown spectroscopy[12], and laser/light-induced fluorescence (LIF)[13-22].

LIF instruments can reveal the fraction of PBAP and concentration of PBAP[23] based on the fact that PBAP exhibit autofluorescence[24] under ultraviolet (UV) excitation. However, some potential interfering particles may also exhibit fluorescence under UV excitation such as combustion-related particles[25, 26], and secondary organic aerosols (SOA)[27] including aromatic organic acid aerosols[20].

Recently, Lee et al.[27] measured the fluorescence property of fresh SOA and aged SOA dissolved in water, which suggests that aged SOA particles may exhibit sufficient fluorescence to interfere with that of PBAP. However, the fluorescence property measured in the liquid phase[27] might be different from that measured in the *particle* phase. Besides, the interference of fresh SOA and aged SOA can not be quantified by measurement of SOA in the liquid phase.

Here we directly measured the fluorescence properties of fresh SOA and aged SOA in the *particle* phase by using the recently developed size-resolved single-particle fluorescence spectrometer (S2FS) (Figure 1). The fluorescence spectra of particles can be directly

obtained without dissolving them in water. Furthermore, the interference of fresh SOA and aged SOA can be quantified by measurement in the particle phase.

2. Experiment

2.1. Generation of fresh SOA and aged SOA

Fresh SOA and aged SOA were generated in a 0.7 m^3 Teflon chamber. Fresh SOA were generated by using the method according to Lee et al.[17]. In brief, ~400 ppb of O_3 was flushed through the chamber. O_3 was generated by photolysis of O_2 using an UV light (O_3 generator SOG-2). The O_3 concentrations were measured by an O_3 analyzer (Model 49*i*, Thermo Fisher Scientific, USA, lower detection limit: 1 ppbv). Then the outlets of the chamber were closed and the fan was turned on. Afterwards, 2 μL of *d*-limonene or *α*-pinene was flushed into the chamber by the compressed air with a flow rate of 4 LPM for 2 min, corresponding to a concentration of ~400 ppb assuming there was no loss. Then the inlet of the chamber was closed and the fan continued working for another 3 min. The reaction last 20 h in the darkness. According to Atkinson et al.[28], the OH radical formation yields from the gas phase reactions O_3 of with *d*-limonene or *α*-pinene were 0.86 and 0.85, respectively. Therefore, the particles measured are a mixture of O_3 and OH radical products.

For the generation of aged SOA, ~400 ppb of O_3 was flushed through the chamber. Then the outlets of the chamber were closed and the fan was turned on. ~0.18 M ammonia solution was flushed into the chamber with a flow rate of 0.5 LPM for 5 min. The concentration of ammonia in the chamber was ~50 ppm by using a cavity-ring-down spectroscopy. Afterwards, 2 μL of *d*-limonene or *α*-pinene was flushed into the chamber by the compressed air with a flow rate of 4 LPM for 2 min. Then the inlet of the chamber was closed and the fan continued working for another 3 min. The aging process last 20 h in the darkness.

After the generation of fresh SOA or aged SOA, the chamber outlet was connected to a differential mobility analyzer (DMA). The sheath flow of the DMA was 2 LPM and the aerosol flow was 1 LPM; the diameter was set to be 850 nm. Under this setting, the

concentration was high enough for the subsequent measurement. The DMA was then directly connected to the S2FS (Figure 1).

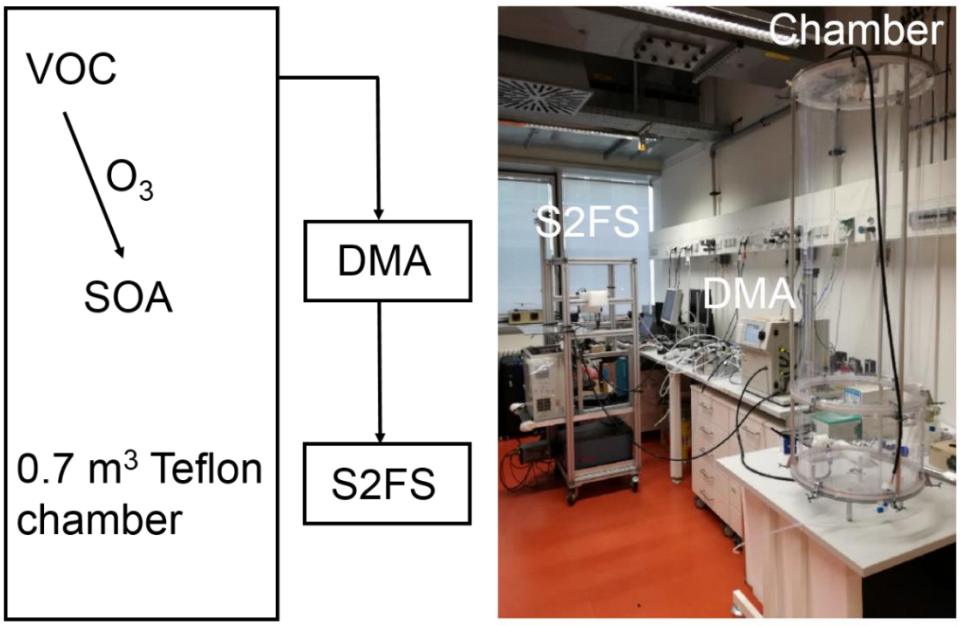

Figure 1. The construction of the reaction chamber and the size-resolved single-particle fluorescence spectrometer (S2FS). The SOA particles were selected by a differential mobility analyzer (DMA). Afterwards, the fluorescence property was directly measured by the S2FS.

2.2. Construction of the S2FS

The S2FS can measure the fluorescence property of the single particle in the *particle* phase. The aerosol flow was 1 LPM. λ_{ex} is 355 nm and the measured fluorescence emission is from 370 to 610 nm dispersed in 512 channels.

3. Results and discussion

3.1. Fluorescence spectra of fresh SOA and aged SOA

By using an offline fluorescence spectrometer, Lee et al.[27] observed the peak emission occurring at ~440 nm or ~450 nm for fresh SOA and aged SOA. To be more specific, aged-LIM/O_3 and aged-PIN/O_3 exhibited the peak emission at ~441 nm and ~440 nm, respectively[27]. Fresh LIM/O_3 (Control) and fresh PIN/O_3 (Control) exhibited the peak

emission at ~444 nm and ~454 nm, respectively[27]. The integrated fluorescence intensity of the aged SOA was 5-12 times higher than the corresponding fresh SOA[27].

A similar trend of fluorescence spectra and integrated fluorescence intensities was observed by the online fluorescence spectrometer S2FS. As shown in Figure 2, aged LIM/O_3 and aged PIN/O_3 exhibit the peak emission at ~480 nm and ~480 nm, respectively. Fresh LIM/O_3 (Control) and fresh PIN/O_3 (Control) exhibit the peak emission at ~467 nm and ~478 nm, respectively. Both fresh SOA and aged SOA in the *particle* phase exhibit the fluorescence peaking at a longer wavelength compared to that measured in the liquid phase[27].

Consistent with the offline results, the integrated fluorescence intensity of the aged SOA measured by the online spectrometer is 3-7 times higher than the corresponding fresh SOA.

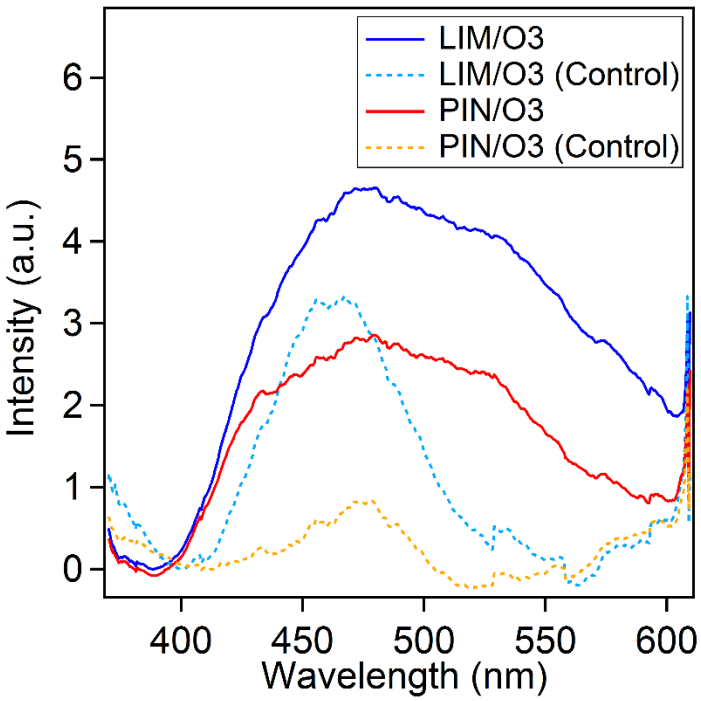

Figure 2. Fluorescence spectra of aged and fresh SOA (control) particles, which are averaged over 20,000 particles and smoothed over 64 pixels. Solid lines indicate aged SOA while dashed lines indicate fresh SOA (control).

3.2. Possible chemical compounds responsible for the fluorescence

The assignment of the fluorescence spectra to individual chemical compounds in mixtures of fresh SOA and aged SOA is based on the published literatures. The relatively weak fluorescence of fresh SOA is predictable since fresh SOA are dominated by molecules with carbonyl, carboxyl, and hydroxyl functional groups[29]. Carboxyl and hydroxyl functional groups have high-energy electronic transitions[29, 30] while carbonyl has relatively low-energy electronic transitions[30], thus having weak absorption and fluorescence properties.

The chemical compounds of aged SOA are attracting more attention in recent years[30]. Bones et al.[31] suggested that the fluorescence of aged SOA could be attributed to nitrogen containing aromatic heterocyclic compounds from intermediate imine compounds. Kampf et al.[32, 33] tested the light absorbance properties of a series of nitrogen containing compounds, among which a coupled 2,5-dimethylpyrrole unit and a substituted dihydropyridine have the absorbance maximum at around 355 nm[32]. Therefore, the nitrogen containing heterocycles including a coupled 2,5-dimethylpyrrole unit or a substituted dihydropyridine could possibly explain fluorescence of aged SOA.

3.3. Fractions of fluorescent particles of fresh SOA and aged SOA

To what extent do fresh SOA or aged SOA influence the LIF instruments is an unsolved question. We used thresholding mode of photon counting of ICCD camera to calculate the fractions of fluorescent particles. When the incoming intensity exceeds the defined threshold (set to be 200 in this study) at one pixel, the incoming intensity was recorded as one photon.

Aged-LIM/O_3 have the largest fraction of 10.9% while aged-PIN/O_3 have the fraction of 6.1%. Fresh LIM/O_3 (Control) also have a large fraction of 4.5% above the background threshold. Fresh LIM/O_3 (Control) have the smallest fraction of 1.4%, which is the nearly the same as that of NaCl. According a previous field measurement in Central Europe, the fractions of fluorescent submicron particles were between 1% and 10%[23]. The fractions of fluorescent particles of fresh SOA and aged SOA are in the same range as the fractions of fluorescent submicron particles. It could be that fresh SOA and aged SOA contribute to the

fluorescent particles to some degree in the submicron range but the effect of PBAP in the submicron range[11] can not be excluded.

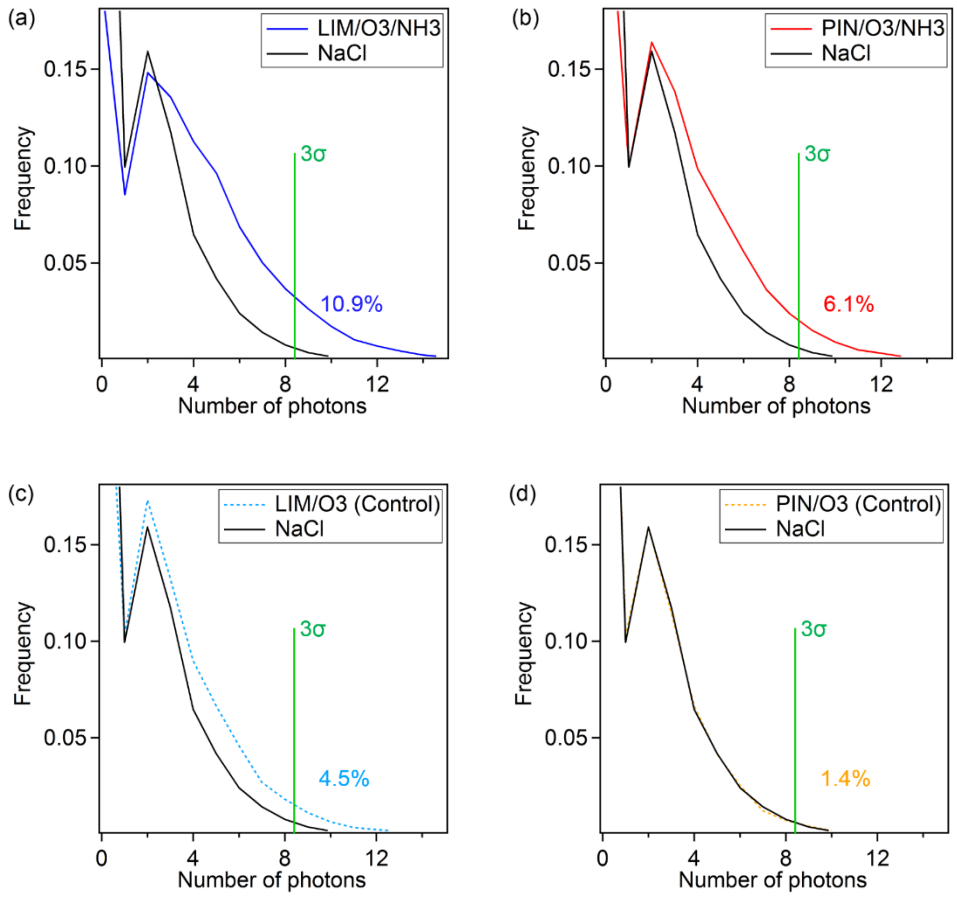

Figure 3. The distribution of number of photons for aged SOA and fresh SOA. Solid lines indicate aged SOA while dashed lines indicate fresh SOA (control). Fresh PIN/O3 reveal the same intensity distribution as that of NaCl.

3.4. Effect of relative humidity (RH)

The above results were measured when the initial RH of the chamber before reaction was 90%. A lower initial RH of 10% was also measured and the corresponding results were illustrated in Figure 4. The influence of RH on fresh SOA and aged SOA is different. For aged SOA, a decrease was observed in the longer wavelength when the RH decreased; meanwhile, for fresh SOA, a decrease was observed in the shorter wavelength when the

RH decreased (Figure 4). After subtraction, the aged SOA have a peak at ~ 530 nm while fresh SOA have a peak at ~470 nm (Figure 5).

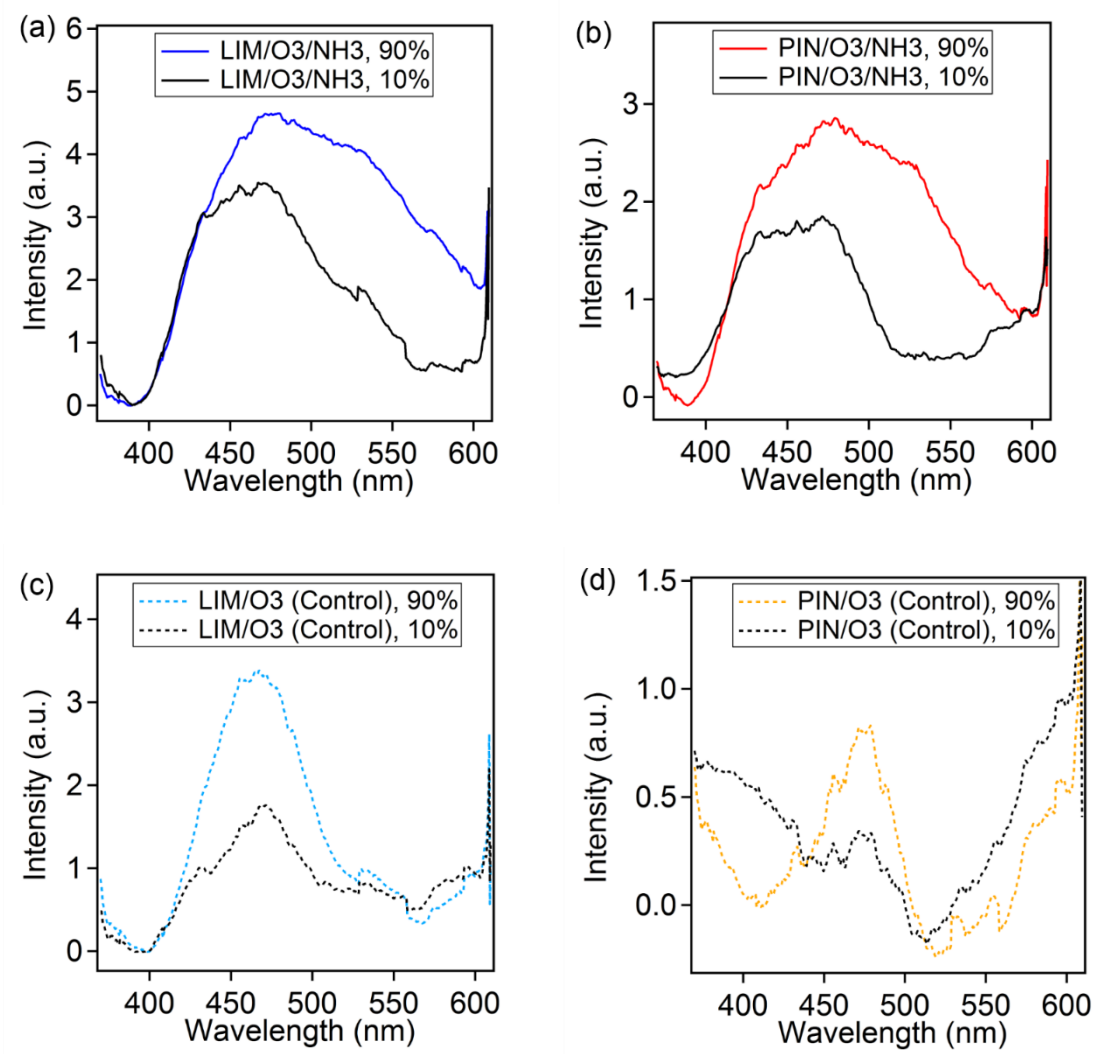

Figure 4. The fluorescence spectra of aged SOA and fresh SOA (control) under different relative humidities. The fluorescence spectra are averaged over 20,000 particles and smoothed over 64 pixels. Solid lines indicate aged SOA while dashed lines indicate fresh SOA (control).

One possible mechanism to explain the RH effect is that the hydration state of particles is different under different RH[14]. In order to test this mechanism, a Nafion dryer with a sheath flow of 5 LPM was used in front of the DMA. The fluorescence spectra of SOA particles with the Nafion dryer are nearly the same as those without the Nafion dryer (Figure 6),

suggesting that the difference of fluorescence is not caused by the hydration state of particles.

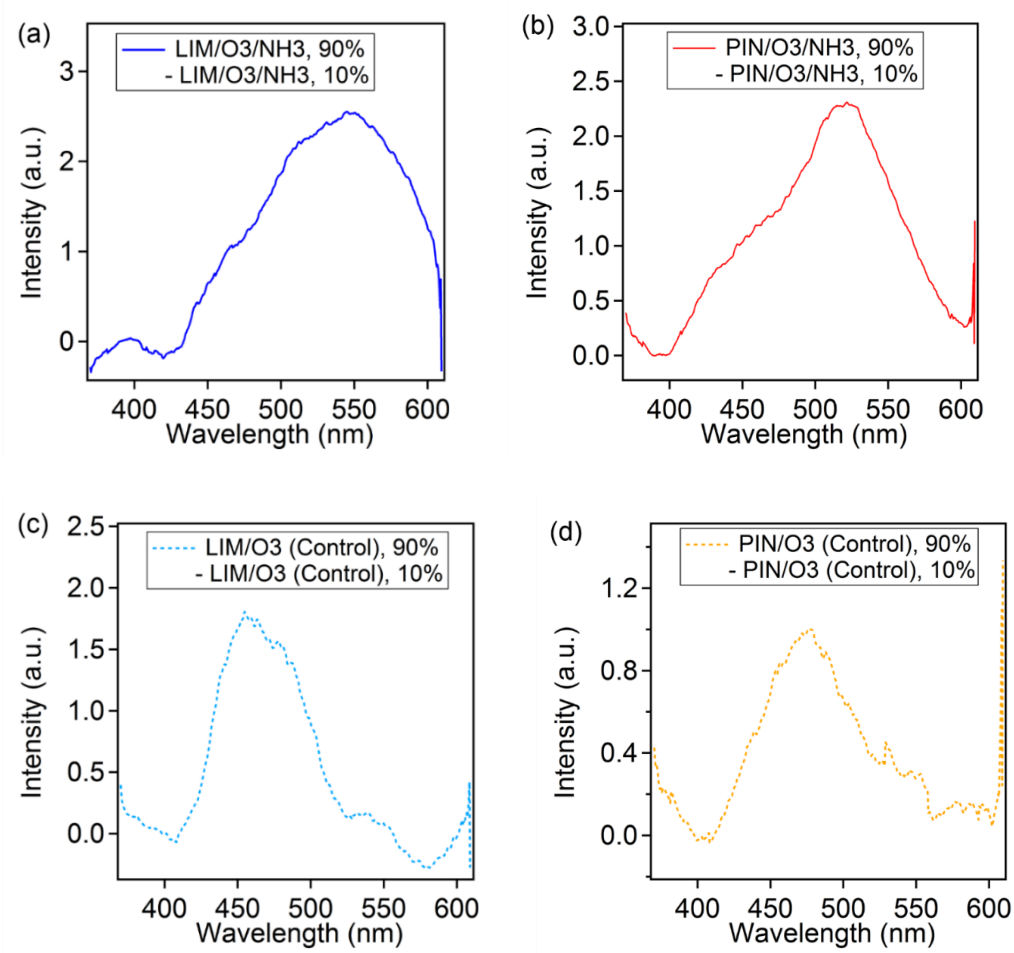

Figure 5. The subtracted fluorescence spectra of aged SOA and fresh SOA (control) under different relative humidities. The fluorescence spectra are averaged over 20,000 particles and smoothed over 64 pixels. Solid lines indicate aged SOA while dashed lines indicate fresh SOA (control).

The other possible mechanism is that RH influenced the final chemical compounds of particles[31, 34]. Nguyen et al.[34] demonstrated that when the relative humidity (RH) dropped and the droplets of aqueous solutions of biogenic SOA mixed with ammonium sulfate evaporated, the rate of chromophore formation increased by three orders of magnitude. Although the molar fraction of chromophores induced by RH was small (2%)[34], these products have a significant influence on the absorption property[34] and the fluorescence property of aerosol particles (Figure 4, 5).

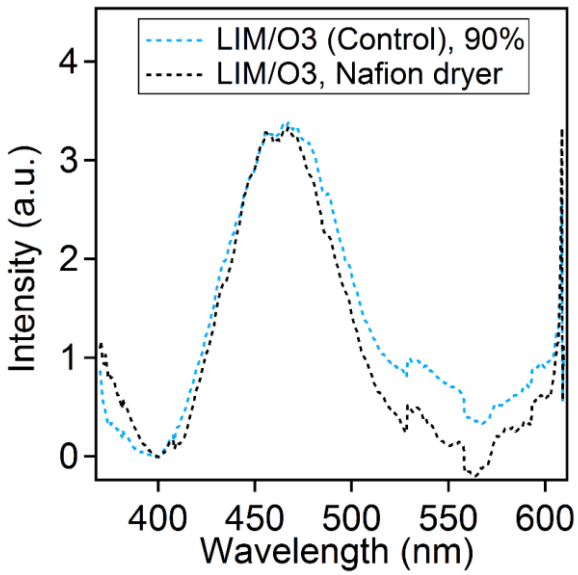

Figure 6. The fluorescence spectra of fresh LIM/O3 without (Control) a Nafion dryer and with a Nafion dryer. The fluorescence spectra are averaged over 20,000 particles and smoothed over 64 pixels.

4. Conclusions

In summary, the fluorescence spectra of fresh SOA and aged SOA were measured in the *particle* phase for the first time. Fresh SOA exhibit fluorescence from 400-500 nm with the emission peaking at ~467 nm or 478 nm while aged SOA cover a broader range from 400-610 nm with the emission peaking at ~480 nm. The fluorescence of fresh SOA could possibly be explained by carbonyl while the florescence of aged SOA could be due to nitrogen containing heterocycles. The fractions of fluorescent fresh SOA and fluorescent aged SOA account for1-4% and 6-10%, respectively. RH influences fluorescence of fresh SOA in the shorter wavelength while RH influences fluorescence of aged SOA in the longer wavelength. The fluorescence spectra of particles measured with the Nafion dryer and without the Nafion drier are nearly the same, suggesting that RH influences the chemical compositions of the SOA and aged SOA.

ACKNOWLEDGMENTS

We acknowledge the National Natural Science Foundation of China (91644218), EU-BACCHUS project (No. 603445), and Guangdong Innovative and Entrepreneurial Research Team Program (2016ZT06N263). J. Schneider is acknowledged for his kind help with UV-APS. M. Zhang would like to thank China Scholarship Council (CSC). This work is supported by the Max Planck Society (MPG).

References

1. Jones, A. M.; Harrison, R. M., The effects of meteorological factors on atmospheric bioaerosol concentrations - a review. *Sci Total Environ* **2004,** *326*, (1-3), 151-180.
2. Sun, J. M.; Ariya, P. A., Atmospheric organic and bio-aerosols as cloud condensation nuclei (CCN): A review. *Atmos Environ* **2006,** *40*, (5), 795-820.
3. Lacey, J.; Dutkiewicz, J., Bioaerosols and Occupational Lung-Disease. *J Aerosol Sci* **1994,** *25*, (8), 1371-1404.
4. Poschl, U.; Martin, S. T.; Sinha, B.; Chen, Q.; Gunthe, S. S.; Huffman, J. A.; Borrmann, S.; Farmer, D. K.; Garland, R. M.; Helas, G.; Jimenez, J. L.; King, S. M.; Manzi, A.; Mikhailov, E.; Pauliquevis, T.; Petters, M. D.; Prenni, A. J.; Roldin, P.; Rose, D.; Schneider, J.; Su, H.; Zorn, S. R.; Artaxo, P.; Andreae, M. O., Rainforest Aerosols as Biogenic Nuclei of Clouds and Precipitation in the Amazon. *Science* **2010,** *329*, (5998), 1513-1516.
5. Cao, C.; Jiang, W. J.; Wang, B. Y.; Fang, J. H.; Lang, J. D.; Tian, G.; Jiang, J. K.; Zhu, T. F., Inhalable Microorganisms in Beijing's PM2.5 and PM10 Pollutants during a Severe Smog Event. *Environ Sci Technol* **2014,** *48*, (3), 1499-1507.
6. Despres, V. R.; Huffman, J. A.; Burrows, S. M.; Hoose, C.; Safatov, A. S.; Buryak, G.; Frohlich-Nowoisky, J.; Elbert, W.; Andreae, M. O.; Poschl, U.; Jaenicke, R., Primary biological aerosol particles in the atmosphere: a review. *Tellus B* **2012,** *64*.
7. Jaenicke, R., Abundance of cellular material and proteins in the atmosphere. *Science* **2005,** *308*, (5718), 73-73.
8. Bozzetti, C.; Daellenbach, K. R.; Hueglin, C.; Fermo, P.; Sciare, J.; Kasper-Giebl, A.; Mazar, Y.; Abbaszade, G.; El Kazzi, M.; Gonzalez, R.; Shuster-Meiseles, T.; Flasch, M.; Wolf, R.; Krepelova, A.; Canonaco, F.; Schnelle-Kreis, J.; Slowik, J. G.; Zimmermann, R.; Rudich, Y.; Baltensperger, U.; El Haddad, I.; Prevot, A. S. H., Size-resolved Identification, Characterization and Quantification of Primary Biological Organic Aerosol at a European Rural Site (vol 50, pg 3425, 2016). *Environ Sci Technol* **2016,** *50*, (23), 13177-13178.
9. Peccia, J.; Hernandez, M., Incorporating polymerase chain reaction-based identification, population characterization, and quantification of microorganisms into aerosol science: A review. *Atmos Environ* **2006,** *40*, (21), 3941-3961.
10. van Wuijckhuijse, A. L.; Stowers, M. A.; Kleefsman, W. A.; van Baar, B. L. M.; Kientz, C. E.; Marijnissen, J. C. M., Matrix-assisted laser desorption/ionisation aerosol

time-of-flight mass spectrometry for the analysis of bioaerosols: development of a fast detector for airborne biological pathogens. *J Aerosol Sci* **2005,** *36*, (5-6), 677-687.
11. Schneider, J.; Freutel, F.; Zorn, S. R.; Chen, Q.; Farmer, D. K.; Jimenez, J. L.; Martin, S. T.; Artaxo, P.; Wiedensohler, A.; Borrmann, S., Mass- spectrometric identification of primary biological particle markers and application to pristine submicron aerosol measurements in Amazonia. *Atmos Chem Phys* **2011,** *11*, (22), 11415-11429.
12. Hybl, J. D.; Lithgow, G. A.; Buckley, S. G., Laser-induced breakdown spectroscopy detection and classification of biological aerosols. *Appl Spectrosc* **2003,** *57*, (10), 1207-1215.
13. Hill, S. C.; Pinnick, R. G.; Niles, S.; Pan, Y. L.; Holler, S.; Chang, R. K.; Bottiger, J.; Chen, B. T.; Orr, C. S.; Feather, G., Real-time measurement of fluorescence spectra from single airborne biological particles. *Field Anal Chem Tech* **1999,** *3*, (4-5), 221-239.
14. Ruske, S.; Topping, D. O.; Foot, V. E.; Kaye, P. H.; Stanley, W. R.; Crawford, I.; Morse, A. P.; Gallagher, M. W., Evaluation of machine learning algorithms for classification of primary biological aerosol using a new UV-LIF spectrometer. *Atmos Meas Tech* **2017,** *10*, (2), 695-708.
15. Huang, H. C.; Pan, Y. L.; Hill, S. C.; Pinnick, R. G.; Chang, R. K., Real-time measurement of dual-wavelength laser-induced fluorescence spectra of individual aerosol particles. *Opt Express* **2008,** *16*, (21), 16523-16528.
16. Pan, Y. L.; Pinnick, R. G.; Hill, S. C.; Chang, R. K., Particle-Fluorescence Spectrometer for Real-Time Single-Particle Measurements of Atmospheric Organic Carbon and Biological Aerosol. *Environ Sci Technol* **2009,** *43*, (2), 429-434.
17. Gabey, A. M.; Gallagher, M. W.; Whitehead, J.; Dorsey, J. R.; Kaye, P. H.; Stanley, W. R., Measurements and comparison of primary biological aerosol above and below a tropical forest canopy using a dual channel fluorescence spectrometer. *Atmos Chem Phys* **2010,** *10*, (10), 4453-4466.
18. Huffman, J. A.; Sinha, B.; Garland, R. M.; Snee-Pollmann, A.; Gunthe, S. S.; Artaxo, P.; Martin, S. T.; Andreae, M. O.; Poschl, U., Size distributions and temporal variations of biological aerosol particles in the Amazon rainforest characterized by microscopy and real-time UV-APS fluorescence techniques during AMAZE-08. *Atmos Chem Phys* **2012,** *12*, (24), 11997-12019.
19. Kiselev, D.; Bonacina, L.; Wolf, J. P., A flash-lamp based device for fluorescence detection and identification of individual pollen grains. *Rev Sci Instrum* **2013,** *84*, (3).
20. Saari, S. E.; Putkiranta, M. J.; Keskinen, J., Fluorescence spectroscopy of atmospherically relevant bacterial and fungal spores and potential interferences. *Atmos Environ* **2013,** *71*, 202-209.
21. Healy, D. A.; Huffman, J. A.; O'Connor, D. J.; Pohlker, C.; Poschl, U.; Sodeau, J. R., Ambient measurements of biological aerosol particles near Killarney, Ireland: a comparison between real-time fluorescence and microscopy techniques. *Atmos Chem Phys* **2014,** *14*, (15), 8055-8069.
22. Ratnesar-Shumate, S.; Pan, Y. L.; Hill, S. C.; Kinahan, S.; Corson, E.; Eshbaugh, J.; Santarpia, J. L., Fluorescence spectra and biological activity of aerosolized bacillus spores and MS2 bacteriophage exposed to ozone at different relative humidities in a rotating drum. *J Quant Spectrosc Ra* **2015,** *153*, 13-28.

23. Huffman, J. A.; Treutlein, B.; Poschl, U., Fluorescent biological aerosol particle concentrations and size distributions measured with an Ultraviolet Aerodynamic Particle Sizer (UV-APS) in Central Europe. *Atmos Chem Phys* **2010,** *10*, (7), 3215-3233.
24. Pohlker, C.; Huffman, J. A.; Poschl, U., Autofluorescence of atmospheric bioaerosols - fluorescent biomolecules and potential interferences. *Atmos Meas Tech* **2012,** *5*, (1), 37-71.
25. Yu, X. W.; Wang, Z. B.; Zhang, M. H.; Kuhn, U.; Xie, Z. Q.; Cheng, Y. F.; Poschl, U.; Su, H., Ambient measurement of fluorescent aerosol particles with a WIBS in the Yangtze River Delta of China: potential impacts of combustion-related aerosol particles. *Atmos Chem Phys* **2016,** *16*, (17), 11337-11348.
26. Pan, Y. L.; Houck, J. D. T.; Clark, P. A.; Pinnick, R. G., Single particle size and fluorescence spectra from emissions of burning materials in a tube furnace to simulate burn pits. *Appl Phys B-Lasers O* **2013,** *112*, (1), 89-98.
27. Lee, H. J.; Laskin, A.; Laskin, J.; Nizkorodov, S. A., Excitation-Emission Spectra and Fluorescence Quantum Yields for Fresh and Aged Biogenic Secondary Organic Aerosols. *Environ Sci Technol* **2013,** *47*, (11), 5763-5770.
28. Atkinson, R.; Aschmann, S. M.; Arey, J.; Shorees, B., Formation of Oh Radicals in the Gas-Phase Reactions of O3 with a Series of Terpenes. *J Geophys Res-Atmos* **1992,** *97*, (D5), 6065-6073.
29. Larsen, B. R.; Lahaniati, M.; Calogirou, A.; Kotzias, D., Atmospheric oxidation products of terpenes: A new nomenclature. *Chemosphere* **1998,** *37*, (6), 1207-1220.
30. Laskin, A.; Laskin, J.; Nizkorodov, S. A., Chemistry of Atmospheric Brown Carbon. *Chem Rev* **2015,** *115*, (10), 4335-4382.
31. Bones, D. L.; Henricksen, D. K.; Mang, S. A.; Gonsior, M.; Bateman, A. P.; Nguyen, T. B.; Cooper, W. J.; Nizkorodov, S. A., Appearance of strong absorbers and fluorophores in limonene-O-3 secondary organic aerosol due to NH4+-mediated chemical aging over long time scales. *J Geophys Res-Atmos* **2010,** *115*.
32. Kampf, C. J.; Filippi, A.; Zuth, C.; Hoffmann, T.; Opatz, T., Secondary brown carbon formation via the dicarbonyl imine pathway: nitrogen heterocycle formation and synergistic effects. *Phys Chem Chem Phys* **2016,** *18*, (27), 18353-18364.
33. Kampf, C. J.; Jakob, R.; Hoffmann, T., Identification and characterization of aging products in the glyoxal/ammonium sulfate system - implications for light-absorbing material in atmospheric aerosols. *Atmos Chem Phys* **2012,** *12*, (14), 6323-6333.
34. Nguyen, T. B.; Lee, P. B.; Updyke, K. M.; Bones, D. L.; Laskin, J.; Laskin, A.; Nizkorodov, S. A., Formation of nitrogen- and sulfur-containing light-absorbing compounds accelerated by evaporation of water from secondary organic aerosols. *J Geophys Res-Atmos* **2012,** *117*.

D.4 Yu et al., Atmos. Chem. Phys., 2018

Ambient measurement of fluorescent aerosol particles with a WIBS in the Yangtze River Delta of China: potential impacts of combustion-related aerosol particles

Xiawei Yu[1,2], Zhibing Wang[2], **Minghui Zhang**[2], Uwe Kuhn[2], Zhouqing Xie[1], Yafang Cheng[2], Ulrich Pöschl[2], Hang Su[2]

[1]School of Earth and Space Sciences, University of Science and Technology of China, Hefei 230026, China

[2]Multiphase Chemistry Department, Max Planck Institute for Chemistry, Mainz 55128, Germany

Correspondence to Zhibin Wang (Zhibin.Wang@mpic.de) and Zhouqing Xie (zqxie@ustc.edu.cn)

Atmos. Chem. Phys., 16, 11337–11348, 2016
www.atmos-chem-phys.net/16/11337/2016/
doi:10.5194/acp-16-11337-2016

Atmospheric Chemistry and Physics Open Access EGU

Ambient measurement of fluorescent aerosol particles with a WIBS in the Yangtze River Delta of China: potential impacts of combustion-related aerosol particles

Xiawei Yu[1,2], Zhibin Wang[2], Minghui Zhang[2], Uwe Kuhn[2], Zhouqing Xie[1], Yafang Cheng[2], Ulrich Pöschl[2], and Hang Su[2]

[1]School of Earth and Space Sciences, University of Science and Technology of China, Hefei 230026, China
[2]Multiphase Chemistry Department, Max Planck Institute for Chemistry, Mainz 55128, Germany

Correspondence to: Zhibin Wang (zhibin.wang@mpic.de) and Zhouqing Xie (zqxie@ustc.edu.cn)

Received: 15 March 2016 – Published in Atmos. Chem. Phys. Discuss.: 17 March 2016
Revised: 29 July 2016 – Accepted: 23 August 2016 – Published: 13 September 2016

Abstract. Fluorescence characteristics of aerosol particles in a polluted atmosphere were studied using a wideband integrated bioaerosol spectrometer (WIBS-4A) in Nanjing, Yangtze River Delta area of China. We observed strong diurnal and day-to-day variations of fluorescent aerosol particles (FAPs). The average number concentrations of FAPs (1–15 µm) detected in the three WIBS measurement channels (FL1: 0.6 cm^{-3}, FL2: 3.4 cm^{-3}, FL3: 2.1 cm^{-3}) were much higher than those observed in forests and rural areas, suggesting that FAPs other than bioaerosols were detected. We found that the number fractions of FAPs were positively correlated with the black carbon mass fraction, especially for the FL1 channel, indicating a large contribution of combustion-related aerosols. To distinguish bioaerosols from combustion-related FAPs, we investigated two classification schemes for use with WIBS data. Our analysis suggests a strong size dependence for the fractional contributions of different types of FAPs. In the FL3 channel, combustion-related particles seem to dominate the 1–2 µm size range while bioaerosols dominate the 2–5 µm range. The number fractions of combustion-related particles and non-combustion-related particles to total aerosol particles were ∼ 11 and ∼ 5 %, respectively.

1 Introduction

From the beginning of atmospheric aerosol studies, airborne biological particles have been found as an important class of aerosol particles (Bary et al., 1887; Després et al., 2012; Fröhlich-Nowoisky et al., 2016). They are ubiquitous in the atmosphere with a wide size range from approximately several nanometers to a few hundred micrometers (Pöschl, 2005; Després et al., 2012). Primary biological aerosol particles (PBAPs) are a subset of biological particles, usually defined as the aerosols of biological origin or carry living organisms, including viruses, bacteria, fungal, pollen, cell or plant debris, and animal tissue (Huffman et al., 2012; Fröhlich-Nowoisky et al., 2016). PBAPs can affect the Earth's radiation balance directly by absorbing and scattering solar radiation, and indirectly by serving as giant cloud condensation nuclei (CCN) and ice nuclei (IN), and thereby influence cloud microphysical and climate-relevant properties (Christner et al., 2008; Pöschl et al., 2010; Deleon-Rodriguez et al., 2013; Morris et al., 2013). These impacts are not only restricted to a local scale, but also may be effective in a regional scale due to the transport of bioaerosols, e.g., by dust storms (Griffin, 2007; Polymenakou et al., 2008; Hallar et al., 2011; Creamean et al., 2013). In addition, PBAPs can spread human, animal, and plant disease and influence public health (Després et al., 2012; Cao et al., 2014). Considering its comprehensive impacts in diverse scientific fields, a better understanding of PBAPs such as its concentration, composition, and spatial and temporal variability becomes critically important.

Table 1. Definition of abbreviations used in the text.

Short name	Description
PBAPs	Primary biological aerosol particles
FAPs	Fluorescent aerosol particles
FL1	Fluorescent particles detected in channel FL1_280 (excitation at 280 nm, detection 310–400 nm)
FL2	Fluorescent particles detected in channel FL2_280 (excitation at 280 nm, detection 420–650 nm)
FL3	Fluorescent particles detected in channel FL2_370 (excitation at 370 nm, detection 420–650 nm)
Type A	Fluorescent particles detected in channel FL1 only
Type B	Fluorescent particles detected in channel FL2 only
Type C	Fluorescent particles detected in channel FL3 only
Type AB	Fluorescent particles detected in channels FL1 and FL2
Type AC	Fluorescent particles detected in channels FL1 and FL3
Type BC	Fluorescent particles detected in channels FL2 and FL3
Type ABC	Fluorescent particles detected in channels FL1, FL2 and FL3
N_x	Number concentration of each type particles
F_x	Number fraction of each type particles
M_{BC}	Mass concentration of black carbon
$PM_{0.8}$	Mass concentration of particles in the size range of 0.006–0.8 µm
D_o	Optical diameter
a.u.	Arbitrary units

Despite its importance, information of PBAPs in the atmosphere is still very limited. Further investigation is hindered due to the lack of automatic measurement techniques. Most previous studies are based on the analysis of cultivable PBAPs or DNA (deoxyribonucleic acid) from filter samples (Henningson and Ahlberg, 1994; Duchaine et al., 2001; Yu et al., 2013; Fröhlich-Nowoisky et al., 2016). These methods are time-consuming and their results may differ depending on the cultivation condition and procedures, especially considering the ubiquity of microorganisms that cannot be cultivated (Oliver, 2005; Pöhlker et al., 2012). The low time resolution of cultivation methods makes it difficult to investigate the emission mechanisms of PBAPs, which happen at a timescale of less than a few hours.

Since most biological materials contain fluorophores, instruments based on the fluorescence detection, such as a UV-APS (ultraviolet aerodynamic particle sizer; Brosseau et al., 2000), WIBS (wideband integrated bioaerosol spectrometer), and other custom-made instruments based on the LIF (laser induced fluorescence) technology (Pan et al., 2009; Taketani et al., 2013; Miyakawa et al., 2015), have recently been developed for online measurements of PBAPs. These instruments have been applied in various atmospheric environments, including rainforest (Gabey et al., 2010; Huffman et al., 2012), forest (Huffman et al., 2013; Schumacher et al., 2013; Crawford et al., 2014), high-altitude (Gabey et al., 2013; Valsan et al., 2016), rural (Healy et al., 2014), suburban (Huffman et al., 2010; Toprak and Schnaiter, 2013), and urban environments (Gabey et al., 2011; Miyakawa et al., 2015; Wei et al., 2016). Besides settled sampling sites, a WIBS has also been used for airborne observations (Perring et al., 2015). In clean environments, these techniques can effectively distinguish PBAPs from other kinds of aerosol particles. For example, Huffman et al. (2012) found similar size distributions of PBAPs measured by UV-APS and scanning electron microscopy (SEM) in the Amazon rainforest.

PBAPs, however, are not the only fluorescent aerosol particles (FAPs) in the atmosphere. Other materials such as polycyclic aromatic hydrocarbons (PAHs) and humic-like substances (HULIS) may also fluoresce and contribute to the measured fluorescence signals (Pöhlker et al., 2012). Hence, the fluorescence information given by the instruments based on the fluorescence detection may include both fluorescent biological and non-biological particles.

In order to have a deeper insight into the ambient FAPs in a polluted area, we have performed WIBS measurements in Nanjing, China, in the autumn of 2013. In this study, we first present the number concentration of FAPs in Nanjing in comparison to previous studies. Then we demonstrate the potential impacts of combustion-related aerosol particles in discrimination of bioaerosols under the polluted atmosphere. Finally, we introduce alternative methods to quantify the relative contributions of different fluorescent materials (combustion- and bioaerosol-type particles) to FAPs.

2 Methods and instrumentation

2.1 Site description

WIBS measurements were performed at the Station for Observing Regional Processes of the Earth System (SORPES station), Xianlin campus of Nanjing University (32.12° N, 118.95° E). Nanjing lies in the Yangtze River Delta with a total population of 8.18 million (data of 2013), and it is a

Table 2. Comparisons between the results of this study and previous studies. Unit for the number concentration of fluorescent particles is L^{-1}. Numbers in parentheses are the number fractions of fluorescent particles (%).

Site location	Site category	Season	N_{FL1}	N_{FL2}	N_{FL3}	N_{FAPs}	References
Nanjing, China	sub-urban	autumn	570 (4.6)	3350 (25.3)	2090 (15.6)	–	This study
Manchester, UK	urban	winter	29 (3)	52 (6)	110 (11)	–	Gabey et al. (2011)
Puy de Dôme mountain, France	high-altitude	summer	12 (4.4)	–	95 (35.2)	–	Gabey et al. (2013)
Killarney, Ireland	rural	summer	175 (0.5)	95 (0.3)	35 (0.1)	15 (0.05)[a]	Healy et al. (2014)
Borneo, Malaysis	rainforest	summer	–	–	–	150[b]	Gabey et al. (2010)
Karlsruhe, Germany	semi-rural	1 year	–	–	–	31 (7.3)[b]	Toprak and Schnaiter (2013)
Amazon, Brazil	rainforest	spring	–	–	–	93 (26.3)[a]	Huffman et al. (2012)
Mainz, Germany	semi-urban	summer, autumn, winter	–	–	–	27 (3.9)[a]	Huffman et al. (2010)
Helsinki, Finland	urban	summer	–	–	–	13 (8)[a]	Saari et al. (2015)
Hyytiälä, Finland	boreal forest	spring	–	–	–	15 (4.4)[a]	Schumacher et al. (2013)
		summer	–	–	–	46 (13)[a]	
		autumn	–	–	–	27 (9.8)[a]	
		winter	–	–	–	4 (1.1)[a]	
Colorado, USA	rural	spring	–	–	–	15 (2.5)[a]	Schumacher et al. (2013)
		summer	–	–	–	30 (8.8)[a]	
		autumn	–	–	–	17 (5.7)[a]	
		winter	–	–	–	5.3 (3)[a]	
Ghats, India	high-altitude	summer				20 (2)[a]	Valsan et al. (2016)

[a] Results of UV-APS. [b] Combine with the FL1 and FL3 channels.

large commercial center in the East China region. The measurement site is ∼ 20 km to the east of the urban center. The SORPES station is located on a hill about 40 m above the surroundings. Details of this station were described by Ding et al. (2013). A 0.75 inch stainless-steel tube inlet was installed ∼ 3 m above the roof, and sample air was dried by a vertical silica gel drier prior to entering the WIBS. Data were collected from 29 October to 15 November 2013.

2.2 Instruments

Measurements of FAPs were performed with a WIBS-4A. It uses the single-particle elastic scattering intensity at 535 nm to calculate the optical size of particles. The scattering signal is used to trigger the flash of two xenon lamps with a UV wavelength of 280 and 370 nm, respectively. The fluorescent signals are recorded at two wavelength bands (310–400 and 420–650 nm). This design results in three wavelength channels: FL1 with excitation at 280 nm and detection 310–400 nm, FL2 with excitation wavelength at 280 nm and detection wavelength at 420–650 nm, and FL3 with excitation wavelength at 370 nm and detection wavelength at 420–650 nm. Respective abbreviations are listed in Table 1. During the measurement period, we used 1 and 2 µm fluorescent and non-fluorescent PSL microspheres (3K-990, B0100, 4K-02 and B0200, Duke Scientific, Inc.) for calibration. The fluorescence noise threshold is defined as

$$E_{\text{Threshold}} = E + 3\sigma, \quad (1)$$

where E is the modal baseline and σ is the standard deviations in each channel. Particles with fluorescence signals above the noise threshold are classified as FAPs. Single-particle data were converted into a size distribution with a 5 min integration time and particles with an optical diameter (D_o) of 1–15 µm were analyzed in this study.

Meteorological data were collected with an automatic weather station (AG1000, CAMPBEL co.). The differential mobility particle sizer (DMPS; built at Helsinki University) was used to measure the number size distribution of submicron particles between 6 and 800 nm mobility diameter (Herrmann et al., 2014). Particle mass concentration below 0.8 µm ($PM_{0.8}$) was calculated from the measured size distributions assuming a density of 1.6 g cm^{-3} (Wang et al., 2014). A 7-wavelength "Spectrum" Aethalometer (AE-31, Magee Scientific co.) was used to measure the black carbon (BC) mass concentration M_{BC}.

3 Results and discussion

3.1 Non-biological fluorescent aerosol particles

Figure 1 shows the time series of number concentrations and fractions of FAPs during the measurement period. The number concentration of FAPs was dominated by the FL2 channel with a mean number concentration N_{FL2} of 3.4 cm^{-3}, followed by N_{FL3} of 2.1 cm^{-3}, and N_{FL1} of 0.6 cm^{-3}. These number concentrations were 1–2 orders of magnitudes higher

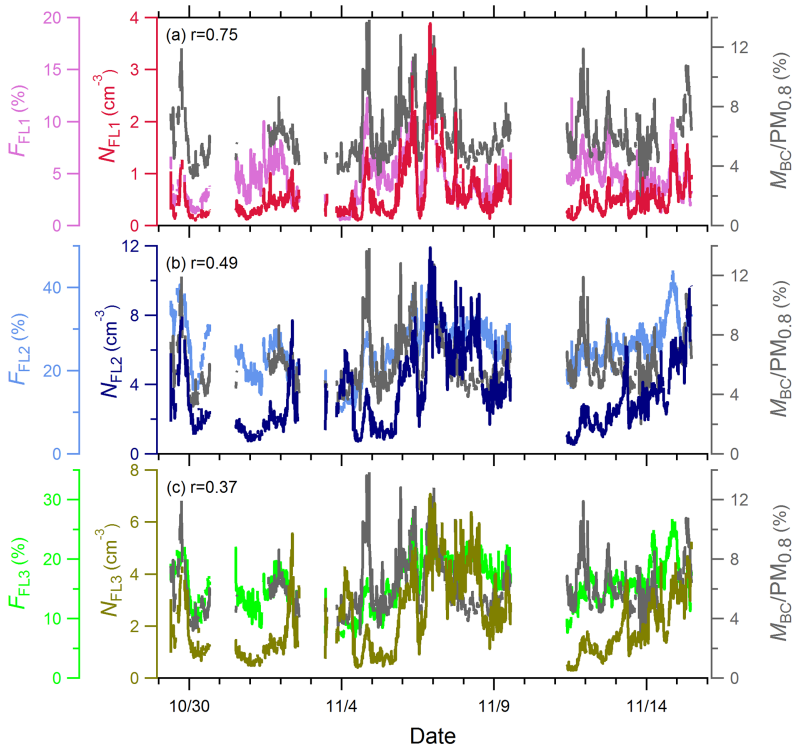

Figure 1. Time series of $M_{BC}/PM_{0.8}$ (gray, right axis), number concentration of fluorescent particles in each channel (primary left axis) and relative number fractions of fluorescent particles in each channel (secondary left axis). **(a)** FL1 channel: N_{FL1} (crimson) and F_{FL1} (orchid). **(b)** FL2 channel: N_{FL2}, (navy) and F_{FL2} (cornflower blue). **(c)** FL3 channel: N_{FL3} (olive) and F_{FL3} (lime). r is the correlation coefficient between F_x and $M_{BC}/PM_{0.8}$.

than those observed in clean areas where bioaerosols dominate the FAPs (Table 2). For example, FAPs of 0.093, 0.15, and 0.023 cm^{-3} were reported for the Amazon, Borneo, and Hyytiälä forests, respectively (Gabey et al., 2010; Huffman et al., 2012; Toprak and Schnaiter, 2013). Since polluted areas are characterized by fewer plants and natural biological processes, fewer bioaerosols are expected compared to the forests. This much higher number concentration of FAPs observed in Nanjing suggests other kinds of FAPs being detected by a WIBS.

Previous studies (Pöhlker et al., 2012; Miyakawa et al., 2015; Perring et al., 2015) reported that non-biological compounds like PAHs, mineral dust, and HULIS can also fluoresce. Several non-biological fluorophores such as SOA (secondary organic aerosol), pyrene, humic acid, and naphthalene have fluorescent property in the same excitation and emission wavelength bands as the FL1 channel (Chang and Thompson, 2010; Pöhlker et al., 2012). These materials originate from sources different from bioaerosols. For example, PAHs enrich on the surface of soot particles from biomass burning and fuel combustion, challenging the interpretation of ambient particle fluorescence measurements.

Our sampling site is located in the vicinity of the polluted Nanjing city and is intensively affected by human activities. To check the potential influences of PAHs and combustion processes, we compared the variability of FAPs with that of BC, on which the PAHs are often coated. To minimize the impacts of transport and boundary layer dynamics, we compared the ratio of BC and FAPs to the total particles in their respective size range, i.e., $M_{BC}/PM_{0.8}$ and F_x, instead of using absolute concentrations. Miyakawa et al. (2015) used factor analysis based on carbon monoxide, elemental carbon, and other markers (using concentration instead of ratio) to identify "combustion-type" and "dust-type" aerosols in urban areas. In our study, we found that $M_{BC}/PM_{0.8}$ showed a good correlation with the number fraction of FAPs, especially in the FL1 channel ($r = 0.75$, Fig. 1). For the FL2 and FL3 channels, the number fractions also nicely followed the variation of $M_{BC}/PM_{0.8}$ except for 8 November, which deteriorated the overall correlation. Since BC and PAHs are products of incomplete combustion, the similar variability suggests a large contribution from combustion-related aerosols to the measured FAPs, especially in the FL1 channel. Our findings strongly support the previous results (Toprak and Schnaiter, 2013; Miyakawa et al., 2015) that FAPs (FL1 channel) may come from the combustion process and anthropogenic interference.

Table 3. Integrated number concentrations (cm^{-3}) of each FAPs and fractions (%) of FAPs number concentrations to the total particle number concentrations. Type AC is not listed.

Category	25th percentile	Mean	Median	75th percentile	Standard deviation	Fraction
Type A	0.03	0.05	0.04	0.06	0.03	0.45
Type B	0.79	1.77	1.42	2.55	1.27	12.95
Type C	0.23	0.66	0.43	0.95	0.55	4.40
Type AB	0.07	0.15	0.11	0.18	0.12	1.20
Type BC	0.52	1.06	0.87	1.51	0.73	8.26
Type ABC	0.17	0.37	0.28	0.43	0.31	2.91
CR-type	0.63	1.45	1.10	2.11	1.06	10.50
NCR-type	0.32	0.64	0.54	0.83	0.46	4.69

3.2 Spectral patterns of fluorescent aerosol particles

The complex nature of FAPs in polluted areas challenges the interpretation of ambient measurements. Different fluorophores have their characteristic excitation–emission matrices (EEMs) maps, which can be useful for discrimination of biological from non-biological FAPs (Pöhlker et al., 2012). Since a WIBS only has two excitation and emission wavebands, a high-resolution EEMs map cannot be retrieved. But we can still consider the two wavebands as low-resolution EEMs, of which the distribution (i.e., the ratio of the two wavebands) may also contain information about the nature of FAPs. For example, we can assume two kinds of fluorescent compounds I and II have different fluorescent spectra, as shown in Fig. 2a. For each compound, the integrated fluorescence intensity is determined in two wavebands by a WIBS (Fig. 2b). For qualitative analysis, a normalized EEM is often used providing the relative wavelength dependence of fluorescent materials. For a WIBS, we simply used the ratio of fluorescence intensity from different WIBS channels to represent the wavelength dependence (Fig. 2c).

Figure 3 shows the intensity distributions of aerosol particles in different fluorescence bands/channels. Due to the instrument setting, fluorescence signal intensities beyond 2200 arbitrary units (a.u.) are forced to the range of 2000–2200 a.u., regarding as saturated signal. Hence we only discussed fluorescence signal intensities below 2000 a.u. We first investigated the intensity ratio between channel FL1 and FL2, as shown in Fig. 3a. With increasing fluorescence intensity, the number concentrations sharply dropped, i.e., most of the abundant aerosol particles exhibited no or only weak fluorescence. Using the intensity ratio of FL1 to FL2 (I_{FL1}/I_{FL2}) as a fluorescence fingerprint, we obtained two prominent groups of aerosols with I_{FL1}/I_{FL2} approaching 0 or infinity. $I_{FL1}/I_{FL2} \sim 0$ means that the aerosols have a low FL1 intensity below the detection limit and a high FL2 intensity, while I_{FL1}/I_{FL2} approaching infinity means the opposite. According to the detection thresholds of both FL1 and FL2 channels, we then classified the aerosol particles into four groups with FL1/FL2 above or below the detection threshold (labeled as g1 to g4 in Fig. 3). We further investigated the FL3 proper-

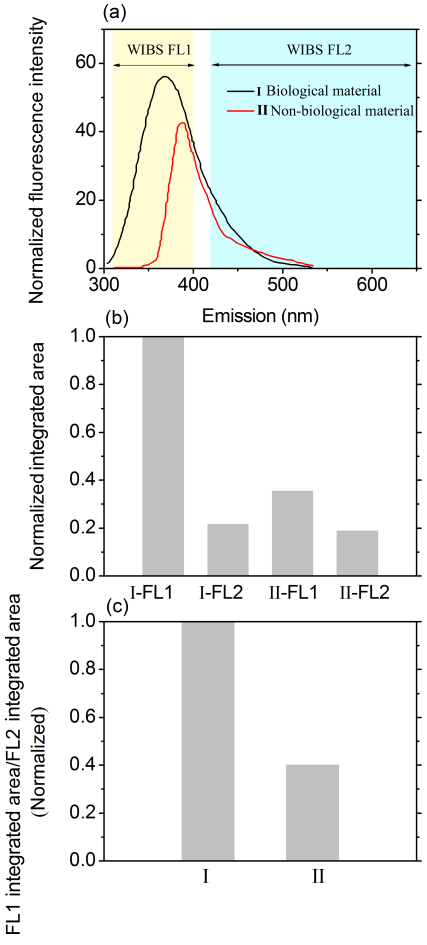

Figure 2. (a) Normalized fluorescence emission spectra of two fluorescent compounds: I (black line, biological material) and II (red line, non-biological material) for excitation wavelengths at $\lambda_{ex} = 280$ nm. Shadow areas indicate the excitation wavebands of FL1 and FL2 channels of WIBS. **(b)** Integrated fluorescence intensity of two compounds in two bands (FL1 and FL2). **(c)** The ratio of fluorescence intensity from different WIBS channels (I_{FL1}/I_{FL2}) of I and II compounds. The fluorescence emission spectra are obtained from Pöhlker et al. (2012).

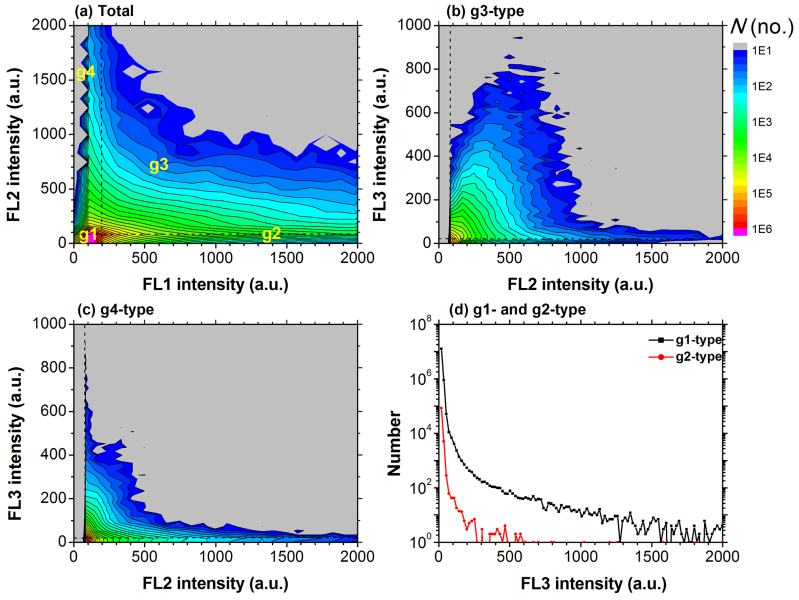

Figure 3. Spectral pattern of the classified fluorescence intensity. FL1 intensity is grouped at 100 intervals, FL2 intensity is grouped at 80 intervals, and FL3 intensity is grouped at 18 intervals. Color scale is the measured particle number. Non-fluorescent and saturating (FL $\geq$ 2000 a.u.) aerosol particles were excluded. **(a)** FL1 intensity vs. FL2 intensity of total measured particles; **(b)** FL2 intensity vs. FL3 intensity of g3-type particles; **(c)** FL2 intensity vs. FL3 intensity of g4-type particles; **(d)** numbers of g1- and g2-type particles of FL3 fluorescence intensity. Because FL2 intensity of g1 and g2 are below the threshold, the spectral patterns are hence not used. Dotted lines denote the threshold of each channel (200 a.u. for FL1, 80 a.u. for FL2, and 18 a.u. for FL3).

ties of the various groups. As shown in Fig. 3b–d, the aerosol number concentration decreased as FL3 intensity increased resembling the distribution for FL1 and FL2. Similarly we used the fluorescence threshold of FL3 to classify aerosols from g1 to g4 into subgroups.

Our efforts towards a spectral fingerprint resulted in the same classification method as in Perring et al. (2015). Here we adopted the labels of Perring et al. (2015) in which channel A refers to FL1, channel B refers to FL2 and channel C refers to FL3. Any aerosol particle can have signals above/below the fluorescence threshold in any of these channels, leading to seven combinations of fluorescence signals, i.e., particles with fluorescence signals above the threshold in single channel as types A, B and C; particles with fluorescence signals in two channels as types AB, AC and BC and particles with fluorescence signals in all three channels as type ABC (Table 1).

As shown in Fig. 4a, types B, BC and C were the most abundant FAPs, followed by types ABC, AB and A. Type AC had the lowest loading and was not even visible. The mean number concentrations of dominant types B, BC and C were 1.77, 1.06, and 0.66 cm^{-3}, respectively (Table 3). The number concentration of seven-type FAPs exhibited strong diurnal and day-to-day variability (Fig. 5). Number concentration of FAPs peaked in the morning ($\sim$ 08:00 local time) and reached a minimum in the afternoon ($\sim$ 14:00). Their similar diurnal patterns indicate the dominant effect of boundary layer development in controlling the variability of aerosol particles, which was also shown in FL1, FL2, and FL3 channels (Fig. S1 in the Supplement). To better understand the source of FAPs, we also investigated the number fraction of FAPs in total particles. The boundary layer development exerts similar effect on all kinds of aerosol particles. Thus for particles of the same origin, their ratios will remain constant and a difference in their ratios reflects their different sources. As shown in Fig. 5, the fractions of FAPs presented quite different diurnal patterns. The fractions of type BC revealed a substantial diurnal opposite with a clear morning peak and early afternoon minimum. Type A and type B showed a much weaker variability, implying a similar source of FAPs as the total aerosol particles.

The number size distributions of FAPs were shown in Fig. 6. The highest FAPs number concentration came out at $\sim$ 1 µm except type ABC. Type ABC peaked at 1–2 µm with a second peak at 4–6 µm. For type A, type C, and type BC the number concentration monotonously decreased with increasing particle diameter. No fluorescence signals were found in FL1 and FL3 channels (corresponding to type A, type C and type AC FAPs) for the particles of size larger than 4 µm. On the contrary, the number fractions of FAPs generally increased as the particle size increased, reaching $\sim$ 100 % at 3–4 µm for FL2 channel (not shown in Fig. 6). These results reveal that most coarse mode particles contain certain kinds of fluorophores.

Meanwhile, we compared the number fraction of seven-type FAPs with $M_{BC}/PM_{0.8}$; the results indicate that the

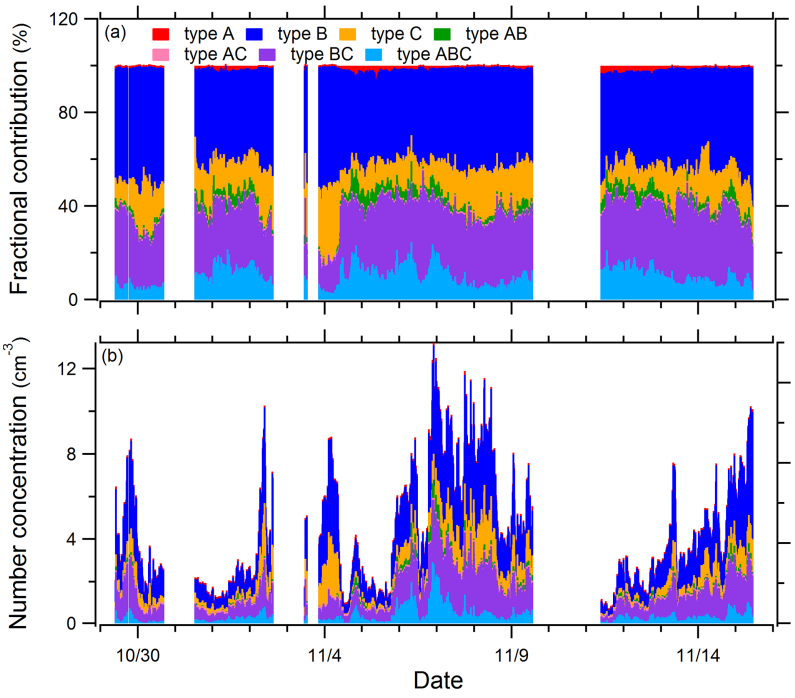

Figure 4. Time series of **(a)** the fractional contribution of each fluorescent type to total FAPs and **(b)** number concentration (left axis) of each fluorescent type. Type A: red; type B: blue; type C: dark yellow; type AB: green; type AC: pink; type BC: purple; type ABC: light blue.

number fractions of types A, AB, and ABC showed good correlations with $M_{BC}/PM_{0.8}$ (Fig. 7), suggesting a large contribution of combustion-related aerosol particles to these types. Note that all these types contain FL1 signals, implying the potential application of FL1 in the identification of biomass burning (or other combustions) events. Likewise, fluorescent types B and BC mostly followed the variation of $M_{BC}/PM_{0.8}$ except for 8 November when elevated fractional contributions were observed 1 day before a rain event on 9 November. A dramatic release of certain fungal spores was often observed before rain (Hjelmroos, 1993). However, the increase on 8 November was mainly contributed by 1–2 µm FAPs rather than fungal spores (> 3 µm) shown by Hjelmroos (1993). So the origin of this elevated FAPs remained inconclusive. Moreover, good correlation ($r = 0.58$) between type B particles in 3–4 µm and $M_{BC}/PM_{0.8}$, suggesting a closer link of this peak with type B particles to the combustion process. Fluorescent type C showed a weak negative correlation with $M_{BC}/PM_{0.8}$, suggesting a minor role of combustion-related aerosols or major contribution of non-combustion-related aerosols (e.g., bioaerosols or dusts).

3.3 Fluorescence intensity

Besides the relative wavelength dependence, the absolute quantum yield is also one of the most important characteristics of a fluorophore. Discrepancies in the quantum yield can directly influence the fluorescence, resulting in different intensity levels. Thus, it is possible to use the intensity information to identify different kinds of FAPs. Huffman et al. (2012) showed that the UV-APS can be used to successfully discriminate bioaerosols from dust particles, both of which have been suggested to fluoresce (Pöhlker et al., 2012).

We first made a hypothesis that there exists a characteristic intensity value I_{cri}, above which most FAPs are bioaerosols. Since I_{cri} cannot be directly inferred from the intensity distribution (Fig. 3), we adopted the parameter $M_{BC}/PM_{0.8}$ to assist our analysis. Because bioaerosols and combustion-related FAPs are of different origins, we scanned different values for I_{cri} until the corresponding FAP (of intensity $> I_{cri}$) fraction showed a non-positive correlation with $M_{BC}/PM_{0.8}$. In this study, we mainly focus on the FL3 channel since it is running in a similar excitation–emission wavelength as the UV-APS and it has been validated against other independent method. We thereby suggest that the FL3 channel can be used to discriminate bioaerosols from combustion-generated FAPs in a similar approach. The analysis of the FL1 and FL2 channels are shown in the Supplement (Figs. S2 and S3). Figure 8 shows the averaged fractional contribution of FAPs with $I_{FL3} > I_{cri}$ at different $M_{BC}/PM_{0.8}$ levels. To account for the size dependence of fluorescence signals, we first classified FAPs according to the particle size. For the 1–2 µm size range, the fraction was always positively correlated with $M_{BC}/PM_{0.8}$ and was independent of the selection of I_{cri}. For the size range of 2–5 µm, the FAPs showed mostly negative correlation with $M_{BC}/PM_{0.8}$ and were also

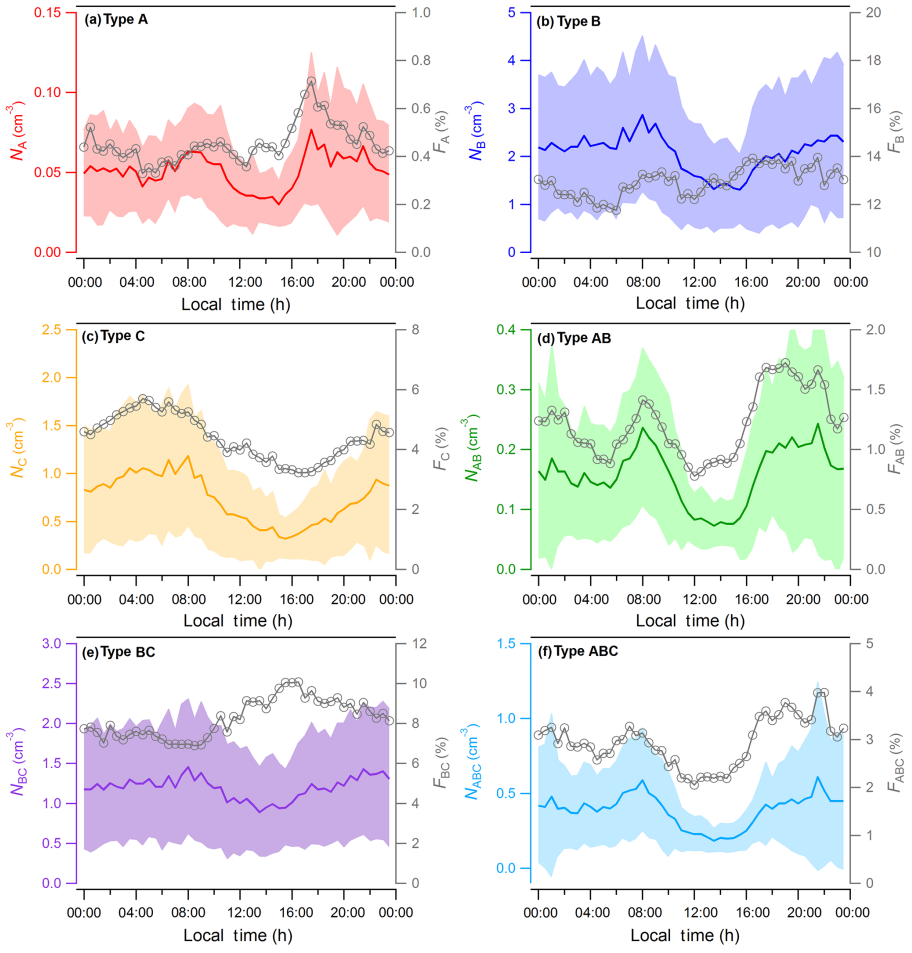

Figure 5. Diurnal variations of number concentrations of **(a)** type A (red), **(b)** type B (blue), **(c)** type C (dark yellow), **(d)** type AB (green), **(e)** type BC (purple), and **(f)** type ABC (light blue). Gray line indicates the number fraction of respective fluorescent particles (right axis). Shading indicates ± 1 standard deviation.

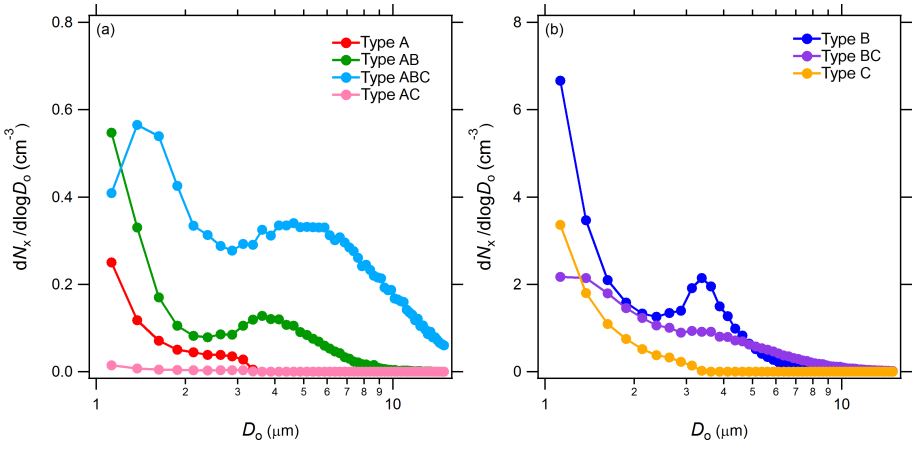

Figure 6. Mean number size distributions of **(a)** type A (red), type AB (green), type AC (pink), and type ABC (light blue); **(b)** type B (blue), type BC (purple), and type C (dark yellow).

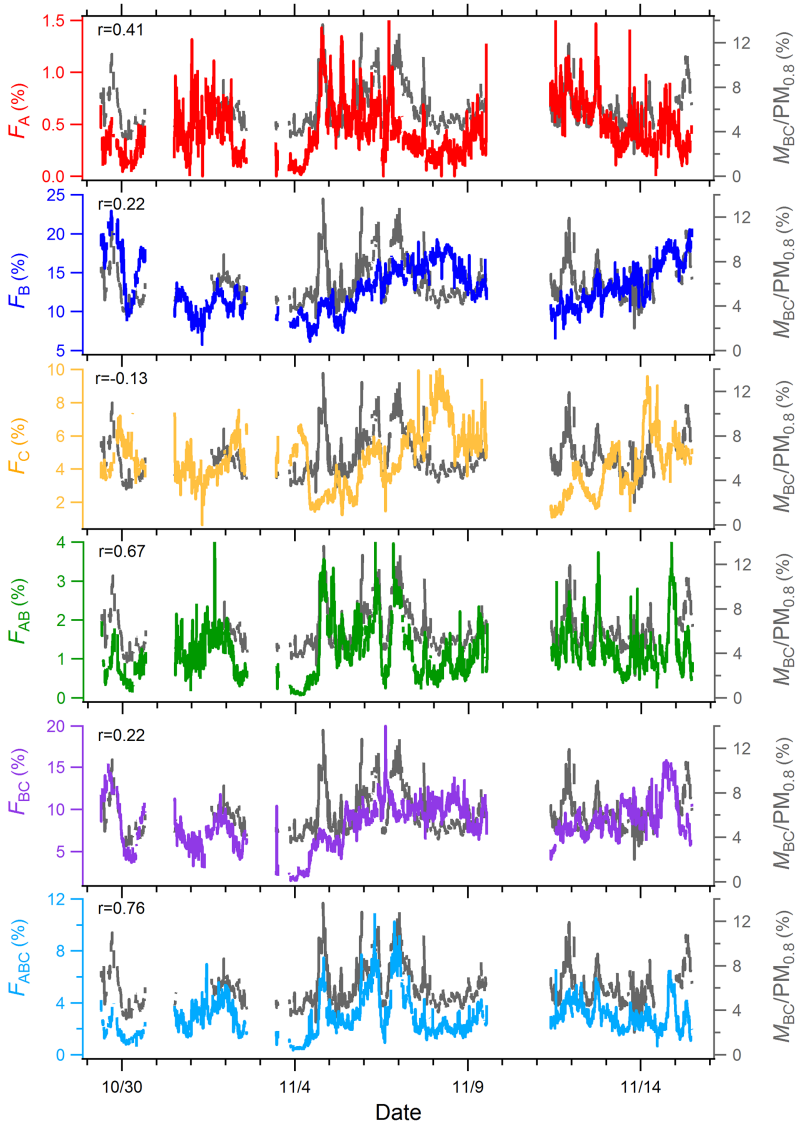

Figure 7. Time series of number fractions of various fluorescent particles (left axis) and $M_{BC}/PM_{0.8}$ (gray, right axis). r is the correlation coefficient between F_x and $M_{BC}/PM_{0.8}$.

independent of the I_{cri} selection. For FAPs larger than 5 µm, the selection of I_{cri} became critical. With increasing I_{cri}, the dependence of FL3 fraction on $M_{BC}/PM_{0.8}$ gradually became weaker and finally turned to negative at $I_{cri} > 40$ a.u. The results at 5–15 µm were consistent with our hypothesis that bioaerosols have stronger fluorescence intensity than combustion-related aerosol particles and can be discriminated from their fluorescence intensity. The different correlation statistics of 1–2 and 2–5 µm may be explained by the different abundance of bioaerosols and combustion-related aerosols at a different size range. The 2–5 µm mode was dominated by bioaerosols, whereas the 1–2 µm mode was dominated by combustion-related aerosol particles. Therefore, there was no clear dependence on the selection of I_{cri}. Saari et al. (2015) reported that FAPs at 0.5–1.5 µm might be due to anthropogenic emissions such as biomass burning, while most fungal spores and pollen dominated the larger size range (Després et al., 2012). It is also possible that I_{cri} had a size dependence because different types of bioaerosols may dominate different size ranges.

By integrating the FAPs of different correlations with $M_{BC}/PM_{0.8}$, we retrieved the number concentrations of "non-combustion-related" (NCR)-type particles (FAPs with $I_{FL3} > 18$ a.u. at 2–5 µm and FAPs with $I_{FL3} > 40$ a.u. at 5–15 µm) and "combustion-related" (CR)-type particles (FAPs with $I_{FL3} > 18$ a.u. at 1–2 µm and FAPs with $40 \geq I_{FL3} > 18$ a.u. at 5–15 µm). The mean number concentrations of NCR-type and CR-type particles were 0.64 ± 0.46

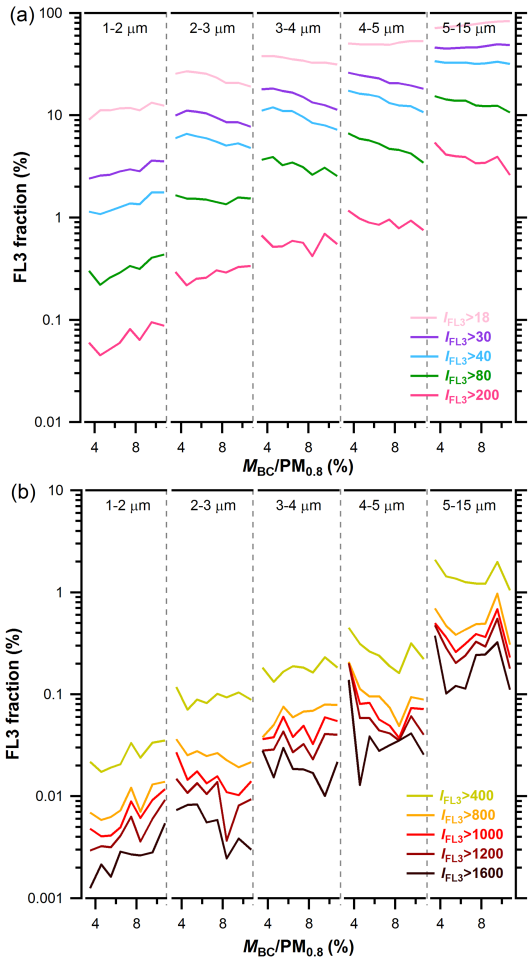

Figure 8. Correlations of FL3 fractions with $M_{BC}/PM_{0.8}$ in different size ranges. The FL3 fraction is the number concentration of the subgroup ratio to the number concentration of total particles in each size bin. **(a)** Low fluorescent intensity group. **(b)** High fluorescent intensity group. The color lines represent the FL3 intensity (I_{FL3}) above the certain I_{cri}.

and $1.45 \pm 1.06\,cm^{-3}$, respectively. The NCR-type FAPs are likely bioaerosols.

In this study, we applied two methods to classify FAPs measured by a WIBS, resulting in two non-combustion-types of particles: type C particles derived from fluorescence spectral pattern analysis and NCR-type particles derived from fluorescence intensity pattern analysis. As shown in Table 3, the mean number concentrations of type C and NCR-type particle were 0.66 and $0.64\,cm^{-3}$, which were still higher than those found in PBAP-dominated regions like the Amazon (Huffman et al., 2012), Hyytiälä (Schumacher et al., 2013), and PdD (Gabey et al., 2013). This indicates that still a residual of these non-combustion-type particles may comprise other fluorescent constituents like mineral dusts (Miyakawa et al., 2015; Perring et al., 2015).

4 Conclusions

Online measurements of FAPs have been performed in Nanjing by using WIBS in the autumn of 2013. Our results showed that the number concentrations of FAPs were 1–2 orders of magnitudes higher than those reported in the previous studies. The observed high values suggested that directly using the FL1, FL2, and FL3 channels to index PBAPs is not suitable for polluted areas. The number fraction of FL1 showed strong correlation with $M_{BC}/PM_{0.8}$ ($r = 0.75$), indicative of a strong bias by anthropogenic emissions.

In this study, we used two methods to classify the FAPs. According to the threshold of each channel, FAPs were divided into seven types. Number fraction of type C showed a negative correlation ($r = -0.13$) with $M_{BC}/PM_{0.8}$, which might be more representative for bioaerosols. Meanwhile, on the basis of the FL3 fluorescent intensity and its correlations with $M_{BC}/PM_{0.8}$, FL3 fluorescent particles were divided into two types. Combustion-related-type particles seemed to dominate 1–2 μm, whereas the non-combustion-related-type particles, which concentrated in the size range of 2–5 μm and showed negative correlation ($r = -0.12$) with $M_{BC}/PM_{0.8}$, might have originated from biological emissions. The number concentrations of the identified two types of bioaerosols ($0.66\,cm^{-3}$ for type C particles and $0.64\,cm^{-3}$ for non-combustion-related type), however, were still higher than those observed in clean background areas and previous studies in Nanjing (Wei et al., 2015), indicating they may also include some other fluorophores, such as dusts.

Our results suggested that fluorescence measurements in polluted areas are prone to interferences and uncertainty introduced by the anthropogenic emissions. Discrimination of biological particles from FAPs still needs further development. Each fluorophore species presents unique fluorescence spectrum; hence, we can effectively distinguish biological particles from other FAPs based on their specific EEMs maps. Due to the limitation of excitation and emission wavebands of WIBS, the development of a multi-wavebands instrument is hence needed. Other methods such as the cluster analysis (Robinson et al., 2013; Crawford et al., 2014, 2015) also exhibited the ability to differentiate various FAPs. Measuring additional particle properties such as size and morphology will help ameliorate the interferences by providing additional dimensions to distinguish fluorescent particles of different emission mechanisms.

5 Data availability

All the data presented in this study are available from the authors upon request (zhibin.wang@mpic.de or h.su@mpic.de).

The Supplement related to this article is available online at doi:10.5194/acp-16-11337-2016-supplement.

Acknowledgements. This study was supported by the Max Plank Society (MPG), the European Commission under the projects BACCHUS (grant no. 603445) and the Natural Science Foundation of China (project no. 91544103). Xiawei Yu and Minghui Zhang would like to thank the China Scholarship Council (CSC) for financial support. We thank the SORPES-NJU station for logistic and instrumentation support.

The article processing charges for this open-access publication were covered by the Max Planck Society.

Edited by: A. Ding
Reviewed by: three anonymous referees

References

Bary, A., Garnsey, H. E. F., and Balfour, I. B.: Comparative morphology and biology of the fungi, mycetozoa and bacteria, Oxford, Clarendon Press, 1887.

Brosseau, L. M., Vesley, D., Rice, N., Goodell, K., Nellis, M., and Hairston, P.: Differences in Detected Fluorescence Among Several Bacterial Species Measured with a Direct-Reading Particle Sizer and Fluorescence Detector, Aerosol Sci. Tech., 32, 545–558, doi:10.1080/027868200303461, 2000.

Cao, C., Jiang, W., Wang, B., Fang, J., Lang, J., Tian, G., Jiang, J., and Zhu, T. F.: Inhalable Microorganisms in Beijing's $PM_{2.5}$ and PM_{10} Pollutants during a Severe Smog Event, Environ. Sci. Technol., 48, 1499–1507, 10.1021/es4048472, 2014.

Chang, J. L. and Thompson, J. E.: Characterization of colored products formed during irradiation of aqueous solutions containing H_2O_2 and phenolic compounds, Atmos. Environ., 44, 541–551, 2010.

Christner, B. C., Morris, C. E., Foreman, C. M., Cai, R., and Sands, D. C.: Ubiquity of Biological Ice Nucleators in Snowfall, Science, 319, 1214, doi:10.1126/science.1149757, 2008.

Crawford, I., Robinson, N. H., Flynn, M. J., Foot, V. E., Gallagher, M. W., Huffman, J. A., Stanley, W. R., and Kaye, P. H.: Characterisation of bioaerosol emissions from a Colorado pine forest: results from the BEACHON-RoMBAS experiment, Atmos. Chem. Phys., 14, 8559–8578, doi:10.5194/acp-14-8559-2014, 2014.

Crawford, I., Ruske, S., Topping, D. O., and Gallagher, M. W.: Evaluation of hierarchical agglomerative cluster analysis methods for discrimination of primary biological aerosol, Atmos. Meas. Tech., 8, 4979–4991, doi:10.5194/amt-8-4979-2015, 2015.

Creamean, J. M., Suski, K. J., Rosenfeld, D., Cazorla, A., DeMott, P. J., Sullivan, R. C., White, A. B., Ralph, F. M., Minnis, P., Comstock, J. M., Tomlinson, J. M., and Prather, K. A.: Dust and Biological Aerosols from the Sahara and Asia Influence Precipitation in the Western US, Science, 339, 1572–1578, doi:10.1126/science.1227279, 2013.

DeLeon-Rodriguez, N., Lathem, T. L., Rodriguez-R, L. M., Barazesh, J. M., Anderson, B. E., Beyersdorf, A. J., Ziemba, L. D., Bergin, M., Nenes, A., and Konstantinidis, K. T.: Microbiome of the upper troposphere: Species composition and prevalence, effects of tropical storms, and atmospheric implications, P. Natl. Acad. Sci. USA, 110, 2575–2580, doi:10.1073/pnas.1212089110, 2013.

Després, V. R., Huffman, J. A., Burrows, S. M., Hoose, C., Safatov, A. S., Buryak, G., Fröhlich-Nowoisky, J., Elbert, W., Andreae, M. O., Pöschl, U., and Jaenicke, R.: Primary biological aerosol particles in the atmosphere: a review, Tellus B, 64, 15598, doi:10.3402/tellusb.v64i0.15598, 2012.

Ding, A. J., Fu, C. B., Yang, X. Q., Sun, J. N., Zheng, L. F., Xie, Y. N., Herrmann, E., Nie, W., Petäjä, T., Kerminen, V.-M., and Kulmala, M.: Ozone and fine particle in the western Yangtze River Delta: an overview of 1 yr data at the SORPES station, Atmos. Chem. Phys., 13, 5813–5830, doi:10.5194/acp-13-5813-2013, 2013.

Duchaine, C., Thorne, P. S., Mériaux, A., Grimard, Y., Whitten, P., and Cormier, Y.: Comparison of endotoxin exposure assessment by bioaerosol impinger and filter-sampling methods, Appl. Environ. Microbiol., 67, 2775–2780, 2001.

Fröhlich-Nowoisky, J., Kampf, C. J., Weber, B., Huffman, J. A., Pöhlker, C., Andreae, M. O., Lang-Yona, N., Burrows, S. M., Gunthe, S. S., Elbert, W., Su, H., Hoor, P., Thines, E., Hoffmann, T., Després, V. R., and Pöschl, U.: Bioaerosols in the Earth system: Climate, health, and ecosystem interactions, Atmos. Res., 182, 346–376, 2016.

Gabey, A. M., Gallagher, M. W., Whitehead, J., Dorsey, J. R., Kaye, P. H., and Stanley, W. R.: Measurements and comparison of primary biological aerosol above and below a tropical forest canopy using a dual channel fluorescence spectrometer, Atmos. Chem. Phys., 10, 4453–4466, doi:10.5194/acp-10-4453-2010, 2010.

Gabey, A. M., Stanley, W. R., Gallagher, M. W., and Kaye, P. H.: The fluorescence properties of aerosol larger than 0.8 µm in urban and tropical rainforest locations, Atmos. Chem. Phys., 11, 5491–5504, doi:10.5194/acp-11-5491-2011, 2011.

Gabey, A. M., Vaitilingom, M., Freney, E., Boulon, J., Sellegri, K., Gallagher, M. W., Crawford, I. P., Robinson, N. H., Stanley, W. R., and Kaye, P. H.: Observations of fluorescent and biological aerosol at a high-altitude site in central France, Atmos. Chem. Phys., 13, 7415–7428, doi:10.5194/acp-13-7415-2013, 2013.

Griffin, D. W.: Atmospheric movement of microorganisms in clouds of desert dust and implications for human health, Clin. Microbiol. Rev., 20, 459–477, doi:10.1128/Cmr.00039-06, 2007.

Hallar, A. G., Chirokova, G., McCubbin, I., Painter, T. H., Wiedinmyer, C., and Dodson, C.: Atmospheric bioaerosols transported via dust storms in the western United States, Geophys. Res. Lett., 38, L17801, doi:10.1029/2011GL048166, 2011.

Healy, D. A., Huffman, J. A., O'Connor, D. J., Pöhlker, C., Pöschl, U., and Sodeau, J. R.: Ambient measurements of biological aerosol particles near Killarney, Ireland: a comparison between real-time fluorescence and microscopy techniques, Atmos. Chem. Phys., 14, 8055–8069, doi:10.5194/acp-14-8055-2014, 2014.

Henningson, E. W. and Ahlberg, M. S.: Evaluation of microbiological aerosol samplers: a review, J. Aerosol Sci., 25, 1459–1492, 1994.

Herrmann, E., Ding, A. J., Kerminen, V.-M., Petäjä, T., Yang, X. Q., Sun, J. N., Qi, X. M., Manninen, H., Hakala, J., Nieminen, T., Aalto, P. P., Kulmala, M., and Fu, C. B.: Aerosols and nucleation in eastern China: first insights from the new SORPES-NJU station, Atmos. Chem. Phys., 14, 2169–2183, doi:10.5194/acp-14-2169-2014, 2014.

Hjelmroos, M.: Relationship between airborne fungal spore presence and weather variables: Cladosporium and Alternaria, Grana, 32, 40–47, 1993.

Huffman, J. A., Treutlein, B., and Pöschl, U.: Fluorescent biological aerosol particle concentrations and size distributions measured with an Ultraviolet Aerodynamic Particle Sizer (UV-APS) in Central Europe, Atmos. Chem. Phys., 10, 3215–3233, doi:10.5194/acp-10-3215-2010, 2010.

Huffman, J. A., Sinha, B., Garland, R. M., Snee-Pollmann, A., Gunthe, S. S., Artaxo, P., Martin, S. T., Andreae, M. O., and Pöschl, U.: Size distributions and temporal variations of biological aerosol particles in the Amazon rainforest characterized by microscopy and real-time UV-APS fluorescence techniques during AMAZE-08, Atmos. Chem. Phys., 12, 11997–12019, doi:10.5194/acp-12-11997-2012, 2012.

Huffman, J. A., Prenni, A. J., DeMott, P. J., Pöhlker, C., Mason, R. H., Robinson, N. H., Fröhlich-Nowoisky, J., Tobo, Y., Després, V. R., Garcia, E., Gochis, D. J., Harris, E., Müller-Germann, I., Ruzene, C., Schmer, B., Sinha, B., Day, D. A., Andreae, M. O., Jimenez, J. L., Gallagher, M., Kreidenweis, S. M., Bertram, A. K., and Pöschl, U.: High concentrations of biological aerosol particles and ice nuclei during and after rain, Atmos. Chem. Phys., 13, 6151–6164, doi:10.5194/acp-13-6151-2013, 2013.

Miyakawa, T., Kanaya, Y., Taketani, F., Tabaru, M., Sugimoto, N., Ozawa, Y., and Takegawa, N.: Ground-based measurement of fluorescent aerosol particles in Tokyo in the spring of 2013: Potential impacts of nonbiological materials on autofluorescence measurements of airborne particles, J. Geophys. Res.-Atmos., 120, 1171–1185, doi:10.1002/2014jd022189, 2015.

Morris, C. E., Sands, D. C., Glaux, C., Samsatly, J., Asaad, S., Moukahel, A. R., Gonçalves, F. L. T., and Bigg, E. K.: Urediospores of rust fungi are ice nucleation active at $> -10\,^{\circ}\mathrm{C}$ and harbor ice nucleation active bacteria, Atmos. Chem. Phys., 13, 4223–4233, doi:10.5194/acp-13-4223-2013, 2013.

Oliver, J. D.: The viable but nonculturable state in bacteria, J. Microbiol., 43, 93–100, 2005.

Pan, Y.-L., Pinnick, R. G., Hill, S. C., and Chang, R. K.: Particle-Fluorescence Spectrometer for Real-Time Single-Particle Measurements of Atmospheric Organic Carbon and Biological Aerosol, Environ. Sci. Technol., 43, 429–434, doi:10.1021/es801544y, 2009.

Perring, A. E., Schwarz, J. P., Baumgardner, D., Hernandez, M. T., Spracklen, D. V., Heald, C. L., Gao, R. S., Kok, G., McMeeking, G. R., McQuaid, J. B., and Fahey, D. W.: Airborne observations of regional variation in fluorescent aerosol across the United States, J. Geophys. Res.-Atmos., 120, 1153–1170, doi:10.1002/2014JD022495, 2015.

Pöhlker, C., Huffman, J. A., and Pöschl, U.: Autofluorescence of atmospheric bioaerosols – fluorescent biomolecules and potential interferences, Atmos. Meas. Tech., 5, 37–71, doi:10.5194/amt-5-37-2012, 2012.

Polymenakou, P. N., Mandalakis, M., Stephanou, E. G., and Tselepides, A.: Particle size distribution of airborne microorganisms and pathogens during an intense African dust event in the eastern Mediterranean, Environ. Health Perspect., 116, 292–296, doi:10.1289/Ehp.10684, 2008.

Pöschl, U.: Atmospheric aerosols: Composition, transformation, climate and health effects, Angew. Chem. Int. Edit., 44, 7520–7540, doi:10.1002/anie.200501122, 2005.

Pöschl, U., Martin, S. T., Sinha, B., Chen, Q., Gunthe, S. S., Huffman, J. A., Borrmann, S., Farmer, D. K., Garland, R. M., Helas, G., Jimenez, J. L., King, S. M., Manzi, A., Mikhailov, E., Pauliquevis, T., Petters, M. D., Prenni, A. J., Roldin, P., Rose, D., Schneider, J., Su, H., Zorn, S. R., Artaxo, P., and Andreae, M. O.: Rainforest Aerosols as Biogenic Nuclei of Clouds and Precipitation in the Amazon, Science, 329, 1513–1516, doi:10.1126/science.1191056, 2010.

Robinson, N. H., Allan, J. D., Huffman, J. A., Kaye, P. H., Foot, V. E., and Gallagher, M.: Cluster analysis of WIBS single-particle bioaerosol data, Atmos. Meas. Tech., 6, 337–347, doi:10.5194/amt-6-337-2013, 2013.

Saari, S., Niemi, J., Rönkkö, T., Kuuluvainen, H., Järvinen, A., Pirjola, L., Aurela, M., Hillamo, R., and Keskinen, J.: Seasonal and Diurnal Variations of Fluorescent Bioaerosol Concentration and Size Distribution in the Urban Environment, Aerosol Air Qual. Res., 15, 572–581, 2015.

Schumacher, C. J., Pöhlker, C., Aalto, P., Hiltunen, V., Petäjä, T., Kulmala, M., Pöschl, U., and Huffman, J. A.: Seasonal cycles of fluorescent biological aerosol particles in boreal and semi-arid forests of Finland and Colorado, Atmos. Chem. Phys., 13, 11987–12001, doi:10.5194/acp-13-11987-2013, 2013.

Taketani, F., Kanaya, Y., Nakamura, T., Koizumi, K., Moteki, N., and Takegawa, N.: Measurement of fluorescence spectra from atmospheric single submicron particle using laser-induced fluorescence technique, J. Aerosol Sci., 58, 1–8, doi:10.1016/j.jaerosci.2012.12.002, 2013.

Toprak, E. and Schnaiter, M.: Fluorescent biological aerosol particles measured with the Waveband Integrated Bioaerosol Sensor WIBS-4: laboratory tests combined with a one year field study, Atmos. Chem. Phys., 13, 225–243, doi:10.5194/acp-13-225-2013, 2013.

Valsan, A. E., Ravikrishna, R., Biju, C. V., Pöhlker, C., Després, V. R., Huffman, J. A., Pöschl, U., and Gunthe, S. S.: Fluorescent biological aerosol particle measurements at a tropical high-altitude site in southern India during the southwest monsoon season, Atmos. Chem. Phys., 16, 9805–9830, doi:10.5194/acp-16-9805-2016, 2016.

Wang, H., Zhu, B., Shen, L., Liu, X., Zhang, Z., and Yang, Y.: Size distributions of aerosol during the Spring Festival in Nanjing, Huan jing ke xue, 35, 442–450, 2014 (in Chinese).

Wei, K., Zheng, Y., Li, J., Shen, F., Zou, Z., Fan, H., Li, X., Wu, C.-Y., and Yao, M.: Microbial aerosol characteristics in highly polluted and near-pristine environments featuring different climatic conditions, Sci. Bull., 60, 1439–1447, doi:10.1007/s11434-015-0868-y, 2015.

Wei, K., Zou, Z., Zheng, Y., Li, J., Shen, F., Wu, C.-y., Wu, Y., Hu, M., and Yao, M.: Ambient bioaerosol particle dynamics observed during haze and sunny days in Beijing, Sci. Total Environ., 550, 751–759, doi:10.1016/j.scitotenv.2016.01.137, 2016.

Yu, J., Hu, Q., Xie, Z., Kang, H., Li, M., Li, Z., and Ye, P.: Concentration and Size Distribution of Fungi Aerosol over Oceans along a Cruise Path during the Fourth Chinese Arctic Research Expedition, Atmosphere, 4, 337–348, 2013.

E CV

Minghui Zhang

Education:

2014 – present Ph.D. in Chemistry, Max Planck Institute for Chemistry, Germany

2010 - 2013 Master in Applied Chemistry, Beihang University, China

2006 - 2010 Bachelor in Applied Chemistry, Qingdao University, China

Awards & Honors (selected):

2016 Prizewinner by Zentrum für Technologietransfer der HZZK, Germany

2013 Runner up prize by European Aeronautic Defence and Space, France

2012 National Scholarship by Ministry of Education, China

Publications:

1. **M. Zhang**, T. Klimach, N. Ma, Z. Wang, T. Könemann, C. Pöhlker, N. Scheck, U. Kuhn, U. Pöschl, H. Su, Y. Cheng, Size-resolved Single-particle Fluorescence Spectrometer (S2FS) for Real-time Measurements of Biological Aerosols and Non-biological Fluorescent Aerosols, *EGU General Assembly Conference Abstracts* 20, 14774, 2018

2. **M. Zhang**, T. Klimach, N. Ma, T. Könemann, C. Pöhlker, Z. Wang, N. Scheck, U. Kuhn, U. Pöschl, H. Su, Y. Cheng, Size-resolved Single-particle Fluorescence Spectrometer (S2FS) for analysis of bioaerosols: Laboratory evaluation and atmospheric measurement, submitted.

3. **M. Zhang**, U. Pöschl, H. Su, Y. Cheng, Intensity calibration of an online/in situ fluorescence spectrometer (OFS) using the volume of single particles, to be submitted.

4. **M. Zhang**, T. Hoffmann, G. Li, U. Kuhn, U. Pöschl, H. Su, Y. Cheng, Fluorescence of fresh and aged biogenic secondary organic aerosols (SOA), in preparation

5. **M. Zhang**, X. Hou, J. Wang, Y. Tian, X. Fan, J. Zhai, L. Jiang, Light and pH cooperative nanofluidic diode using a spiropyran-functionalized single nanochannel, *Advanced Materials* 24 (18), 2424-2428, 2012

6. **M. Zhang**, Z. Meng, J Zhai, L. Jiang, Photo-induced current amplification in L-histidine modified nanochannels based on a highly charged photoacid in solution, *Chemical Communications* 49 (23), 2284-2286, 2013
7. J. Wang, **M. Zhang**, J. Zhai, L. Jiang, Theoretical simulation of the ion current rectification (ICR) in nano-pores based on the Poisson–Nernst–Planck (PNP) model, *Physical Chemistry Chemical Physics* 16 (1), 23-32, 2014
8. Y. Xu, **M. Zhang**, T. Tian, Y. Shang, Z. Meng, J. Jiang, J. Zhai, Y. Wang, Mimicking how plants control CO2 influx: CO2 activation of ion current rectification in nanochannels, *NPG Asia Materials* 7 (9), 215, 2015
9. X. Yu, Z. Wang, **M. Zhang**, U. Kuhn, Z. Xie, Y. Cheng, U. Pöschl, H. Su, Ambient measurement of fluorescent aerosol particles with a WIBS in the Yangtze River Delta of China: potential impacts of combustion-related aerosol particles, *Atmospheric Chemistry and Physics* 16 (17), 11337-11348, 2016
10. Y. Kong, X. Fan, **M. Zhang**, X. Hou, Z. Liu, J. Zhai, L. Jiang, Nanofluidic diode based on branched alumina nanochannels with tunable ionic rectification, *ACS applied materials & interfaces* 5 (16), 7931-7936, 2013
11. Z. Meng, H. Bao, J. Wang, C Jiang, **M. Zhang**, J. Zhai, L. Jiang, Artificial Ion Channels Regulating Light-Induced Ionic Currents in Photoelectrical Conversion Systems, *Advanced Materials* 26 (15), 2329-2334, 2014